COMPREHENSIVE STUDY OF THE INFLUENCE OF SURFACE ROUGHNESS OF PLATINUM ELECTRODES ON THEIR INTERFACIAL MASS CHANGES AS EXAMINED USING THE ELECTROCHEMICAL QUARTZ-CRYSTAL NANOBALANCE

by

Jutae Kim

A thesis submitted to the Graduate Program in Chemistry

in conformity with the requirements for the

Degree of Doctor of Philosophy

Queen's University

Kingston, Ontario, Canada

(May, 2017)

Abstract

The electrochemical quartz-crystal nanobalance (EQCN) is an electroanalytical technique used to measure *in-situ* minute mass changes (Δm) associated with interfacial electrochemical phenomena. The results acquired by combining the EQCN and electrochemical techniques provide a new insight into the nature of electrochemical processes and contribute to the understanding of their mechanisms at the atomic/molecular level. The EQCN has been used for over three decades; however, its limits of detection (LOD) and quantification (LOQ) have never been studied. We propose a methodology for determining the values of LOD and LOQ for Pt electrodes in aqueous H_2SO_4 solutions. The values of LOD and LOQ decrease as the concentration of the electrolyte decreases. The EQCN measures changes in frequency (Δf) of a quartz-crystal resonator, which are converted into Δm using the Sauerbrey equation containing the characteristic constant (C_f); C_f is determined by physical parameters of the quartz and refers to an atomically smooth surface. However, real electrodes are not atomically flat and it is unknown how surface roughness factor (R) affects Δm. We examine Δm associated with H adsorption/desorption and surface oxide formation/reduction on Pt electrodes. The value of R is fine-tuned through Pt electrodeposition and the surface morphology is examined using atomic force microscopy. The results reveal linear relationships between Δm and R, and their extrapolation to $R = 1.00$ leads to the determination of Δm for atomically flat polycrystalline Pt electrodes. The values of Δm for $R = 1.00$ are analyzed in terms of the number of electrolyte components interacting with each Pt surface atom. A modified Sauerbrey equation, which takes into account the surface roughness, is proposed. Also, we calibrate the system using Ag electrodeposition, and the experimental characteristic constant ($C_{f,exp}$) values are determined by analyzing the slopes of charge density versus Δf plots for the Ag electrodeposition. They are different than the value of C_f and increase logarithmically with R. The C_f and $C_{f,exp}$ values are used in a comparative analysis of Δm for complete cyclic-voltammetry profiles. It reveals that the employment of C_f instead of $C_{f,exp}$ provides inaccurate values of Δm, and the magnitude of discrepancy increases with R.

Co-Authorship

All work reported in this thesis was carried out by the author under the supervision of Professor Gregory Jerkiewicz in the Department of Chemistry at Queen's University. Portions of this thesis contain results that were analyzed in collaboration with Professor Diane Beauchemin in the Department of Chemistry at Queen's University and the group of Professor Christophe Coutanceau at Université de Poitiers, France. Portions of this thesis are published and submitted as manuscripts in peer-reviewed scientific journals:

1. Jutae Kim, Andrew Munro, Diane Beauchemin, Gregory Jerkiewicz, "Limits of Detection and Quantification of Electrochemical Quartz-Crystal Nanobalance in Platinum Electrochemistry and Electrocatalysis Research", *Analytical Chemistry* **2016,** *88,* 10599–10604.

2. Jutae Kim, Patrick Urchaga, Stève Baranton, Christophe Coutanceau, Gregory Jerkiewicz, "Interfacial Structure of Atomically Flat Polycrystalline Pt Electrodes and Modified Sauerbrey Equation", Submitted to *Nature Communications* (2017).

3. Jutae Kim, Gregory Jerkiewicz, "Influence of the Surface Roughness of Platinum Electrodes on the Calibration of the Electrochemical Quartz-Crystal Nanobalance", Submitted to *Analytical Chemistry* (2017).

Acknowledgements

I would like to express my sincere thanks and appreciation to my supervisor Dr. Gregory Jerkiewicz for his support and guidance over the course of my Ph. D. study. He helped me a lot to push my boundaries and to expand my capability.

To the past and present members of the Jerkiewicz Lab, I would like to thank you for your advice, friendship and support throughout all these years: Dr. Julia van Drunen, Dr. Liyan Xing, Dr. Mohammad Akhtar Hossain, Dr. Yoshihisa Furuya, Dr. Min Tian, Mr. Nakkiran Arulmozhi, Ms. Sadaf Tahmasebi, Ms. Ashley McMath, Mr. Derek Esau, Mr. Ram Lamsal, Mr. Marco Gibaldi, Mr. Eduardo de Barros Ferreira, and Dr. Nausheen Sadiq. Also, I would also like to thank Dr. Yongsung Park for being a good friend with a weekly coffee time in the chemistry department.

Most importantly, I would like to thank my parents and wife for their encouragement, patience, support, and love over my Ph.D. study. I love you.

Statement of Originality

I hereby certify that all of the work described within this thesis is the original work of the author. Any published (or unpublished) ideas and/or techniques from the work of others are fully acknowledged in accordance with the standard referencing practices.

Jutae Kim

May, 2017

Table of Contents

List of Figures

List of Tables

List of Abbreviations

A	surface area
A_{ecsa}	electrochemically active surface area
AES	Auger electron spectroscopy
AFM	atomic force microscopy
A_{geom}	geometric surface area
Ar(g)	argon gas
CA	chronoamperometry
C_f	characteristic constant
$C_{f,exp}$	experimental characteristic constant
c_m	molar concentration
CP	chronopotentiometry
CV	cyclic-voltammetry
DLCR	double-layer charging range
E	potential
E_{pmm}	potential of minimum mass
EPR	entire potential range
E_{PtO}	onset potential of platinum surface oxide formation
E_{pzc}	potential of zero charge
EQCM	electrochemical quartz-crystal microbalance
EQCN	electrochemical quartz-crystal nanobalance
F	Faraday constant
f_0	resonant frequency
FV	frequency variation

h	thickness
$H_2(g)$	hydrogen gas
HAR	hydrogen adsorption range
HER	hydrogen evolution reaction
H_{OPD}	over-potential deposited hydrogen
HOR	hydrogen oxidation reaction
H_{UPD}	under-potential deposited hydrogen
I	y-intercepts
j	current density
LOD	limits of detection
LOQ	limits of quantification
ML	monolayer
MV	mass variation
n	number of harmonic
N/A	not available
n_{AN}	number of anion
n_{H2O}	number of water molecule
n_{H3O+}	number of hydronium ion
n_{Ochem}	number of chemisorbed oxygen
O_{ads}	adsorbed oxygen
O_{chem}	chemisorbed oxygen
$O_{chem}^{\delta-}$	chemisorbed oxygen having a partial negative charge
OH_{ads}	adsorbed hydroxyl group
ORR	oxygen reduction reaction
PEMFC	polymer electrolyte membrane fuel cell

PEMWE	polymer electrolyte membrane water electrolyser
PGM	Pt-group metal
Pt(poly)	polycrystalline platinum
$Pt^{\delta+}$	platinum atom having a partial positive charge
q	charge density
QCM	quartz-crystal microbalance
q_{Pt}	effective surface charge of platinum electrode
R	roughness factor
r_{H2O}	radius of water molecule
RHE	reversible hydrogen electrode
r_{Pt}	radius of platinum atom
s	scan rate
S	slope
S/N	signal-to-noise
SHE	standard hydrogen electrode
SOFR	surface oxide formation range
T	temperature
t	time
UHP	ultra-high purity
UPD	under-potential deposition
W	atomic weight
z	number of electron transferred
δE	potential change
Δf	frequency change
Δf_m	frequency change associated with mass change

Δf_p	frequency change associated with pressure change
Δf_r	frequency change associated with surface roughness change
Δf_T	frequency change associated with temperature change
Δf_v	frequency change associated with viscosity change
Δm	mass change
$\delta\Delta M$	magnitude of molar mass change in two potential limit
$\delta\Delta m.$	magnitude of mass change in two potential limit
$\delta\Delta m_{DLCR}$	magnitude of mass change in the double-layer charging range
$\delta\Delta M_{DLCR}$	magnitude of molar mass change in the double-layer charging range
$\delta\Delta m_{EPR}$	magnitude of mass change in the entire potential range
$\delta\Delta M_{EPR}$	magnitude of molar mass change in the entire potential range
$\delta\Delta M_{HAR}$	magnitude of molar mass change in the hydrogen adsorption range
$\delta\Delta m_{HAR},$	magnitude of mass change in the hydrogen adsorption range
$\delta\Delta m_{SOFR}$	magnitude of mass change in the surface oxide formation range
$\delta\Delta M_{SOFR}$	magnitude of molar mass change in the surface oxide formation range
η_L	viscosity of liquid
θ	surface coverage
θ_{AN}	anion coverage
λ	wavelength
μ_q	shear modulus of quartz
v_q	shear velocity of quartz
ρ_L	density of liquid
ρ_q	density of quartz
σ	standard deviation

Chapter 1

Introduction

1.1 General introduction to the electrochemical quartz-crystal nanobalance

The field of interfacial electrochemistry often focuses on heterogeneous chemical reactions, involving the transfer of electrons at the interface between an electrode and a species in the electrolyte. There are two types of electrochemical reactions occurring at the electrode/electrolyte interface: anodic (oxidation) and cathodic (reduction) reactions. In the case of the anodic reaction, a species within the electrolyte or at the electrode is oxidized by the loss of electrons, whereas in the case of the cathodic process, reduction of the species occurs through the gain of electrons. When either of these two reactions takes place at the electrode surface and the reactant and/or the product is stripped from or deposited on the electrode, the mass of the electrode changes. Examples of interfacial electrochemical processes which proceed with mass changes are (i) electro-dissolution of metallic electrodes; (ii) electrodeposition of metals or semiconductors on the electrode surface; (iii) formation of an oxide film on the electrode surface; (iv) electro-polymerization; and so on.[1]

As an *in-situ* nanogravimetry, the electrochemical quartz-crystal nanobalance (EQCN) is a very sensitive technique that is used to measure minute mass changes at an electrode surface during interfacial electrochemical processes. The technique is based on the piezoelectric properties of quartz.[1,2] When a mechanical stress is applied to the surface of quartz-crystal, a proportional electric potential is generated through the crystal. A specific electric field can also

be applied to a quartz-crystal, inducing it to oscillate at a certain frequency, which is called the fundamental resonant frequency. The electric field is applied to the quartz-crystal resonator using two metallic film electrodes (e.g. Pt or Au) that are vapor-deposited on both sides of the resonator. While the resonator oscillates due to the electric field applied between the two electrodes (pads), one electrode (pad) could simultaneously be used as a working electrode on which the electrode processes of interest take place in electrochemical measurements. In 1981, Nomura and Iijima conducted the first EQCM measurements (it was referred to as an electrochemical quartz-crystal microbalance at that time) to measure minute concentrations of Ag^+ in aqueous media.[3] The dissolved Ag^+ was electrodeposited and the resulting EQCM frequency change was converted into a mass change, and subsequently into the concentration of Ag^+. At present, the instrumental measurement resolution is in the nanogram range thanks to improved resonator fabrication and more sensitive electronic signal analysis. Electrochemical quartz-crystal nanobalance measurements in conjunction with classical electrochemical measurements provide changes in mass and changes in electric charge during electrochemical processes taking place at the electrode surface. Through the combination of these two pieces of information, one can obtain new insights into the mechanism of the electrochemical reaction. The mass is a fundamental property of matter and mass changes associated with interfacial electrochemical processes should be examined concurrently with changes in the energy balance. The combination of these three balances together with other information acquired through electrochemical experiments provide new insights into the nature (mechanisms and kinetics) of electrochemical processes.

1.2 The Sauerbrey equation (the frequency-mass correlation)

During electrochemical processes, interfacial mass changes at the working electrode take place through the addition/removal of oxidized/reduced species, disturbing the resonant frequency of the resonator. The EQCN measures the changes in frequency (Δf) of a quartz-crystal resonator upon which the electrode material is coated, and then converts Δf into the changes in mass (Δm) using the Sauerbrey equation.

In 1959, Sauerbrey introduced the quartz-crystal microbalance (QCM) and derived an equation that shows the relationship between frequency changes of the quartz-crystal resonator and corresponding mass changes on the resonator surface.[2] In the derivation, he treated a mass change on the resonator as a thickness change of the resonator (Figure 1.1).

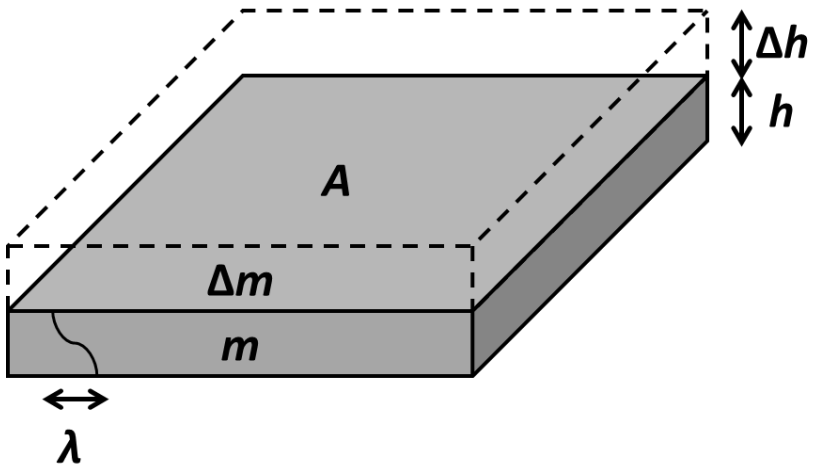

Figure 1.1. Schematic diagram of an oscillating quartz-crystal resonator and an added thin layer on it.

Thus, the increased thickness assumed to be an addition of a flat thin film, which has a uniform distribution over the resonator. This implies that the added foreign material that causes the mass change has the same physical properties as the resonator and perfectly adheres to the substrate resonator. The derivation below follows on the basis of these assumptions.[2,4]

When the quartz-crystal resonator oscillates at a harmonic resonance, the wavelength λ is stated as:

$$\lambda = \frac{2h}{n} \tag{1.1}$$

where h is the thickness of the resonator, $n = 1$ for the first harmonic and $n > 1$ for the higher harmonics. The resonant frequency of the resonator is f_0 at the first harmonic (in the case of the n^{th} harmonic the frequency would be $n \times f_0$), and the shear velocity (v_q) of the resonator is defined as λf_0. Therefore, the shear velocity of the resonator can be presented as:

$$v_q = 2h\ f_0 \tag{1.2}$$

The change in frequency (df_0) which is caused by the infinitesimal thickness change (dh) of the resonator can be expressed by rearranging and differentiating equation 1.2 as follows:

$$df_0 = -\frac{v_q\, dh}{2h^2} \tag{1.3}$$

The shear velocity in equation 1.3 can be isolated and then substituted into equation 1.2, yielding the following:

$$\frac{\mathrm{d}f_0}{f_0} = -\frac{\mathrm{d}h}{h} \tag{1.4}$$

The negative sign indicates that an increase in thickness results in a decrease in resonance frequency. Equation 1.4, which contains infinitesimal changes, can be rewritten with finite changes, and the change in thickness can be presented as the change in mass (Δm), bearing in mind the surface area (A) of the resonator and the density of quartz (ρ_q = 2.648 g cm^{-3}). Introduction of Δm, A, and ρ_q leads to the following expression:

$$\frac{\Delta f}{f_0} = -\frac{\Delta m}{h\,\rho_q\,A} \tag{1.5}$$

Isolation of the thickness of the resonator h from equation 1.2 and its substitution into equation 1.5 yields the following formula:

$$\frac{\Delta f}{f_0} = -\frac{2 f_0\,\Delta m}{\nu_q\,\rho_q\,A} \tag{1.6}$$

The shear velocity of the resonator can be expressed as:

$$\nu_q = \sqrt{\frac{\mu_q}{\rho_q}} \tag{1.7}$$

where μ_q is the shear modulus of quartz (2.947 × 10^{11} g cm^{-1} s^{-2}).

Therefore, substitution of equation 1.7 into equation 1.6 and simple rearrangements provides the Sauerbrey equation:

$$\Delta f = -\frac{2 f_0^{\,2}\, \Delta m}{A\sqrt{\mu_q\, \rho_q}} \tag{1.8}$$

In order to calculate the changes in mass per unit area (cm^{-2}) from the changes in frequency, the following equation is commonly used:

$$\Delta m = -\frac{\Delta f \sqrt{\mu_q\, \rho_q}}{2 f_0^{\,2}} = -C_f\, \Delta f \tag{1.9}$$

where C_f is the characteristic constant containing all of the above properties of the quartz. In the case of a resonator possessing the f_0 value of 9.00 MHz, the calculated value of C_f is 5.45 ng Hz^{-1} cm^{-2}. The value of C_f implies that for $\Delta f = -1.00$ Hz the interfacial mass change (here addition) equals Δm = 5.45 ng cm^{-2}.

Since the resolution of modern electronic instrumentation is in the 0.1–0.01 Hz range, the theoretical (ideal) limit of detection of the EQCN could be down to 54.5 pg cm^{-2}. Such a high detection limit (such a small mass change) would allow measuring mass changes due to deposition/stripping of sub-monolayers of H. However, this 54.5 pg cm^{-2} limit only refers to ideal conditions and does not take into account various sources of interferences, such as external mechanical vibrations, electromagnetic interferences, and natural convection of the electrolyte liquid, which is in contact with the resonator. In the next section, the isolation of the EQCN system from the outer interferences will be discussed, and the experimental determination of the limits of detection and quantification (LOD and LOQ, respectively) will be treated in *Chapter 2*.

1.3 Mechanical and electromagnetic isolation of the EQCN system

Normally, there are many external sources that can generate minute mechanical vibrations in a research laboratory, for example, opening or closing the entrance doors, operating fume hoods, and people talking or simply walking in the laboratory. Such actions are typically not given much thought and are therefore deemed insignificant. However, when it comes to a technique which is very sensitive to an external mechanical disturbance, e.g. the EQCN, they are no longer meaningless. Because the measurement scale of the EQCN is in the nanogram range, the experimental frequency change measurement can be easily affected by mechanical vibrations originating in the surroundings. Also, electromagnetic interference from other instruments, computers, electric motors, or fluorescent lights, just to mention a few, could generate noise during the frequency change measurement. Therefore, it is of great importance to isolate the EQCN system from the external mechanical and electromagnetic disturbances to make proper measurements.

In order to minimize the influence of the external mechanical and electromagnetic disturbances, we use an in-house constructed, vibration-isolated Faraday cage (Figure 1.2). The Faraday cage consists of six walls held together using a metal custom-made frame. Each wall comprises two Plexiglas sheets with copper mesh sandwiched in between. The six copper meshes are electrically connected and the entire Faraday cage is grounded. The front wall is divided into two sliding doors. The entire Faraday cage is suspended by means of flexible rubber bands from an outer frame to reduce and prevent the mechanical disturbance. A thick glass plate, a bag with fine sand, and a stable optical lab jack which holds an oscillator electronic circuit are placed in the Faraday cage to provide a stable base.

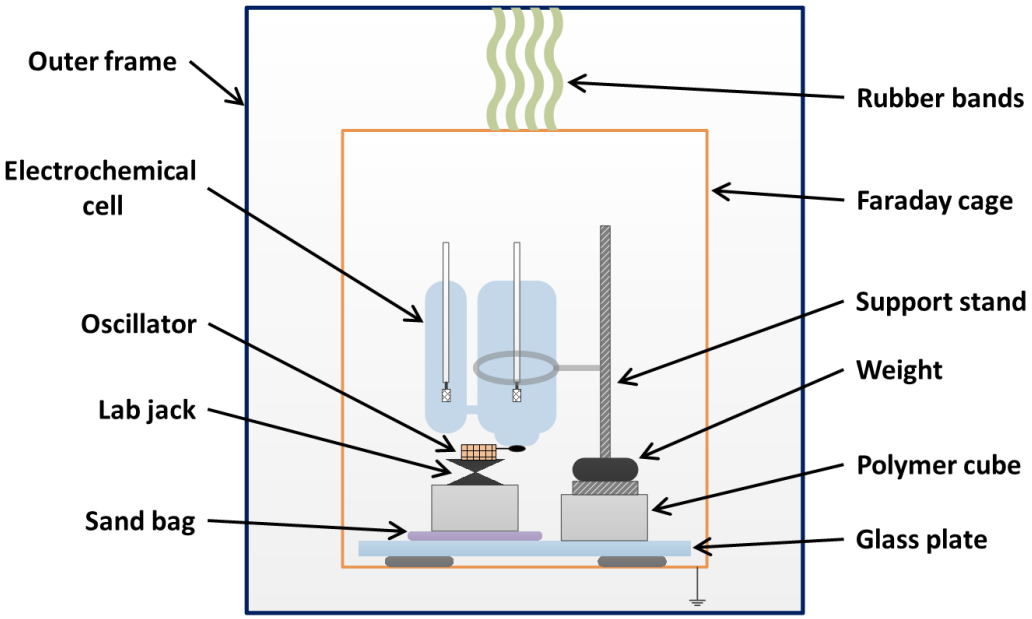

Figure 1.2. A schematic representation of the custom-made vibration-isolated Faraday cage and a two-compartment electrochemical cell within the cage.

In order to improve the stability of the support stand, a heavy weight is attached to its base, and hard polymer cubes are placed beneath the stand and the lab jack as vibration buffers.

Figures 1.3A and 1.3B present frequency variation (FV) transients that were recorded simultaneously with cyclic-voltammetry (CV) measurements for a Pt-coated resonator in 0.50 M aqueous H_2O_4 solution. The FV transient shown in Figure 1.3A was measured outside of the vibration-isolated Faraday cage, while the Figure 1.3B was obtained inside of the cage. They clearly depict the effect of using the vibration-isolated Faraday cage, lowering ca. 60% of the noise level.

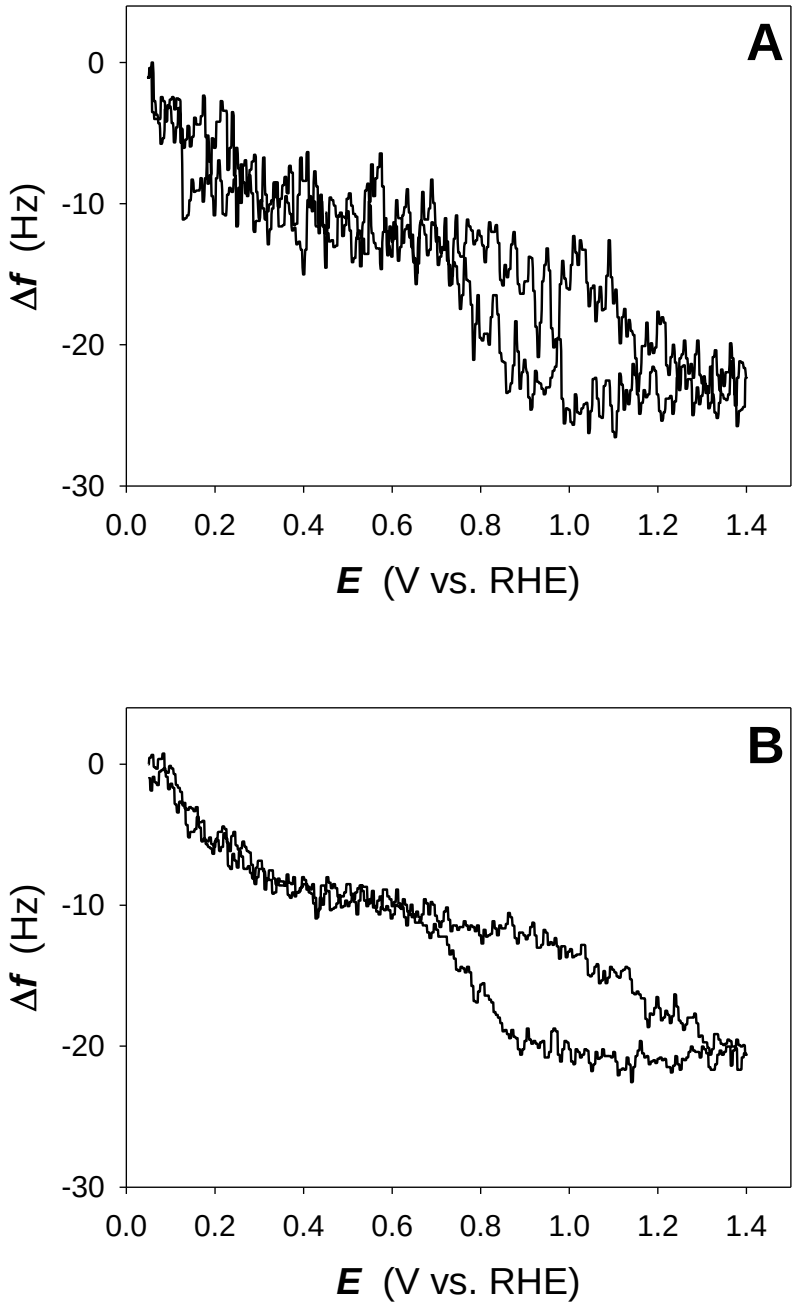

Figure 1.3. Frequency variation transients recorded acquired outside (**A**) and within (**B**) the vibration-isolated Faraday cage. They are obtained simultaneously with the cyclic-voltammetry measurements for a Pt-coated resonator in 0.50 M aqueous H_2SO_4 solution at a scan rate of s = 50.0 mV s^{-1} and T = 298 K.

In order to improve the signal-to-noise (S/N) ratio of the frequency data, in subsequent research, ten consecutively conducted but independent FV transients are acquired and averaged (this will be treated in *Chapter 2*). The resultant averaged FV transient is presented and analyzed.

Therefore, the use of the vibration-isolated Faraday cage is a great benefit to obtaining an interference free frequency signal. In this thesis, all of EQCN experiments were performed within the vibration-isolated Faraday cage to have minimized external disturbance.

1.4 Applications of the EQCN to Platinum Electrochemistry and Electrocatalysis

An ever increasing interest in clean and renewable energy and the emerging hydrogen economy have contributed to the development of a polymer electrolyte membrane fuel cell (PEMFC). The PEMFC is a device that converts chemical energy of fuels, such as hydrogen or low molecular weight alcohols, to electrical energy through electrochemical reactions. The hydrogen PEMFC is the most promising candidate for a power generator and automotive applications for next generations because it does not emit any pollutant and has a high efficiency at a relatively low operating temperature.[5] For the operation of the PEMFC, hydrogen gas and air (oxygen gas) are supplied to the anode and cathode, respectively, then the hydrogen oxidation reaction (HOR) and the oxygen reduction reaction (ORR) take place at each electrode, generating electricity. Platinum shows outstanding electrocatalytic activity towards the HOR and the ORR taking place in the PEMFCs.[6–10] However, Pt is not stable and undergoes electro-oxidation and (electro-)dissolution phenomena, which gradually reduce the mass of the precious electrocatalysts and the electrochemically active surface area at which the HOR and ORR take place. Therefore, understanding the electrocatalytic behavior of Pt-based materials, and especially their durability and stability, is of great importance to the PEMFC science and technology.

Platinum can electrochemically adsorb hydrogen at higher potentials (E) than the standard reduction potential of the H^+/H_2 redox couple, which is 0.00 V versus SHE (the standard hydrogen electrode). This process is referred to as the under-potential deposition of hydrogen (UPD H). A monolayer (ML) of under-potential deposited hydrogen (H_{UPD}) is electro-adsorbed on platinum prior to the onset of the electrolytic $H_2(g)$ generation. The $H_2(g)$ generation referred to as the hydrogen evolution reaction (HER) involves the over-potential deposition of H, and the species is referred to as the over-potential deposited H (H_{OPD}). The UPD H and OPD H are represented by the following half-cell reactions.[9]

$$Pt + H_3O^+ + e^- \rightarrow Pt\text{–}H_{UPD} + H_2O \quad (E > 0 \text{ versus SHE}) \tag{1.10}$$

$$Pt + H_3O^+ + e^- \rightarrow Pt\text{–}H_{OPD} + H_2O \quad (E < 0 \text{ versus SHE}) \tag{1.11}$$

There was a lack of agreement within the literature with regards to the mechanism of the formation of Pt surface oxide and the sequence of elementary steps that the process involved. In 1972, Vetter and Schultze proposed that platinum surface oxide formation involves the following two steps:

$$\text{Step 1: } Pt + H_2O \rightarrow Pt\text{–}O_{ads} + 2H^+ + 2e^- \tag{1.12}$$

$$\text{Step 2: } Pt\text{–}O_{ads} \rightarrow O^{2-}\text{–}Pt^{2+} \tag{1.13}$$

where equation 1.12 refers the oxidation of H_2O starting at E = 0.85 V versus SHE, and equation 1.13 shows the interfacial place exchange that takes place when the surface coverage (θ) of adsorbed oxygen (O_{ads}) is $\theta_O \geq 1.0$.[11,12] On the other hand, in 1973, Conway et al. proposed the following steps:

$$\text{Step 1: } Pt + H_2O \rightarrow Pt\text{–}OH_{ads} + H^+ + e^- \quad (1.14)$$

$$\text{Step 2: } Pt\text{–}OH_{ads} \rightarrow OH_{ads}\text{–}Pt \quad (1.15)$$

$$\text{Step 3: } OH_{ads}\text{–}Pt \rightarrow O\text{–}Pt + H^+ + e^- \quad (1.16)$$

where equation 1.14 refers to the oxidation of H_2O starting at E = 0.85 V versus SHE through the adsorption of a hydroxyl group (OH_{ads}) on Pt; equation 1.15 refers to the interfacial place exchange; and equation 1.16 shows subsequent oxidation of OH_{ads} by the departure of a H^+. According to Conway et al., the interfacial place exchange commences as soon as OH_{ads} is formed.[13,14] The mechanistic models proposed by these two groups were based entirely on electrochemical data and their subsequent interpretation.

With the ability to monitor interfacial mass changes of the electrode/electrolyte interface throughout the electrochemical reaction, we could shed new light on the mechanism of electrochemical reactions taking place on Pt, such as Pt surface electro-oxidation. In 2004, Jerkiewicz et al. reexamined the mechanism of Pt surface oxide formation through a combination of CV, EQCN, and Auger electron spectroscopy (AES) measurements.[15] According to the mass variation data, the mass added during the surface oxide formation points to the formation of Pt–O_{ads} instead of Pt–OH_{ads}. This new finding implies that the Pt oxide formation mechanism is a two-step reaction rather than the three-step process proposed by Conway. Through the analysis of their AES data (the sensitivity of the Auger signal to the electron beam exposure), Jerkiewicz et al. also demonstrated that the interfacial place exchange commences when the O surface coverage is ca. 0.5. In 2011, using the EQCN Jerkiewicz et al. discovered the potential of minimum mass (E_{pmm}) for Pt electrodes.[16] In this paper, the EQCN was used to monitor interfacial mass changes at the starting point of the hydrogen evolution reaction (HER). At the E_{pmm}, the mass at the Pt electrode surface, as measured by EQCN, has the lowest value. The electrochemically adsorbed H reaches a monolayer coverage on the surface of Pt electrode, and

the interactions between the Pt surface and the electrolyte components are the weakest. Consequently, H_3O^+ can be easily discharged to form H_{OPD} (it is an intermediate of the HER) and H_2(g) generation commences. These two papers showed that the EQCN is a very powerful technique that can be used to monitor *in-situ* minute mass changes while an interfacial electrochemical reaction occurs.

The EQCN is a very powerful and relatively inexpensive technique but its applicability in interfacial electrochemistry and electrocatalysis research requires knowledge of its limits of detection and quantification. *Chapter 2* addresses this issue by proposing an experimental approach to their determination and their evaluation for the experimental setup used in this research. Applications of the EQCN to Pt electrochemistry and electrocatalysis offers significant research opportunities through measuring interfacial mass changes accompanied interfacial electrochemical processes. In addition, it offers a unique opportunity through the application of this technique in research on other electrode materials and interfacial phenomena. The applicability of the EQCN in research on the interfacial behavior of Pt materials is of great importance to the PEMFC and PEM water electrolyser (PEMWE) technologies because both employ Pt materials as electrocatalysts. In reality, however, the Pt-based electrocatalysts used in PEMFCs and PEMWEs have very small sizes, typically of the meso- or nano-size, because of their extremely high cost. The application of such meso- and nano-structured materials offers an increase in catalytic activity. However, meso- and nano-sized materials are significantly more reactive towards undesired reactions, such as electro-oxidation and (electro-)dissolution through which they degrade. As mentioned in *Section 1.2*, the Sauerbrey equation, which is employed to convert the changes in frequency to the changes in mass, is based on the assumption that the surface of the electrode is completely flat, which is not the case. Therefore, it is important to understand the influence of the surface roughness on the mass response of EQCN during

electrochemical measurements prior to applying this technique in research on meso- and nano-structured materials. This topic will be treated in *Chapter 3* and *Chapter 4* as of this thesis.

1.5 References

(1) Hepel, M. In *Interfacial Electrochemistry: Theory, Experiment, and Applications;* Wieckowski, A., Ed.; Marcel Dekker: New York, 1999; Chapter 34.

(2) Sauerbrey, G. *Z. Phys.* **1959,** *155*, 206–222.

(3) Nomura, T.; Iijima, M. *Anal. Chim. Acta* **1981,** *131*, 97–102.

(4) Janata, J. *Principles of Chemical Sensors*, 2nd ed.; Springer: New York, 2009; Chapter 4.

(5) Wang, Y.; Chen, K. S.; Mishler, J.; Cho, S. C.; Adroher, X. C. *Appl. Energy* **2011,** *88*, 981–1007.

(6) Trasatti, S. *J. Electroanal. Chem.* **1972,** *39*, 163–184.

(7) Jerkiewicz, G. *Prog. Surf. Sci.* **1998,** *57*, 137–186.

(8) Conway, B. E.; Jerkiewicz, G. *Electrochim. Acta* **2000,** *45*, 4075–4083.

(9) Jerkiewicz, G. *Electrocatalysis* **2010,** *1*, 179–199.

(10) Stephens, I. E. L.; Bondarenko, A. S.; Gronbjerg. U.; Rossmeisl, J.; Chorkendorff, I. *Energy Environ. Sci.* **2012,** *5*, 6744–6762.

(11) Vetter, K. J.; Schultze, J. W. *J. Electroanal. Chem.* **1972**, *34*, 131–139.

(12) Vetter, K. J.; Schultze, J. W. *J. Electroanal. Chem.* **1972**, *34*, 141–158.

(13) Angerstein-Kozlowska, H.; Conway, B. E.; Sharp, W. B. A. *J. Electroanal. Chem.* **1973**, *43*, 9–36.

(14) Conway, B. E. *Prog. Surf. Sci.* **1995**, *49*, 331–452.

(15) Jerkiewicz, G.; Vatankhah, G.; Lessard, J.; Soriaga, M. P.; Park, Y. *Electrochim. Acta* **2004**, *49*, 1451–1459.

(16) Jerkiewicz, G.; Vatankhah, G.; Tanaka, S.; Lessard, J. *Langmuir* **2011**, *27*, 4220–4226.

Chapter 2

Limits of Detection and Quantification of Electrochemical Quartz-Crystal Nanobalance in Platinum Electrochemistry and Electrocatalysis Research

2.1 Introduction

There is a lot of interest in the study of electrocatalytic processes occurring on Pt-group metals (PGMs) due to their application in developing clean and sustainable electrochemical energy systems, such as fuel cells. Electrocatalysis studies shed light on the mechanisms and kinetics of electrochemical reactions in terms of their energy efficiency while providing important information about the stability and durability of electrocatalysts. The electrochemical quartz-crystal microbalance (EQCM) was first employed by Nomura and Iijima to measure *in-situ* small amounts of Ag ion present in aqueous media.[1] Later, it was employed as a reliable technique to study on the nanogram scale *in-situ* interfacial mass changes associated with electrochemical processes taking place at Pt electrodes, thus as the electrochemical quartz-crystal nanobalance (EQCN).[2,3] Conventional electrochemical techniques, such as cyclic-voltammetry (CV), chronopotentiometry, and chronoamperometry, allow one to determine the value of electric charge transferred during electrochemical reactions, while *in-situ* nanogravimetry measurements (i.e. EQCN) can measure the interfacial mass changes during these processes. Through the combination of these two techniques, one can determine *in-situ* the molecular mass of the species residing at or removed from the electrode surfaces.

The EQCN measures changes in frequency (Δf) of a quartz-crystal resonator onto which the working electrode material (e.g. Pt or Au) is coated. When an electrochemical reaction takes place at the working electrode, the resonator undergoes shear deformation and its resonance is disturbed by an addition or a removal of mass to/from the electrode surface. One can convert this resonant frequency change (Δf) to the mass change (Δm) at the electrode surface using the Sauerbrey equation:

$$\Delta m = -\left(\frac{\sqrt{\mu_q \rho_q}}{2 f_0^2}\right)\Delta f = -C_f \Delta f \qquad (2.1)$$

where f_0 is the resonant frequency of the quartz-crystal resonator prior to the addition or removal of mass, $\mu_q = 2.947 \times 10^{11}$ g cm^{-1} s^{-2} is the shear modulus of quartz, $\rho_q = 2.648$ g cm^{-3} is the density of quartz, and C_f is the characteristic constant containing all of the above properties of the quartz crystal.[4] In the case of a resonator possessing the f_0 value of 9.00 MHz, the calculated value of C_f is 5.45 ng Hz^{-1} cm^{-2}; the unit surface area refers to the geometric area of the working electrode. The value of C_f implies that for $\Delta f = -1.00$ Hz the interfacial mass change equals Δm = 5.45 ng cm^{-2}.

The EQCN has found various applications as an electroanalytical technique.[5] In general, when employing an analytical technique with the objective of measuring small quantities of analytes, it is necessary to know the technique's limit of detection (LOD) and limit of quantification (LOQ). For over three decades, the EQCN has played an important role in electrochemical research but the determination of its LOD and LOQ has received practically no attention. Although the manuals of various instruments list a frequency measurement resolution in the 0.01–0.1 Hz range (in our case 0.1 Hz), they refer to ideal conditions and do not take into account various sources of noise, such as electromagnetic interference and mechanical vibration.

Consequently, the LOD and LOQ are defined as a multiple of an arbitrary measurement resolution. In addition, the unique nature of the electrochemical setup/measurement (the Pt-coated resonator with an intermediate layer, the electrolyte undergoing natural convective movement, changes in the electrolyte density and viscosity in the interfacial region, etc.) also contribute to the frequency noise level.

In the field of sensors based on QCM (not on EQCM or EQCN), there exist several experimental methods for determining the values of LOD and LOQ for specific chemical species.[6–9] They employ blanks and calibration curves with known quantities of the species to be quantified, which are subsequently used to determine the values of LOD and LOQ of the QCM. However, in interfacial EQCN experiments, it is practically impossible to perform measurements using a blank solution (e.g. pure water) due to its high resistance. In addition, it is difficult to have a pre-determined calibration curve because the increase in the electrolyte concentration does not translate into an increase of the electrochemical signal. Perfect examples of electrochemical surface processes occurring at Pt electrodes that give rise to very similar electrochemical responses are the under-potential deposition of H (UPD H), and the formation and reduction of surface oxide.[3,10] In this case, an increase in electrolyte concentration does not increase the CV features but only slightly modifies them due to the anion electrostatic interactions with the Pt surface. However, the total charge density values associated with these processes remain practically the same.

In general, the LOD and LOQ are described as three times and ten times the standard deviation (σ) of the instrument signal from blanks, respectively.[11,12] Three times σ is greater than ca. 99% of the normally distributed signals obtained from blanks, but it is still not precise enough for quantitative measurements. The distributed signals of quantification should be above the signals of detection, thus ten times σ has been defined as the LOQ. As explained above, this approach cannot be applied to EQCN analysis of interfacial electrochemical processes and,

consequently, a different method is required. In this study, we propose a convenient method for determining the LOD and LOQ for the EQCN with Pt electrodes, which employs concurrent frequency change and CV measurements in aqueous H_2SO_4 solutions having four different molar concentrations (c_m). The results demonstrate that the LOD and LOQ values depend on the electrolyte concentration. Then, we discuss the applicability of the EQCN in research on electrochemical H adsorption, Pt electro-oxidation, as well as chemical and electrochemical Pt dissolution.

2.2 Experimental

Cyclic-voltammetry and corresponding frequency variation (FV) measurements were conducted using an EQCN setup that consisted of a Bio-Logic model SP-150 potentiostat and a Seiko-EG&G model QCA 922 quartz crystal analyzer, which has an instrumental measurement resolution of 0.1 Hz and a sampling time of 0.1 s. Electrochemical experiments were performed using a custom-made Pyrex two-compartment electrochemical cell. A Pt-coated quartz-crystal resonator (Seiko-EG&G, QA-A9M-PT) having a resonant frequency of ca. 9.00 MHz (the exact value was determined prior to each experiment) was placed in a Teflon holder. It was attached to the bottom of the cell and thus had a horizontal configuration.[2] One of the Pt-coated sides of the quartz-crystal resonator was in contact with the electrolyte and served as the working electrode; its geometric surface area was 0.196 cm^2 and its roughness factor was $R = 1.60$, where $R = A_{ecsa}/A_{geom}$, A_{ecsa} is the electrochemically active surface area and A_{geom} is the geometric surface area and thus a two-dimensional projection of the real surface.[13,14] A Pt gauze (Alfa Aesar, 99.9%) spot-welded to a Pt wire (Alfa Aesar, 99.95%) was used as a counter electrode and its surface area was at least ten times larger than that of the working electrode. A reversible

hydrogen electrode (RHE) which consisted of Pt wire (Alfa Aesar, 99.95%) covered with a thin layer of electrodeposited Pt black was used as the reference electrode. All potentials quoted in this contribution refer to the RHE scale. All glassware employed in the course of research was cleaned according to well-established procedures.[15] Four aqueous H_2SO_4 solutions of different molar concentrations, namely 0.010, 0.10, 0.50, and 1.0 M, were prepared using concentrated H_2SO_4 (Fluka Analytical, TraceSELECT ≥ 95%) and ultra-high purity (UHP) water (Millipore, 18.2 MΩ cm). Ultra-high purity Ar(g) (Praxair, 5.0 grade) was purged through the electrolyte for 60 minutes prior to each electrochemical measurement in order to expel any oxygen or other reactive gasses from the system.

Prior to an electrochemical experiment, the Pt working electrode was preconditioned through repetitive potential cycling in the $0.05 \leq E \leq 1.50$ V potential range (at least 1000 times) at a potential scan rate of $s = 50.0$ mV s^{-1} in degassed aqueous H_2SO_4 solution (of a given concentration) to obtain a CV profile characteristic of a clean system (both clean electrode and clean electrolyte). All experiments were performed in a home-built Faraday cage, which was suspended by means of flexible rubber bands from an outer frame. All experiments were conducted at room temperature ($T = 298 \pm 1$ K). In order to improve the S/N ratio of the frequency changes, ten independent but consecutively conducted FV transients were recorded and their average was computed.[2] In this contribution, both the individual and averaged FV transients are presented and discussed. The CV and FV transients that were used to determine the LOD and LOQ values were acquired simultaneously in the $0.05 \leq E \leq 1.40$ V potential range at a potential scan rate of $s = 50.0$ mV s^{-1} in the four H_2SO_4 solutions having different concentrations.

2.3 Results and discussion

Figure 2.1A presents a single CV profile (the black transient) and a single FV transient (the blue transient) obtained simultaneously for the Pt(poly) electrode coated on the quartz-crystal resonator in the c_m = 0.50 M aqueous H_2SO_4 at a scan rate of s = 50.0 mV s^{-1}. The CV profile and FV transient reveal features associated with the adsorption (E = 0.40–0.05 V) and desorption (E = 0.05–0.40 V) of under-potentially deposited H (H_{UPD}), the double-layer charging, and the surface oxide formation (E = 0.85–1.40 V) and reduction (E = 1.10–0.60 V).[10] Figure 2.1B shows the averaged CV profile and FV transient that are based on 10 independent but consecutive measurements. The ten CV profiles show a great level of reproducibility and extremely low noise level; the charge values associated with the H_{UPD} agree to within 0.05% of the σ of their averaged value. The FV transient shown in Figure 2.1A, which is representative of the other measurements, demonstrates a significant noise level. On the other hand, the averaged FV transient shown in Figure 2.1B reveals a considerably lower noise level as expected.[2] Conversion of these FV transients to mass variation (MV) transients through the Sauerbrey equation (equation 2.1) yields mass changes (Δm) that have the same noise level as the FV transients just multiplied by a constant.[2,16] Because we directly measure frequency changes, and not mass changes, in this contribution, we focus on the determination of the LOD and LOQ values of the frequency measurements. Then, we convert these LOD and LOQ values for *the frequency change* to the corresponding LOD and LOQ values for *the mass change* and analyze their magnitude in the context of the mass changes associated with interfacial electrochemical processes taking place at Pt electrodes.

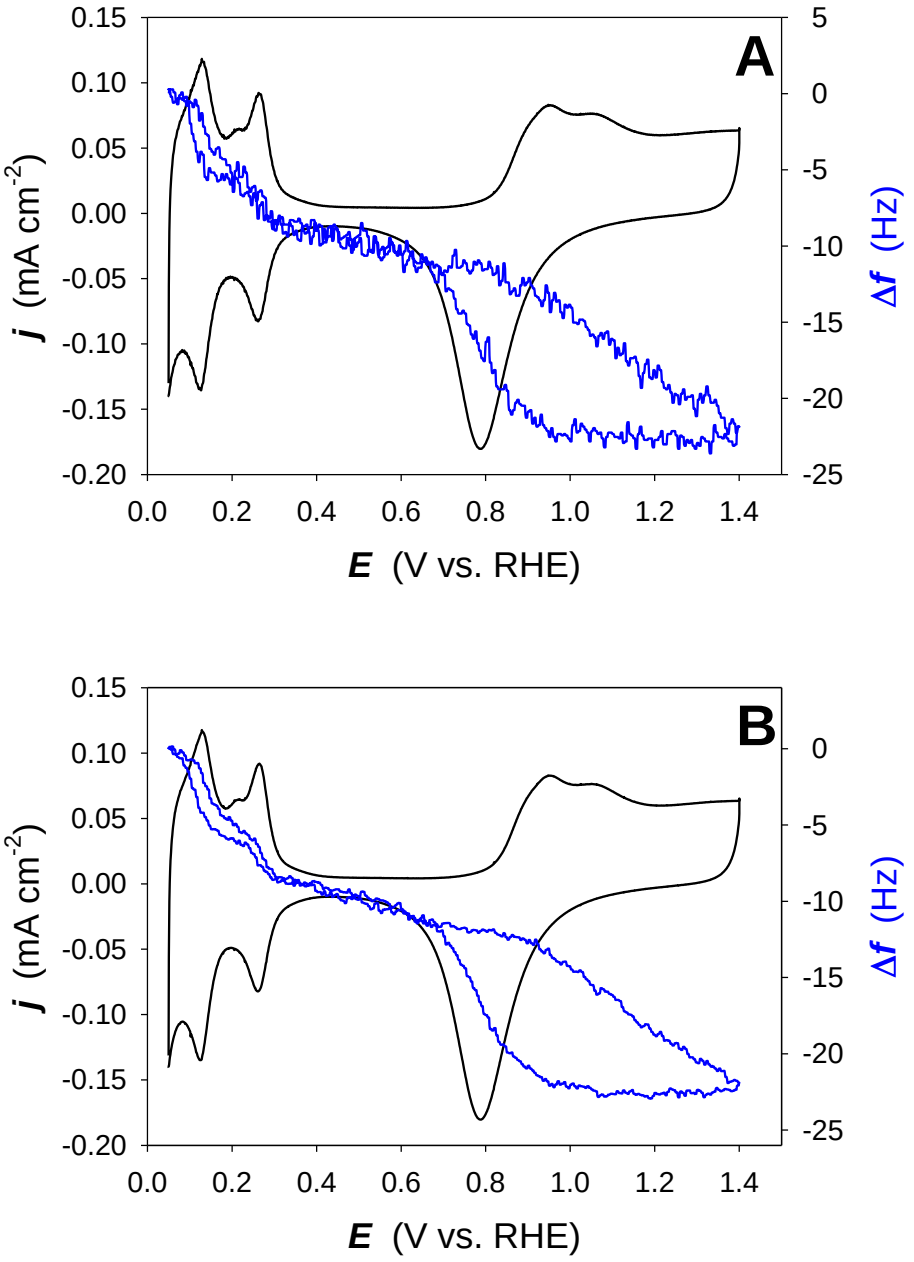

Figure 2.1. Cyclic-voltammetry profiles (black transients) and corresponding frequency variation transients (blue transients) for Pt electrodes in 0.5 M aqueous H_2SO_4 solution at a scan rate of s = 50.0 mV s^{-1}. (**A**) Single CV and FV transients and (**B**) averaged CV and FV transients prepared on the basis of ten CV and FV measurements.

The CV profiles in Figures 2.1A and 2.1B show no faradaic or pseudo-capacitive current in the anodic component of the double-layer charging region (E = 0.40–0.75 V). However, there is a moderate linear increase in Δf, which is attributed to physisorptive interactions of electrolyte components with the Pt(poly) electrode surface.[16–18] The physisorptive interactions of electrolyte components with the electrode are always present and cannot be eliminated; they give rise to responses in both CV profiles and FV transients. Thus, these phenomena cannot be decoupled from the CV and FV features associated with the electrochemical adsorption and desorption of H_{UPD} or the formation and reduction of Pt oxide. The linear double-layer charging region of the Δf versus E transients can serve as a baseline (it is equivalent to a method blank) in the statistical analysis of frequency changes, the objective of which is to determine the values of LOD and LOQ.[11,12] Because the cathodic CV and FV transients do not reveal an extended region due to the double-layer charging, only the anodic profiles are employed in the determination of the LOD and LOQ values.

Figures 2.2A and 2.2B present the single and averaged frequency transients of the anodic double-layer charging region (E = 0.40–0.75 V) prepared using the FV transients shown in Figures 2.1A and 2.1B, respectively (here, they are presented as a series of points without being connected). These frequency transients have a slanted linear trend with background noise. The experimental points were fitted using a linear regression that is shown as a black solid line. Figures 2.2C and 2.2D present residual plots (plots corrected for the respective slopes) based on the graphs shown in Figures 2.2A and 2.2B. The values of σ for the residuals are equal to 0.44 Hz and 0.16 Hz, respectively. Although Figures 2.2A through 2.2D refer to the experimental results obtained in the 0.50 M aqueous H_2SO_4 solution, the same approach was used to determine the values of σ for the 0.010, 0.10, and 1.0 M solutions.

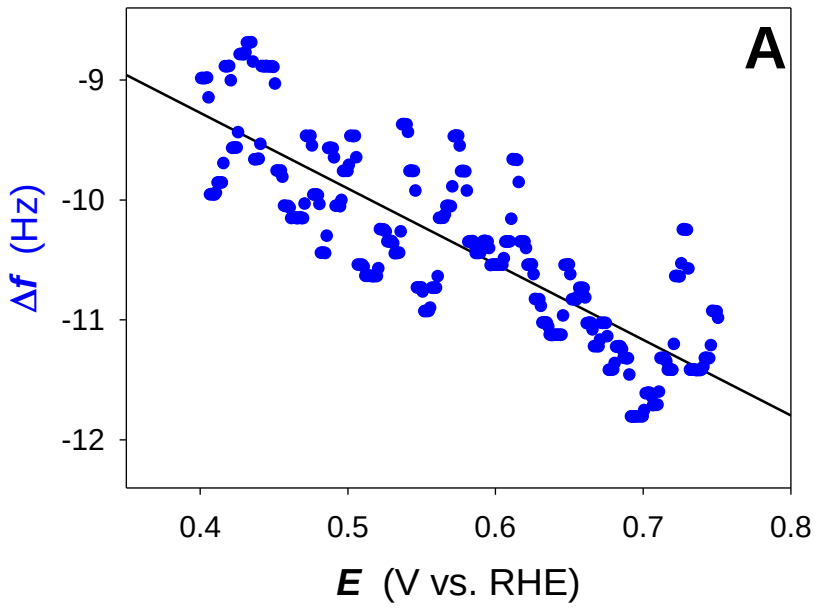
A
-9
-10
-11
-12
Δf (Hz)
0.4
0.5
0.6
0.7
0.8
E (V vs. RHE)

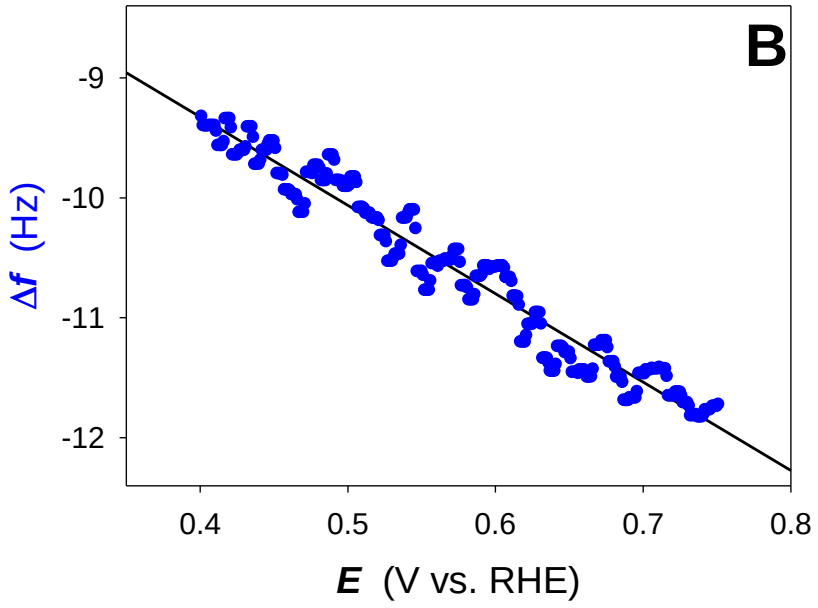
B
-9
-10
-11
-12
Δf (Hz)
0.4
0.5
0.6
0.7
0.8
E (V vs. RHE)

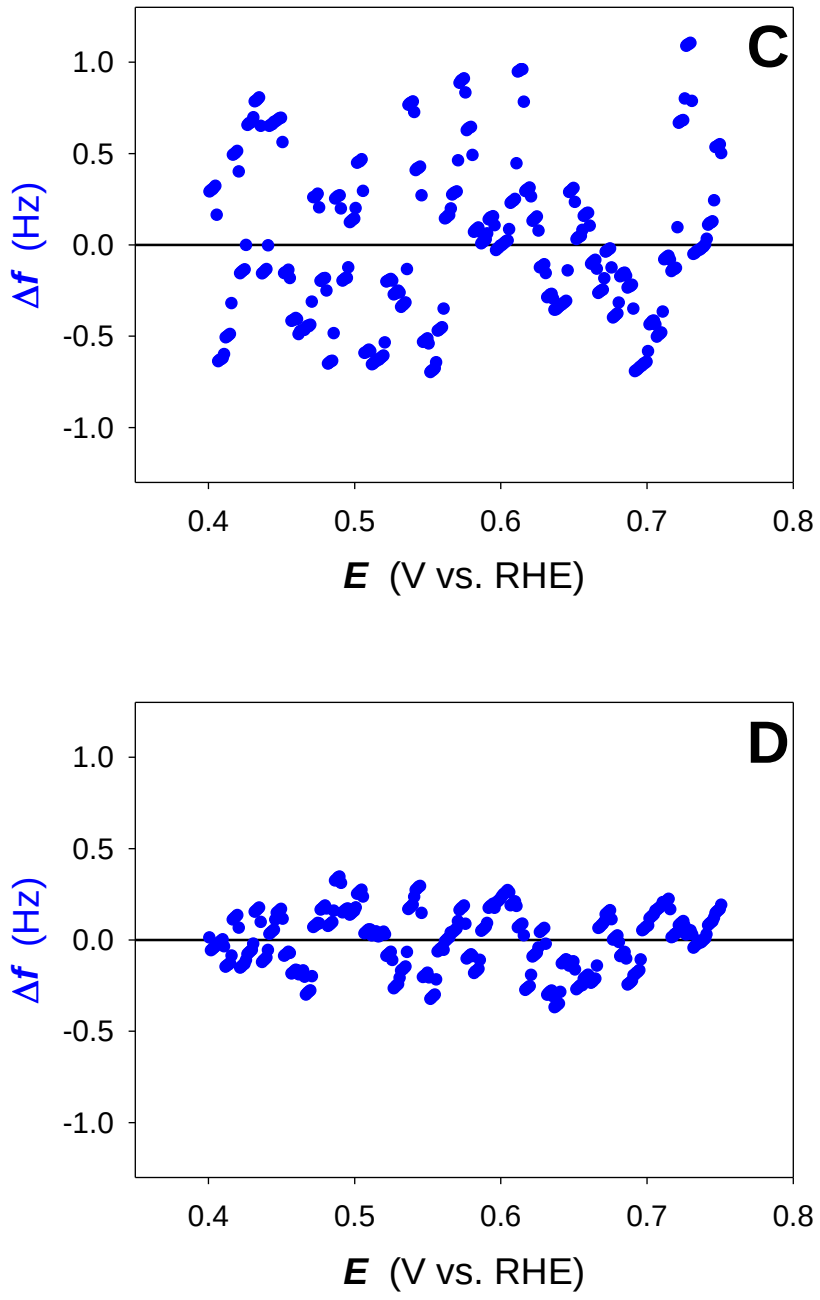

Figure 2.2. Single (**A**) and averaged (**B**) frequency variation transients of the anodic double-layer charging region (E = 0.40–0.75 V) presented as a series of points with the linear regressions shown as black solid lines. Residual plots (corrected for the respective slopes) for the single (**C**) and averaged (**D**) frequency variation transients.

The slope of the linear Δf versus E plots is the same in the four electrolytes. This behavior is expected because the surface coverage of the specifically adsorbed anions, which contribute to the interfacial mass change in the double-layer region, reaches its saturation values already in the case of the 0.010 M aqueous H_2SO_4 solution. However, in the case of lower concentrations the slope of the Δf versus E plots could possibly be concentration-dependent. However, CV and FV transients in very diluted electrolyte solutions would suffer from substantial solution resistance and, consequently, distorted CV and FV transients.

Figure 2.3 presents the calculated σ values of the residuals of the averaged frequency transients as a function of the H_2SO_4 solution concentration (σ versus c_m plot). The results demonstrate that the value of σ increases as c_m is raised.

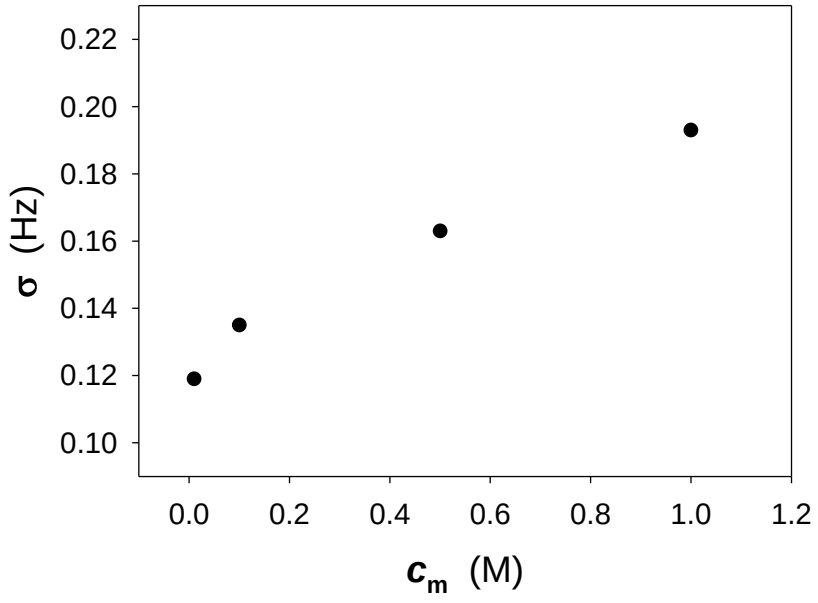

Figure 2.3. Plot of standard deviation (σ) values as a function of the concentration of aqueous H_2SO_4 solution (c_m).

The increase is substantial because an increase in the electrolyte solution concentration from 0.010 M to 1.0 M enhances the value of σ by ca. 62%. In an attempt to understand the phenomena responsible for this increase in the value of σ, we examined the changes in the FV transients associated with the adsorption of H_{UPD}, anodic double layer charging, and Pt oxide formation. Figures 2.4A and 2.4B present averaged CV profiles and FV transients for the Pt(poly) electrode recorded at T = 298 K and s = 50.0 mV s^{-1} in the four electrolyte solutions, respectively. The results demonstrate that when the Pt(poly) electrode is scanned between the 0.05 V and 1.40 V limits, the magnitude of Δf increases by ca. 21% as the c_m rises from 0.010 M to 1.0 M. This behavior is expected and is related to the anion interactions (specific adsorption) with the Pt(poly) electrode. Elsewhere, it was explained that the minimum attainable frequency noise level increases with the resonant frequency (f_0) and a square root of the $\rho_L\eta_L$ product, where ρ_L and η_L are the density and viscosity of the liquid medium, respectively.[19] In the case of f_0 = 9.00 MHz and the four concentrations of aqueous H_2SO_4 solutions at T = 298 K (ρ_L = 0.9976 g cm^{-3} and η_L = 0.902 cP for 0.010 M; ρ_L = 1.004 g cm^{-3} and η_L = 0.921 cP for 0.10 M; ρ_L = 1.028 g cm^{-3} and η_L = 1.00 cP for 0.50 M; ρ_L = 1.059 g cm^{-3} and η_L = 1.10 cP for 1.0 M), the respective calculated value of the oscillatory detection limit is 3×10^{-4} Hz.[19,20] The calculated value of the minimum attainable frequency noise is very small (below 1 mHz in all cases, which is lower than the instrumental measurement resolution as defined in the manual) and refers to ideal conditions. However, even if its value were to increase ten-fold under real conditions, it would still be much smaller than the σ values reported in Figure 2.3. Consequently, the increase in the value of σ with c_m may not be attributed to the changes in the density and viscosity of the electrolyte solutions and an alternative explanation is required.

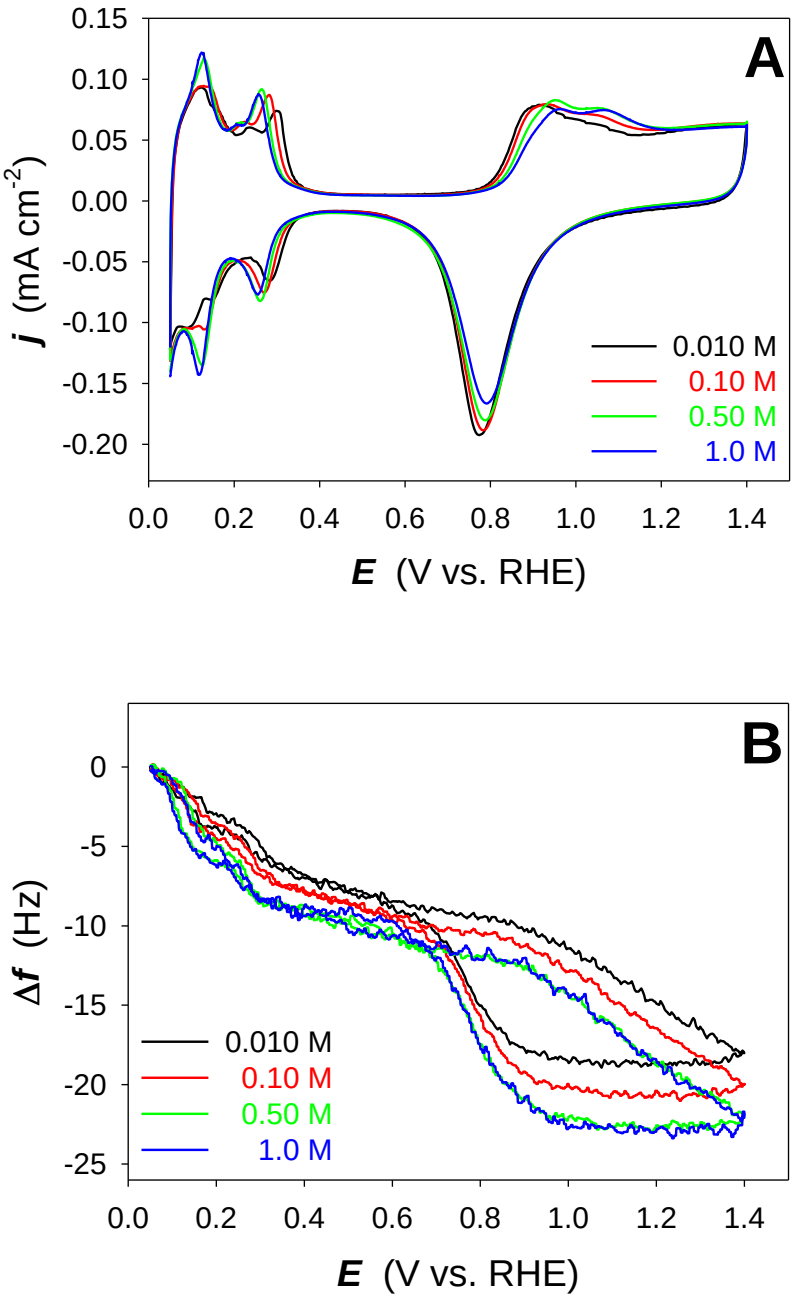

Figure 2.4. Averaged CV profiles (**A**) and their corresponding averaged FV transients (**B**) for a Pt(poly) electrode in aqueous H_2SO_4 solutions having four different concentrations acquired at a scan rate of s = 50.0 mV s^{-1} and T = 298 K.

Recent molecular dynamics simulations of hydrated electrode interfaces comprising water molecules and hydrated ions point to the existence of structural inhomogeneities. It is reported that the water layer parallel to the electrode surface is slowly evolving, thereby influencing the dynamics of the electrolyte solution adjacent to it. Consequently, densities and mobilities of water molecules and hydrated ions are spatially heterogeneous on the nanosecond timescale.[21] Although these calculations do not discuss any changes in the electrolyte viscosity, it is assumed that it evolves as well. On the basis of these simulations, we propose that the evolving electric double layer is responsible for the gradual increase in the value of σ as the c_m of H_2SO_4 rises. It is reasonable to expect that the magnitude of σ would also depend on the nature of the cation and anion (their size and charge), as well as on the electrolyte temperature, which modifies the electrolyte density and viscosity. These observations call for additional research on experimental parameters and variables, and their effect on the magnitude of σ.

Table 2.1 presents the σ values in Hz (for 350 residuals) for the four concentrations of H_2SO_4 and the calculated LOD and LOQ values also in Hz, bearing in mind that LOD = 3 σ and LOQ = 10 σ. They are converted to ng cm^{-2} using the Sauerbrey equation and the value of C_f = 5.45 ng Hz^{-1} cm^{-2} (equation 2.1). In the case of 0.50 M aqueous H_2SO_4, which is one of the most commonly used electrolytes, the values of LOD and LOQ are 3 ng cm^{-2} and 9 ng cm^{-2}, respectively. Because the interfacial mass changes associated with the adsorption of H_{UPD}, double layer charging, and oxide formation are ca. 38 ng cm^{-2}, 19 ng cm^{-2}, and 57 ng cm^{-2} in Figure 1B, respectively, the EQCN is a suitable technique to study these phenomena and can provide an important new insight (here the interfacial mass changes) that other experimental approaches are unable to provide.

Table 2.1. The values of σ (for 350 residuals), LOD, and LOQ in Hz and ng cm^{-2} of the EQCN for Pt(poly) electrodes in aqueous H_2SO_4 solutions of four different concentrations.

		c_m of H_2SO_4 (M)			
		0.010	0.10	0.50	1.0
σ	Hz	0.12	0.14	0.16	0.19
	ng cm^{-2}	0.65	0.74	0.89	1.1
LOD	Hz	0.4	0.4	0.5	0.6
	ng cm^{-2}	2	2	3	3
LOQ	Hz	1	1	2	2
	ng cm^{-2}	6	7	9	10

Platinum dissolution in aqueous acidic solutions is an important and timely topic, and can follow different pathways involving either metallic Pt or its oxides (PtO or PtO_2). Thus, research on Pt electro-oxidation and dissolution attracts considerable attention.[3,22–28] The process is examined using both experimental and theoretical approaches, and the results are discussed with the objective of identifying the parameters that impact (enhance) the process the most. The amount of Pt oxide formed is typically expressed in monolayers (ML) of O and can be converted to a mass in ng cm^{-2}. The amount of dissolved Pt is also expressed as a number of ML. Such quantified amounts of formed oxide and dissolved Pt refer either to a single potential transient or to a series of repetitive potential transients. The value of LOD of the EQCN setup employed in this research is 3 ng cm^{-2} (in 0.50 M H_2SO_4 solution) and corresponds to 8×10^{-2} ML of added or removed O atoms, and 6×10^{-3} ML of added or removed Pt surface atoms. Elsewhere, it was reported that, in the case of potential cycling between 0.70 V and 1.20 V, the average amount of dissolved Pt per single transient is 9.82×10^{-4} ML of Pt atoms, which corresponds to 0.417 ng cm^{-2}.[28] Because this value is about six times smaller than the LOD value, the EQCN is not

capable of measuring and quantifying the dissolved Pt per single potential transient. The LOD and LOQ values reported in this contribution represent an instrumental limitation of typical commercial EQCN instrumentation. Substantial improvements in the EQCN instrumentation would be required in order to improve the LOD and LOQ values so that the technique would be sensitive enough to study metal and metal oxide dissolution of the order of a few percent of ML. Although there might exist some fluctuations in the amount of dissolved Pt per single potential transients, it is unlikely that the amount would increase by a factor of six making it detectable. However, single CV transients are frequently employed to study under-potential deposition of metallic species that typically form one or two monolayers. Because the interfacial mass changes associated with this process are orders of magnitude larger, EQCN is a suitable experimental method that can be employed to study it and can provide new and important insight. The observation that the amount of dissolved Pt per single potential transients is smaller than the LOD value is a very important because the development of catalysts for polymer electrolyte membrane fuel cells (PEMFC) relies on a broad range of experimental techniques that evaluate their catalytic properties as well as their stability and durability. Evaluation of the stability of PEMFC catalysts requires reproducible and reliable experimental data because inaccurate results might lead to erroneous observations and incorrect conclusions.

2.4 Conclusions

We developed a methodology for determining the values of LOD and LOQ of EQCN measurements for Pt electrodes in aqueous H_2SO_4. The approach is based on concurrent and repetitive cyclic-voltammetry and frequency variation experiments. The values of the LOD and LOQ are in the 2–3 ng cm^{-2} and 6–10 ng cm^{-2} ranges, respectively, and depend on the electrolyte

concentration. The behavior is explained in terms of structural inhomogeneities of the electrolyte in the interfacial region adjacent to the Pt electrode surface. These inhomogeneities increase the values of the electrolyte density and viscosity as the concentration is raised. The values of LOD and LOQ are sufficiently small to make this technique suitable for measuring interfacial mass changes associated with the electrochemical adsorption of H, double layer charging, surface oxide formation and reduction, and metallic under-potential deposition. However, the technique is not sensitive enough to study interfacial mass losses associated with the dissolution of Pt or Pt oxide during a single cyclic-voltammetry transient in the 0.05–1.40 V range. This limitation could be circumvented by using large surface roughness materials but the influence of the electrode roughness on the frequency response needs to be first understood. Although the methodology of determining the values of LOD and LOQ is developed with the objective of studying Pt catalytic materials due to their importance to hydrogen fuel cells, the approach is universal and could be applied to other metallic materials.

2.5 References

(1) Nomura, T.; Iijima, M. *Anal. Chim. Acta* **1981,** *131,* 97–102.

(2) Jerkiewicz, G.; Vatankhah, G.; Zolfaghari, A.; Lessard, J. *Electrochem. Commun.* **1999,** *1,* 419–424.

(3) Jerkiewicz, G.; Vatankhah, G.; Lessard, J.; Soriaga, M. P.; Park, Y. S. *Electrochim. Acta* **2004,** *49,* 1451–1459.

(4) Sauerbrey, G. *Z. Phys.* **1959,** *155,* 206–222.

(5) Hepel, M. Electrode-Solution Interface Studied with Electrochemical Quartz Crystal Nanobalance. In *Interfacial Electrochemistry: Theory, Experiment, and Applications;* Wieckowski, A., Ed.; Marcel Dekker: New York, 1999; pp 599–630.

(6) Marrazza, G. *Biosensors* **2014,** *4*, 301–317.

(7) Vashist, S. K.; Vashist, P. *J. Sens.* **2011,** *2011*, ID 571405.

(8) Cooper, M. A.; Singleton, V. T. *J. Mol. Recognit.* **2007,** *20*, 154–184.

(9) Marx, K. A. *Biomacromolecules* **2003,** *4*, 1099–1120.

(10) Jerkiewicz, G. *Electrocatalysis* **2010,** *1*, 179–199.

(11) Harris, D. C. *Quantitative Chemical Analysis*, 8th ed.; W. H. Freeman and Company: New York, 2010; pp 96–116.

(12) Miller, J. N.; Miller, J. C. *Statistics and Chemometrics for Analytical Chemistry*, 5th ed.; Pearson Education Limited: Harlow, 2005; pp 107–149.

(13) Rodriguez, J. M. D.; Melian, J. A. H.; Pena, J. P. *J. Chem. Educ.* **2000,** *77*, 1195–1197.

(14) Chen, D.; Tao, Q.; Liao, L. W.; Liu, S. X.; Chen, Y.X.; Ye, S. *Electrocatalysis* **2011,** *2*, 207–219.

(15) Angerstein-Kozlowska, H.; Conway, B. E.; Sharp, W. B. A. *J. Electroanal. Chem.* **1973,** *43*, 9–36.

(16) Jerkiewicz, G.; Vatankhah, G.; Tanaka, S.; Lessard, J. *Langmuir* **2011,** *27*, 4220–4226.

(17) Gamboa-Aldeco, M. E.; Herrero, E.; Zelenay, P. S.; Wieckowski, A. *J. Electroanal. Chem.* **1993,** *348*, 451–457.

(18) Kolics, A.; Wieckowski, A. *J. Phys. Chem. B* **2001,** *105*, 2588–2595.

(19) Rodriguez-Pardo, L.; Farina, J.; Gabrielli, C.; Perrot, H.; Brendel, R. *Sens. Actuator B-Chem.* **2004,** *103*, 318–324.

(20) *CRC Handbook of Chemistry and Physics*, 75th ed.; Boca Raton, FL, 1994; Chapter 6, pp 10–246.

(21) Limmer, D. T.; Willard, A. P. *Chem. Phys. Lett.* **2015,** *620,* 144–150.

(22) Darling, R. M.; Meyers, J. P. *J. Electrochem. Soc.* **2003,** *150,* A1523–A1527.

(23) Topalov, A. A.; Katsounaros, I.; Auinger, M.; Cherevko, S.; Meier, J. C.; Klemm, S. O.; Mayrhofer, K. J. J. *Angew. Chem. Int. Ed.* **2012,** *51,* 12613–12615.

(24) Topalov, A. A.; Cherevko, S.; Zeradjanin, A. R.; Meier, J. C.; Katsounaros, I.; Mayrhofer, K. J. J. *Chem. Sci.* **2014,** *5,* 631–638.

(25) Guilminot, E.; Corcella, A.; Charlot, F.; Maillard, F.; Chatenet, M. *J. Electrochem. Soc.* **2007,** *154,* B96–B105.

(26) Rice, C. A.; Betancourt,D.; Hepel. M. *Electrocatalysis* **2015,** *6,* 1–6.

(27) Rinaldo, S. G.; Lee, W.; Stumper, J; Eikerling, M. *Electrocatalysis* **2014,** *5,* 262–272.

(28) Xing, L.; Hossain, M. A.; Tian, M.; Beauchemin, D.; Adjemian, K. T.; Jerkiewicz, G. *Electrocatalysis* **2014,** *5,* 96–112.

Chapter 3

Interfacial Structure of Atomically Flat Polycrystalline Platinum Electrodes and Modified Sauerbrey Equation

3.1 Introduction

In 1959, Sauerbrey introduced the quartz-crystal microbalance (QCM) as a new interfacial science technique to monitor the deposition rate of thin films under vacuum conditions.[1] In 1981, Nomura and Iijima applied the QCM as an *in-situ* tool to measure minute concentrations of Ag^+ in aqueous media in conjunction with electrodeposition.[2] By combining QCM with electrochemical measurements, they created the first electrochemical quartz-crystal microbalance (EQCM). At present, the method is applied to measure interfacial mass changes under electrochemical conditions on the ng cm^{-2} scale and is referred to as the electrochemical quartz-crystal nanobalance (EQCN). Cyclic-voltammetry (CV), chronoamperometry (CA), and chronopotentiometry (CP) are typical methods employed in conjunction with nanogravimetry measurements.

The EQCN measures changes in the resonant frequency (Δf) of the quartz-crystal resonator upon which the working electrode material is coated. The quartz-crystal has a fundamental resonant frequency associated with its unaltered state. When an electrochemical reaction takes place at the electrode surface and mass is added or removed, the resonance is disturbed and a new resonant frequency is established. This resonant frequency change (Δf) is related to the interfacial mass variation (Δm) through the Sauerbrey equation:

$$\Delta m = -\left(\frac{\sqrt{\mu_q \, \rho_q}}{2 \, f_0^{\,2}} \right) \Delta f = -C_f \, \Delta f \tag{3.1}$$

where μ_q is the shear modulus of quartz ($\mu_q = 2.947 \times 10^{11}$ g cm^{-1} s^{-2}), ρ_q is the density of quartz ($\rho_q = 2.648$ g cm^{-3}), f_0 is the resonant frequency of the resonator prior to the addition or removal of mass, and C_f is the characteristic constant.[1] In the case of $f_0 = 9.00$ MHz, the calculated value of C_f is equal to 5.45 ng Hz^{-1} cm^{-2} and the corresponding mass detection limit is $\Delta m = 5.45$ ng cm^{-2}, provided that the frequency detection limit is $\Delta f = 1$ Hz. This detection limit refers to a flat surface but metal-coated quartz-crystal resonators are never atomically flat. Consequently, an intrinsic surface roughness together with other factors contributes to the experimentally measured resonant frequency change.[3–5] When the EQCN is applied to analyze interfacial electrochemical processes typically in aqueous media, the following phenomena contribute to the frequency change: (i) the mass addition or removal (Δf_m); (ii) the change in the surface roughness (Δf_r); (iii) the change in the electrolyte viscosity (Δf_v); (iv) the change in pressure (Δf_p); and (v) the change in temperature (Δf_T).[4,5] If all processes contribute simultaneously, the overall resonant frequency change equals:

$$\Delta f = \Delta f_m + \Delta f_r + \Delta f_v + \Delta f_p + \Delta f_T \tag{3.2}$$

Because typical interfacial electrochemical measurements take 1–2 min, the pressure and temperature do not change (any heat evolved is absorbed by the electrolyte that has a large heat capacity), and the corresponding Δf_p and Δf_T values are practically nil. In the case of the electrochemical H adsorption/desorption or surface oxide formation/reduction on Pt electrodes, there are no changes in the electrolyte viscosity and Δf_v also equals zero. Because metallic deposits on quartz-crystal resonators are polycrystalline in nature and are never atomically flat,

their surface roughness factor (R) needs to be taken into account when employing the Sauerbrey equation (equation 3.1) with the objective of assigning interfacial mass changes to specific electrochemical phenomena. This is of particular importance when employing the technique in electrochemical research on meso- and nano-structured materials because by default they have a large value of R and the interpretation of results is not straightforward.[6–8]

Platinum due to its application in hydrogen fuel cells is an important catalyst and its interfacial behavior needs to be examined using a variety of complementary techniques. Platinum possesses the unique ability to electrochemically adsorb H prior to the onset of the hydrogen evolution reaction (HER), which is referred to as the under-potential deposition of H, and to form a surface oxide layer.[9–17] The CV features associated with these two processes can be used to examine the system's cleanliness. The charge associated with the adsorption and desorption of the under-potential deposited H (H_{UPD}) is used to determine the electrochemically active surface area (A_{ecsa}) of the electrode, thus its roughness factor defined as $R = A_{esca}/A_{geom}$, where A_{geom} is the geometric area (a two-dimensional projection of a rough surface). Consequently, Pt is the most suitable material for evaluation of the influence of surface roughness on the resonant frequency change (thus the mass change) response. The influence of the surface roughness of the response of EQCM has never been examined in detail. Elsewhere, it was reported that an increase in the roughness of Au and Ag electrodes brought about higher than expected changes in the resonant frequency.[18,19] Because those surfaces could be represented by rolling hills separated by valleys, the unexpected behavior was explained in terms of electrolyte in the valleys.

In this contribution, we report on the interfacial mass response of Pt electrodes of gradually increasing surface roughness on the nanoscopic scale. The surface roughness is modified through Pt electrodeposition and the surface morphology is examined using atomic force microscopy (AFM), with A_{ecsa} being determined by using H_{UPD} as a surface-probing species. Analysis of the values of Δm as a function of R facilitates the determination of interfacial mass

changes for an ideal atomically flat, polycrystalline Pt electrode. In addition, an examination of the Δm versus R plots leads to a modified version of the Sauerbrey equation that takes into account the surface roughness and can be employed to predict the interfacial mass response of roughened Pt electrodes. This knowledge is of great importance to the understanding of the mechanism and kinetics of the degradation of Pt catalysts employed in hydrogen fuel cells. In addition, the approach developed and discussed in this contribution is transferable to other metallic materials, and can be used to analyze a broad range of interfacial phenomena, including electrodeposition of ultra-thin layers, formation of structured nanomaterials, degradation and dissolution of nanoparticles, adsorption of reaction intermediates, early stage of corrosion, self-assembly, and others.

3.2 Experimental

Platinum electrodeposition, cyclic-voltammetry (CV), and mass variation (MV) measurements were conducted using a Bio-Logic potentiostat/galvanostat (SP-150) and a Seiko-EG&G quartz crystal analyzer (QCA 922). Electrochemical experiments were performed using a custom-made Pyrex two-compartment electrochemical cell. The working electrode and counter electrode were located in the main compartment of the cell, whereas the reference electrode was placed in the second compartment that was connected to the main compartment by means of a Luggin capillary. The glassware employed in the measurements was cleaned using well-established and broadly accepted procedures.[15] The working electrode was a Pt-coated quartz-crystal resonator (Seiko-EG&G, QA-A9M-PT) having ca. 9.00 MHz resonant frequency; it was attached to the bottom of the main compartment in a horizontal configuration using a Teflon holder.[20] The geometric surface area (A_{geom}) of the Pt working electrode deposited on the

resonator was 0.196 cm^2. A platinum gauze (99.9% in purity, Alfa Aesar) was used as the counter electrode; its surface area was at least ten times greater than that of the working electrode. A reversible hydrogen electrode (RHE) in the form of a Pt wire (99.95% in purity, Alfa Aesar) coated with electrodeposited Pt black was used as the reference electrode. A high purity 0.50 M aqueous H_2SO_4 electrolyte solution and 0.20 mM H_2PtCl_6 in 0.50 M aqueous H_2SO_4 electrolyte solution were prepared using concentrated H_2SO_4 (Fluka Analytical, TraceSELECT ≥95%), $H_2PtCl_6 \cdot 6H_2O$ (Alfa Aesar, 99.9%), and ultra-high purity (UHP) water (Millipore, 18.2 MΩ cm). Ultra-high purity Ar(g) (5.0 grade, Praxair) was purged through the main cell compartment for at least 1 hour prior to electrochemical experiments to expel any gases. The electrochemical cell was placed in a custom-built Faraday cage. It was suspended from an outer frame by means of bungee cords to minimize mechanical interferences from the environment during electrochemical experiments.

Prior to the commencement of all measurements, as received Pt working electrode was preconditioned through repetitive potential cycling 1000 times in the E = 0.05–1.50 V range at a potential scan rate of s = 50.0 mV s^{-1} in 0.50 M aqueous H_2SO_4 solution. After preconditioning, the electrolyte was switched to a fresh and outgassed 0.50 M aqueous H_2SO_4 solution; then, CV and MV measurements were carried out in the E = 0.05 V–1.40 V range at a potential scan rate of s = 50.0 mV s^{-1}. In order to improve the signal-to-noise ratio of the MV transients, ten consecutively performed but independent MV transients were recorded and their average was calculated.

The roughness of the Pt surface was fine-tuned through Pt electrodeposition on the Pt-coated resonator. The Pt electrodeposition designed to increase the surface roughness was performed at a deposition potential of E = 0.20 V for 30 s using 0.20 mM H_2PtCl_6 in 0.50 M aqueous H_2SO_4 solution. Afterward, the electrochemical cell was thoroughly rinsed several times with UHP water followed by rinsing with a fresh stock solution of 0.50 M aqueous H_2SO_4. Each

electrodeposited Pt electrode having higher surface roughness was pretreated by repetitive potential cycling (ca. 300 times) in the E = 0.05–1.40 V range at a potential scan rate of s = 50.0 mV s^{-1} in outgassed 0.50 M aqueous H_2SO_4 solution. This procedure known as "electrochemical annealing" resulted in the release of any stress from the near-surface region of the electrodeposited Pt and generated a CV profile characteristic of a polycrystalline Pt electrode.[21] Afterward, the electrolyte was changed for a fresh outgassed 0.50 M aqueous H_2SO_4 solution; then, CV and MV measurements were carried out in the E = 0.05 V–1.40 V range at a potential scan rate of s = 50.0 mV s^{-1}. All experiments were conducted at a constant temperature of T = 298 ± 1 K. In order to prepare Pt electrode of gradually increasing surface roughness, the aforementioned sequence of experimental steps was repeated several times until a comprehensive set of CV and MV transients for a range of surface roughness values was obtained.

The electrochemically active surface area (A_{ecsa}) of each Pt electrodeposit was determined by examining the charge associated with the under-potential deposition of H and comparing it to the charge density of 210 μC cm^{-2} associated with the deposition of 1 monolayer (ML) of under-potential deposited H (H_{UPD}).[22] The topography of the as-received and gradually roughened Pt electrodes was examined using an atomic force microscope (AFM), Veeco Instruments MultiMode V. The Pt electrodes were scanned in a contact mode using a silicon nitride tip (k = 0.12 N m^{-1}) at a tip speed of 1.0 μm s^{-1} under ambient conditions.

3.3 Results and discussion

Figure 3.1 presents a CV profile (the black transient) for a Pt-coated quartz-crystal resonator having a roughness factor of R = 1.61 and a simultaneously recorded MV transient (the green transient) acquired in 0.50 M aqueous H_2SO_4 solution at a potential scan rate of s = 50.0

mV s^{-1} and a temperature of T = 298 K. The features observed in these transients are characteristic of a clean system, thus impurity-free Pt(poly) electrode, electrolyte, and cell. The CV profile shows features corresponding to: (i) the electrochemical H adsorption in the 0.40–0.05 V range; (ii) the electrochemical H desorption in the 0.05–0.40 V range; (iii) the surface oxide formation in the 0.85–1.40 V range; and (iv) the surface oxide reduction in the 1.20–0.60 V range. The interfacial mass decrease upon the adsorption of H_{UPD} is due to the desorption of H_2O molecules and modification of the wetting ability of Pt(poly).[23–25] The mass changes in the double layer region are due to the physisorption of H_2O molecules and anion adsorption.[23,26,27] The mass changes at higher potentials are assigned to the surface oxide formation and reduction, respectively.[17,28]

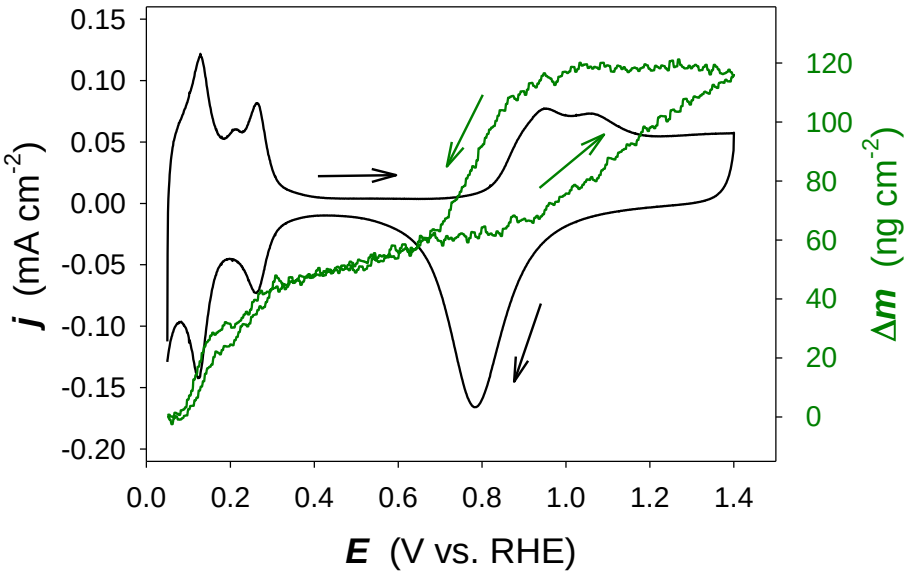

Figure 3.1. A cyclic-voltammetry profile (black) and a corresponding mass variation transient (green) for a polycrystalline Pt electrode having a surface roughness factor of R = 1.61 acquired in 0.50 M aqueous H_2SO_4 at a potential scan rate of s = 50.0 mV s^{-1} and T = 298 K.

It is important to add that prior to electrochemical measurements, each Pt-coated resonator was preconditioned by applying repetitive potential cycling between 0.05 and 1.50 V in 0.50 M aqueous H_2SO_4. This approach releases excessive surface stress by rearranging surface atoms; it involves Pt oxide formation and reduction as well as Pt dissolution and re-deposition. The treatment produces a CV profile characteristic of Pt(poly) electrode and the surface roughness of such preconditioned resonators was always in the R = 1.50–1.70 range.[21]

Figure 3.2 presents chronoamperometry (current density versus time, j vs. t; the black profile) and chronocoulometry (charge density versus time, q vs. t; the mauve transient) profiles for Pt electrodeposition at E = 0.20 V in the solution of 0.20 mM H_2PtCl_6 in 0.50 M aqueous H_2SO_4 (equation 3.3). The chronocoulometry profile was obtained by integrating the j versus t transient.

$$PtCl_6^{-2}(aq) + 4e^- \rightarrow Pt(s) + 6Cl^-(aq) \qquad (3.3)$$

As expected, the charge density associated with Pt electrodeposition increases with time and in the case of t = 30.0 s reaches a value of q = 15.5 mC cm^{-2}. Using Faraday's law and bearing in mind that the process involves 4 electrons per Pt atom, this charge density value corresponds to 7.82 μg cm^{-2} of solid Pt. Because Pt has a large surface tension, the deposit does not develop a smooth finish mimicking the topography of the underlying substrate and, consequently, its surface morphology needs to be examined using a suitable technique, such as atomic force microscopy (AFM).

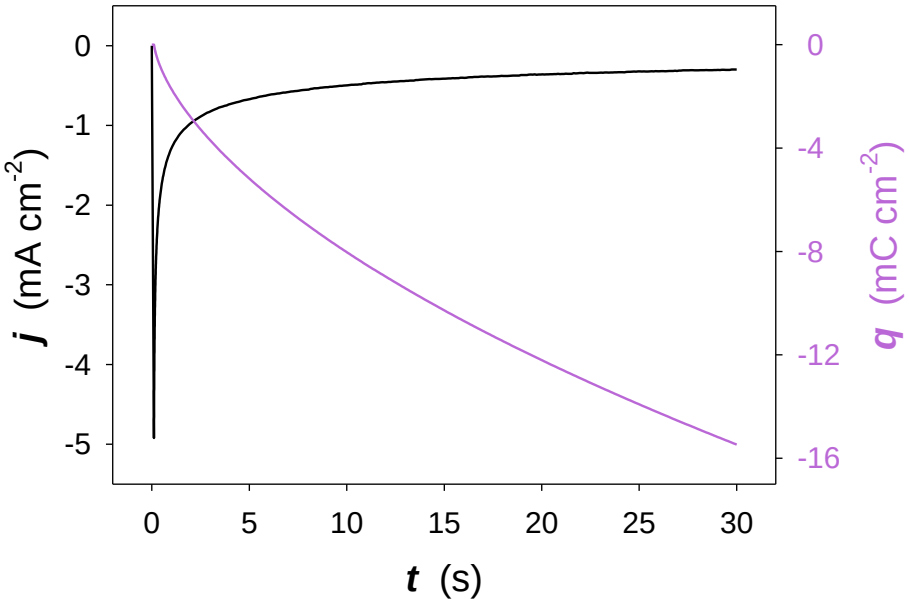

Figure 3.2. A current density profile (black) and a corresponding charge density transient (mauve) for Pt electrodeposition at E = 0.20 V in 0.50 M aqueous H_2SO_4 solution containing 0.20 mM H_2PtCl_6 at T = 298 K.

Figure 3.3A presents an AFM image of a preconditioned Pt-coated resonator (R = 1.70) showing interconnected grains with smooth faces and edges. The x and y axes cover the 0.00–5.00 μm range, while the z axis covers the range from −200 nm to +200 nm. The same scale is employed for the x, y and z axes, thus the AFM images represent the true and undistorted images of surface features. Figures 3.3B through 3.3D show AFM images of Pt-coated resonators with gradually increasing roughness that was achieved by repeating several times the Pt electrodeposition process. The values of R for the three images are 6.85, 12.1, and 22.8, and the number of Pt deposition cycles (for all other parameters being the same as described above) are 7, 14, and 30, respectively.

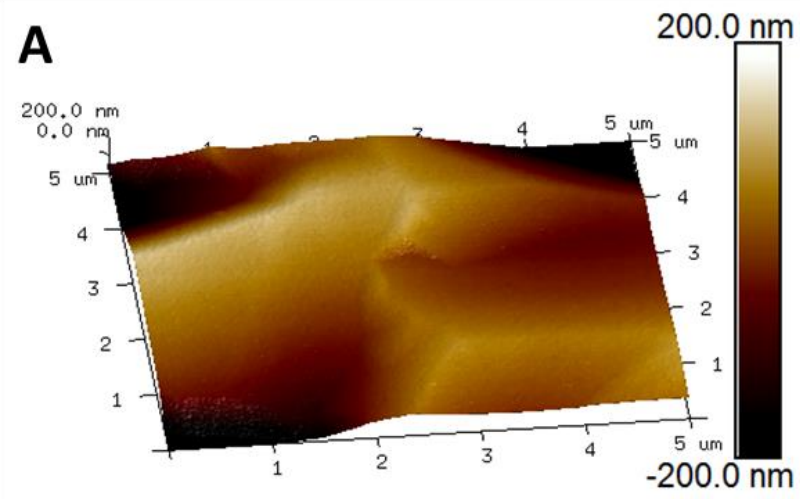
A
200.0 nm
200.0 nm
0.0 nm
5 um
4
3
2
1
5 um
-200.0 nm

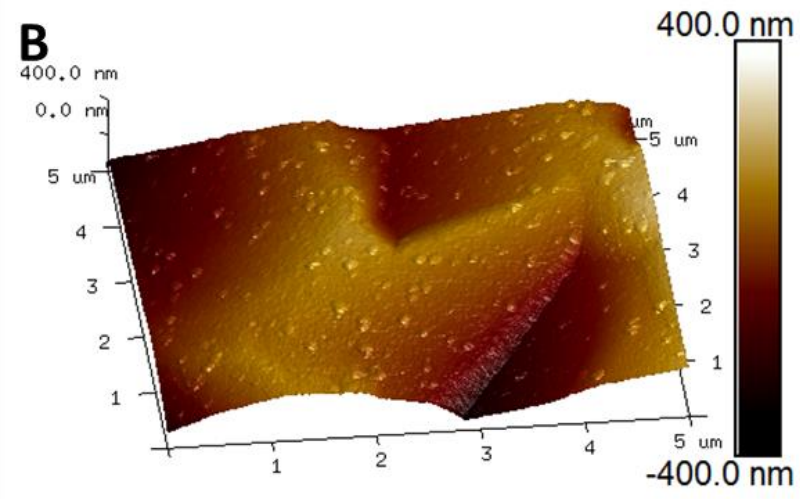
B
400.0 nm
400.0 nm
0.0 nm
5 um
4
3
2
1
5 um
-400.0 nm

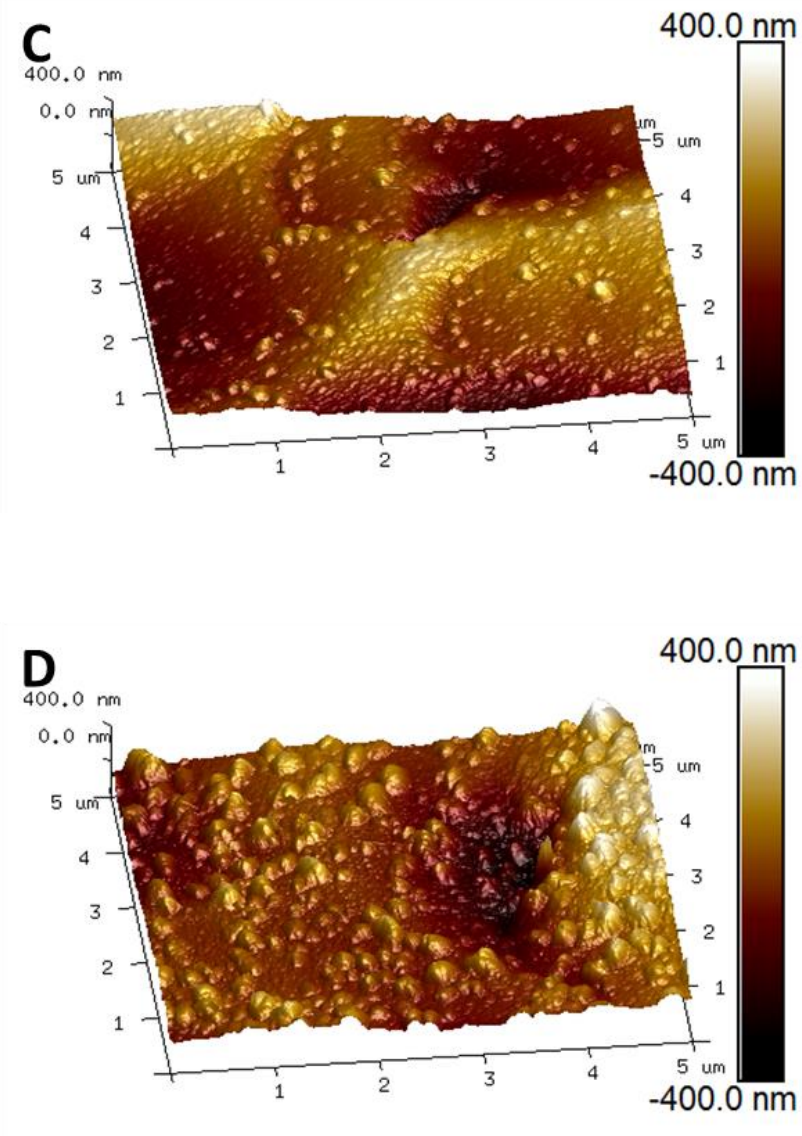

Figure 3.3. Atomic force microscopy images for pretreated Pt electrodes having a gradually increasing surface roughness. (**A**) R = 1.70; (**B**) R = 6.85; (**C**) R = 12.1; and (**D**) R = 22.8.

The scale of the *x* and *y* axes is the same as in Figure 3.3A but the *z* axis covers the range from −400 nm to +400 nm. The images demonstrate that the electrodeposition of Pt roughens the faces and creates small islands (Figure 3.3B). As more Pt is electrodeposited (Figure 3.3C), the roughness of the faces increases even more through the formation of wave-like features, development of new small islands, and increase in the size of already existing islands. Additional electrodeposition of Pt (Figure 3.3D) generates a very rough surface comprising wavy faces as well as small, large, and very large islands. The island distribution is non-uniform and some large islands overlap creating ranges; the sides of the islands are also rough. Although we prepared a very rough Pt electrode for an AFM analysis (having a roughness factor of $R = 22.8$), it was not used in CV and MV measurements because its extended surface could give rise to solution trapping in between islands and contribute to uncontrollable secondary hydrodynamic effects.

The preparation of Pt-coated resonators of gradually increasing roughness, thus A_{ecsa}, and known surface morphology creates a basis for subsequent evaluation of their CV profiles and MV transients. Figures 3.4A and 3.4B present CV profiles and MV transients for such prepared Pt electrodes acquired in 0.50 M aqueous H_2SO_4 at a potential scan rate of $s = 50.0$ mV s^{-1} and $T = 298$ K. All CV profiles (Figure 3.4A) reveal the same features and if the respective *j* values are divided by the corresponding values of *R*, then they overlap (see *Appendix A*). This is a very important observation because it indicates that the polycrystalline nature of the electrodes remains the same even when the surface roughness increases up to $R = 13.0$. In other words, the relative ratio of the main crystallographic facets is the same. The MV transients (Figure 3.4B) also reveal the same features and the magnitude of Δm increases with rising *R*.

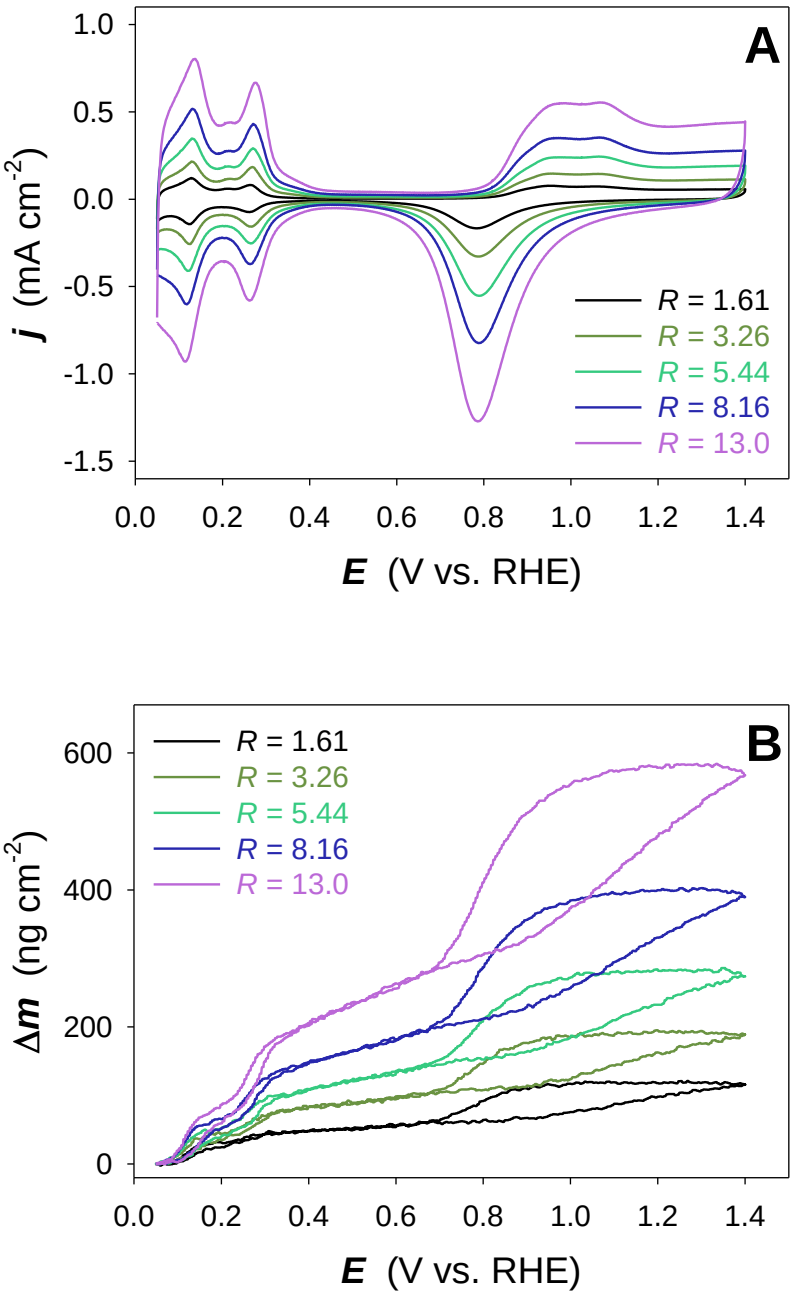

Figure 3.4. A series of CV profiles (**A**) and a set of simultaneously recorded MV transients (**B**) for Pt electrodes of gradually increasing surface roughness ($1.61 \leq R \leq 13.0$) acquired in 0.50 M aqueous H_2SO_4 at a potential scan rate of s = 50.0 mV s^{-1} and T = 298 K.

However, division of the values of Δm by the corresponding values of R does not create overlapping MV transients (see *Appendix A*). This is a very important observation indicating that the current density and the mass density responses do not scale up the same as R rises. In other words, doubling the values of R increases the value of j by a factor of two but does not double the value of Δm (it increases less than twice). In order to understand the origin of this behavior, we analyzed the magnitudes of Δm as a function of R for each MV transient in the following potential ranges: (i) the entire potential range (EPR); (ii) the hydrogen adsorption range (HAR); (iii) the anodic double-layer charging range (DLCR); and (iv) the surface oxide formation range (SOFR). Because this analysis refers to two potential limits ($\delta E = E_2 - E_1$), the corresponding mass variation is presented as $\delta\Delta m$. The qualitative and quantitative analysis that follows is performed with respect to three potentials, namely the potential of zero charge ($E_{pzc} = 0.31 \pm 0.01$ V), the potential of minimum mass ($E_{pmm} = 0.05 \pm 0.01$ V), and the onset potential of Pt surface oxide formation ($E_{PtO} = 0.85 \pm 0.01$ V).[25,29,30] It is important to note that the upper potential limit of HAR and the lower potential limit of DLCR are the same and equal $E_{pzc} = 0.31$ V; it coincides with an inflection in the MV transients. Similarly, the upper potential limit of DLCR and the lower potential limit of SOFR are the same and equal $E_{PtO} = 0.85$ V; it also coincides with an inflection (a different one) in the MV transients. E_{pzc} is an important parameter in the data analysis because its represents the potential at which the effective surface charge of the Pt electrode is zero ($q_{Pt} = 0$). At $E < E_{pzc}$ the effective surface charge is negative ($q_{Pt} < 0$), while at $E > E_{pzc}$ the effective charge is positive ($q_{Pt} > 0$).[29,30] E_{pmm} coincides with completion of saturation (monolayer) of H_{UPD} on Pt and the effective surface charge is negative ($q_{Pt} < 0$).[24,25] At E_{PtO}, the surface oxide formation commences and is accompanied by the desorption of specifically adsorbed anions. The onset potential of PtO development corresponds to the second potential of zero charge due to the existence of surface oxide dipole.[29,31]

Figure 3.5 presents the values of $\delta\Delta m$ as a function of R for the four potential ranges; the $\delta\Delta m$ values are determined on the basis of the MV transients shown in Figure 3.4B. For clarity of presentation, they are abbreviated as $\delta\Delta m_{EPR}$, $\delta\Delta m_{HAR}$, $\delta\Delta m_{DLCR}$, and $\delta\Delta m_{SOFR}$. The results demonstrate that their values increase linearly with R (their fitting using a linear regression yielded the square of the correlation coefficient of at least 0.991; the linear regressions are presented as solid lines). Extrapolation of the four plots to the y-intercept, thus to $R = 1.00$, allows us to determine for the first time the respective $\delta\Delta m$ values for an *atomically flat polycrystalline Pt electrode*.

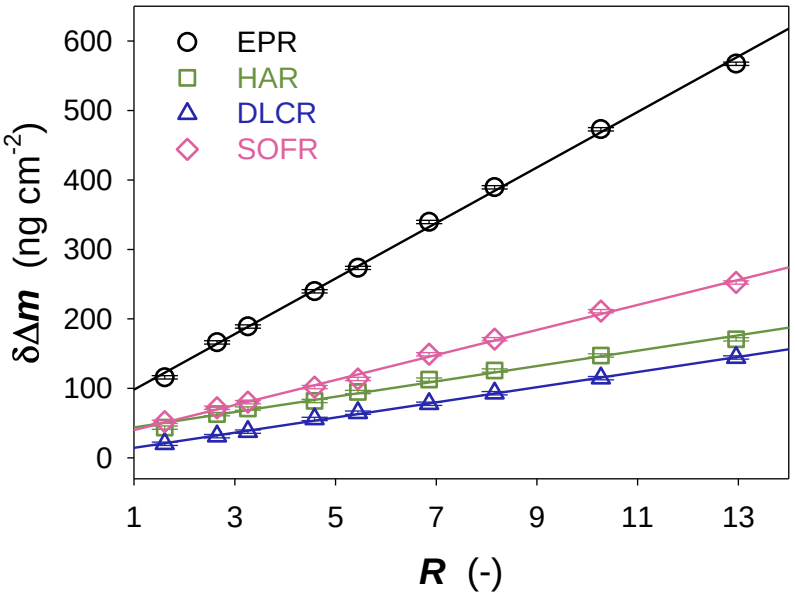

Figure 3.5. The values of $\delta\Delta m$ as a function of R for the entire potential range (EPR, 0.05 V $\leq E \leq$ 1.40 V), the hydrogen adsorption range (HAR, 0.05 V $\leq E \leq$ 0.31 V), the double-layer charging range (DLCR, 0.31 V $\leq E \leq$ 0.85 V), and the surface oxide formation range (SOFR, 0.85 $\leq E \leq$ 1.40 V) obtained from the MV transients presented in Figure 3.4B.

They are as follows: (i) $\delta\Delta m_{EPR}$ = 98.2 ± 4.5 ng cm^{-2}; (ii) $\delta\Delta m_{HAR}$ = 43.7 ± 3.1 ng cm^{-2}; (iii) $\delta\Delta m_{DLCR}$ = 14.5 ± 1.1 ng cm^{-2}; and (iv) $\delta\Delta m_{SOFR}$ = 40.0 ± 2.9 ng cm^{-2} (Table 3.1). In addition, the slopes of these plots determine how the respective values of $\delta\Delta m$ scale up with increasing surface roughness in the low and intermediate surface roughness range, thus for $R \leq 13.0$ (Table 3.1). For molecular-level interpretation of our experimental data, the $\delta\Delta m$ values are converted to mass values per mole of Pt surface atom, thus into molar mass changes designated as $\delta\Delta M_{EPR}$, $\delta\Delta M_{HAR}$, $\delta\Delta M_{DLCR}$, and $\delta\Delta M_{SOFR}$. Their values are as follows: $\delta\Delta M_{EPR}$ = 45.1 ± 2.1 g mol$_{Pt}^{-1}$; $\delta\Delta M_{HAR}$ = 20.1 ± 1.4 g mol$_{Pt}^{-1}$; $\delta\Delta M_{DLCR}$ = 6.66 ± 0.51 g mol$_{Pt}^{-1}$; and $\delta\Delta M_{SOFR}$ = 18.4 ± 1.3 g mol$_{Pt}^{-1}$ (Table 3.1).

Table 3.1. The values of *y*-intercepts at R = 1.00 and slopes of the plots for the four potential ranges shown in Figure 3.5. The values of *y*-intercepts are presented as interfacial mass changes per unit area ($\delta\Delta m$, ng cm^{-2}) and per mole of Pt surface atom ($\delta\Delta M$, g mol$_{Pt}^{-1}$).

	y-intercept in $\delta\Delta m$ (ng cm^{-2})	*y*-intercept in $\delta\Delta M$ (g mol$_{Pt}^{-1}$)	Slope (-)
Entire potential range (EPR)	98.2 ± 4.5	45.1 ± 2.1	40.0 ± 0.5
Hydrogen adsorption range (HAR)	43.7 ± 3.1	20.1 ± 1.4	11.0 ± 0.4
Double-layer charging range (DLCR)	14.5 ± 1.1	6.66 ± 0.51	10.9 ± 0.1
Surface oxide formation range (SOFR)	40.0 ± 2.9	18.4 ± 1.3	18.0 ± 0.4

At E_{pmm} = 0.05 V, the Pt surface is modified with a saturation layer (monolayer) of H_{UPD}. Although it has a negative effective surface charge ($q_{Pt} < 0$), its interactions with H_2O molecules and H_3O^+ cations present in the double-layer region are the weakest because the surface is hydrophobic-like (Figure 3.6A).[24,25] One would expect the surface dipole moment of Pt to be substantial because of the negative effective surface charge but the embedded H_{UPD} adatoms significantly modify (reduce) its magnitude to the lowest possible value that makes the surface hydrophobic-like. Increase of the applied potential from E_{pmm} = 0.05 V to E_{pzc} = 0.31 V leads to gradual desorption of H_{UPD} adatoms (−1.0 g mol_{Pt}^{-1}). The oxidative desorption of H_{UPD} adatoms creates H_3O^+ species in the double-layer region. As the H_{UPD} surface coverage decreases, the unoccupied Pt surface atoms develop physisorptive interactions with H_2O molecules. Because at $E = E_{pzc}$ = 0.31 V (q_{Pt} = 0) the experimentally determined value of $\delta\Delta M_{HAR}$ is 20.1 g mol_{Pt}^{-1} and because the molar mass change due to H_{UPD} desorption is 1.00 g mol_{Pt}^{-1}, the interfacial molar mass change associated with the H_2O interfacial interactions is ca. 21.1 g mol_{Pt}^{-1}. The latter value is attributed to the interaction of H_2O molecules with the Pt surface and corresponds to 1.2 H_2O molecules per Pt surface atom. Since the radius of H_2O molecule (r_{H2O} = ~0.144 nm) is greater than that of Pt atom (r_{Pt} = ~0.139 nm), the value of 1.2 corresponds to an organized water structure that is more than one monolayer in thickness.[32,33] In agreement with spectroscopy results, we propose a visual representation of the interface in which H_2O molecules adjacent to the Pt surface are on the average parallel to the surface.[24] The (bi)sulfate anions and H_3O^+ cations constituting the electrolyte solution are not present in the immediate interfacial region and, consequently, do not interact with the Pt electrode surface (Figure 3.6B).[24,34]

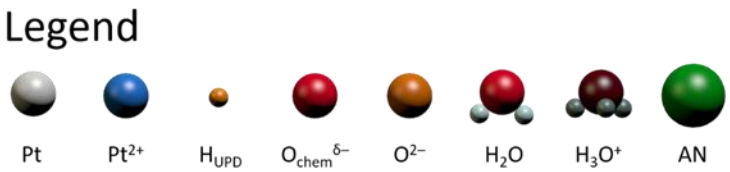

A

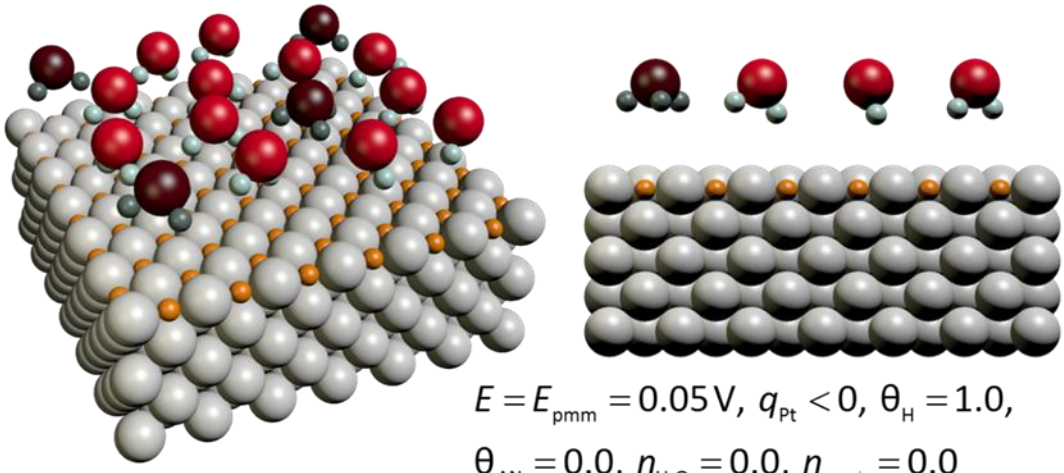

$E = E_{pmm} = 0.05\,V,\ q_{Pt} < 0,\ \theta_H = 1.0,$
$\theta_{AN} = 0.0,\ n_{H_2O} = 0.0,\ n_{H_3O^+} = 0.0$

B

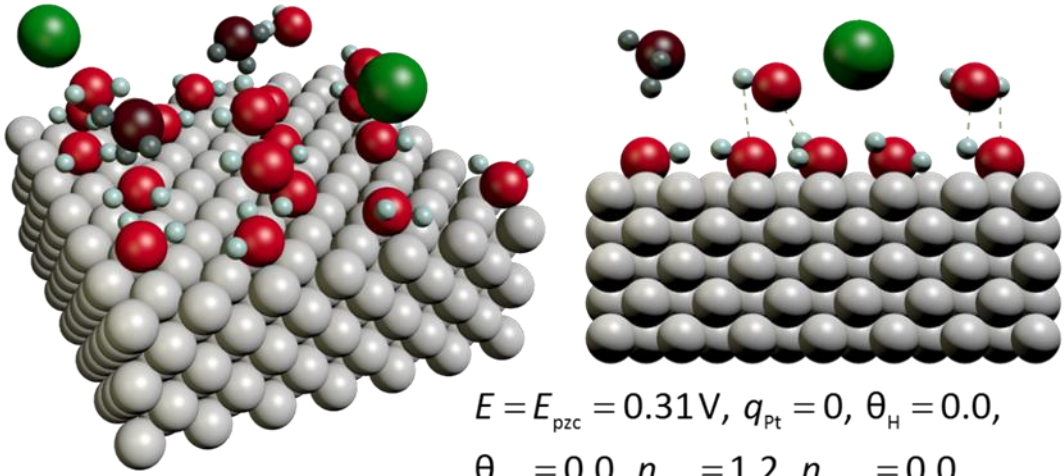

$E = E_{pzc} = 0.31\,V,\ q_{Pt} = 0,\ \theta_H = 0.0,$
$\theta_{AN} = 0.0,\ n_{H_2O} = 1.2,\ n_{H_3O^+} = 0.0$

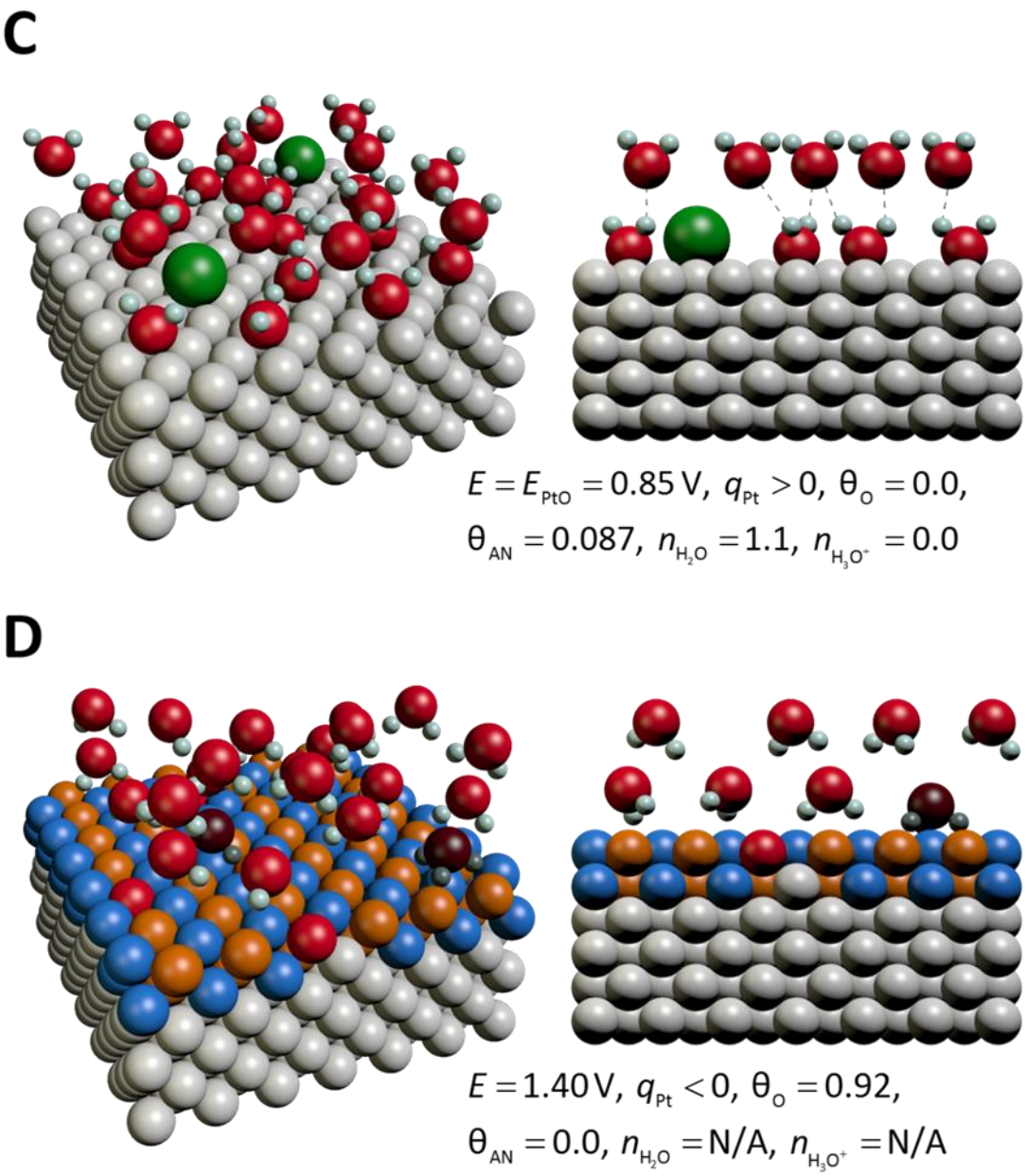

Figure 3.6. Three-dimensional renderings and side views of the Pt/electrolyte interfacial structures at specific potential (E) values corresponding to different sign of the surface charge (q_{Pt}) and characteristic electrode states. The applied potential defines: (i) the surface coverage of electrochemically adsorbed H (θ_H); (ii) the surface coverage of O in the form of O_{chem} or O^{2-} (θ_O); (iii) the surface coverage of specifically adsorbed AN (θ_{AN}); (iv) the number of hydronium cations (n_{H3O+}); and (v) the number of water molecules (n_{H2O}) interacting with each Pt surface atom. (**A**) $E = E_{pmm} = 0.05$ V; (**B**) $E = E_{pzc} = 0.31$ V; (**C**) $E = E_{PtO} = 0.85$ V; and (**D**) $E = 1.40$ V.

As the applied potential increases from E_{pzc} = 0.31 V to E_{PtO} = 0.85 V, the effective surface charge is positive and drives the specific adsorption of anions, in this case (bi)sulfate (+97.1 g mol_{Pt}^{-1}). The specifically adsorbed anions require surface adsorption sites, thus the process is accompanied by partial desorption of H_2O molecules. The anion surface coverage gradually increases and reached a maximum of θ_{AN} = 0.087 at a potential only slightly lower than the onset potential of Pt surface oxide formation that is 0.85 V.[26,35,36] Because the anion surface coverage is small, the desorption of H_2O molecules is only partial and the Pt surface is covered by remaining physisorbed H_2O molecules that on the average are oriented towards the surface through the negatively charged oxygen end. The maximum anion coverage of θ_{AN} = 0.087 can be converted into a molar mass change and produces a value of 8.4 g mol_{Pt}^{-1}. Because the experimentally determined molar mass change in the double layer range is $\delta\Delta M_{DLCR}$ = 6.66 g mol_{Pt}^{-1}, the difference of −1.8 g mol_{Pt}^{-1} is assigned to the desorbed H_2O molecules. This value (i.e. −1.8 g mol_{Pt}^{-1}) corresponds to the surface coverage of desorbed H_2O molecules being 0.10. Thus, in the case of atomically flat polycrystalline Pt electrode, the specific adsorption of anion gives rise to desorption of 1.1 water molecules per adsorbing anion (0.10/0.087 = 1.1). On the basis of in-situ electrochemical spectroscopy data, Osawa et al. explained that the specifically adsorbed anions together with water molecules form an ice-like bilayer structure that is visually represented in Figure 3.6C.[24,34]

As the applied potential increases from E_{PtO} = 0.85 V to E = 1.40 V, chemisorption of oxygen (O_{chem}, +16.0 g mol_{Pt}^{-1}) occurs as a result of the discharge of O from the physisorbed H_2O molecule; the process is accompanied by the departure of hydrated protons. The process is also accompanied by desorption of anions because the surface bond between the Pt surface atoms having a partial positive charge ($Pt^{\delta+}$) and chemisorbed O having a partial negative charge ($O_{chem}^{\delta-}$) is significantly stronger than the Pt–AN bond (the respective thermodynamic driving force is also stronger).[26] Once the amount of $O_{chem}^{\delta-}$ exceeds 0.50 MLs, the interfacial phase

transition (also referred to as the interfacial place exchange) between $Pt^{\delta+}$ and $O_{chem}^{\delta-}$ species commences and leads to the development a quasi-3D lattice comprising Pt^{2+} and O^{2-}; the process is accompanied by the completion of charge transfer between Pt and O. Visual representation of the interfacial structure that develops is shown in Figure 3.6D.[17,37] Elsewhere, it is explained that the formation of Pt surface oxide gives rise to a negative effective surface charge and the onset potential of Pt surface oxide formation coincides with the second potential of zero charge.[31] The negatively charged Pt surface oxide attracts H_2O molecules through the hydrogen end and H_3O^+ cations. The experimentally determined molar mass change of $\delta\Delta M_{SOFR} = 18.4$ g mol_{Pt}^{-1} associated with the Pt surface oxide formation has several contributions, such as the molar interfacial mass change of -8.4 g mol_{Pt}^{-1} due to the anion desorption and the molar interfacial mass change of $+14.7$ g mol_{Pt}^{-1} due to the formation of 0.92 ML of O (in the form of $O_{chem}^{\delta-}$ or O^{2-}). Consequently, the remaining molar mass change of 12.1 g mol_{Pt}^{-1} is attributed to the interaction of H_2O molecules and H_3O^+ cations with the oxidized Pt surface. Because the number of H_3O^+ cations interacting with the oxidized Pt surface is unknown, we are unable to assign the value of 12.1 g mol_{Pt}^{-1} to specific surface coverages of H_2O and H_3O^+ numbers.

To summarize this detailed analysis, the potential of $E = E_{pmm} = 0.05$ V is employed as a reference state and refers to a Pt electrode covered with a saturation layer of H_{UPD} and having no interactions with the electrolyte components. The transition from $E_{pmm} = 0.05$ V to $E_{pzc} = 0.31$ V results in the desorption of H_{UPD} and leads to the formation of an interfacial structure comprising on the average 1.2 water molecules per Pt surface atom. The subsequent transition from $E_{pzc} = 0.31$ V to $E_{PtO} = 0.85$ V results in the development of an interfacial structure comprising both anions and water molecules; on the average, there are 0.087 anions and 1.1 water molecules per Pt surface atom. The final transition from $E_{PtO} = 0.85$ V to $E = 1.40$ V leads to the formation of Pt surface oxide; the process is accompanied by desorption of anions and physisorption of water molecules and H_3O^+ cations; there are 0.92 O_{chem} atoms per Pt surface atom as well as H_2O and

H_3O^+ species but the number of the latter is unknown. The values of interfacial molar mass changes ($\delta\Delta M$) and the corresponding numbers of water molecules (n_{H2O}), H_3O^+ cations (n_{H3O+}), (bi)sulfate anions (n_{AN}), and O_{chem} species (n_{Ochem}) per Pt surface atom in each potential range are presented in Table 3.2. The abbreviation N/A refers to not available data.

Table 3.2. The values of interfacial molar mass changes ($\delta\Delta M$, g mol_{Pt}^{-1}) corresponding to different potential ranges defined by two potential limits ($\delta E = E_2 - E_1$) and the corresponding number of H_2O molecules (n_{H2O}), H_3O^+ cations (n_{H3O+}), (bi)sulfate anions (n_{AN}), and O_{chem} species (n_{Ochem}) interacting with per Pt surface atom. N/A refers to unavailable data.

	E_2 \ E_1	0.05 V	0.31 V	0.85 V	1.40 V
$\delta\Delta M$ (g mol_{Pt}^{-1})	0.05 V	--	–20.1 ± 1.4	–26.8 ± 1.9	–45.1 ± 2.1
	0.31 V	20.1 ± 1.4	0	–6.66 ± 0.51	–25.1 ± 1.8
	0.85 V	26.8 ± 1.9	6.66 ± 0.51	0	–18.4 ± 1.3
	1.40 V	45.1 ± 2.1	25.1 ± 1.8	18.4 ± 1.3	0
n_{H2O} (-)	0.05 V	--	–1.2	–1.1	N/A
	0.31 V	1.2	0	0.10	N/A
	0.85 V	1.1	–0.10	0	N/A
	1.40 V	N/A	N/A	N/A	0
n_{H3O+} (-)	0.05 V	--	0	0	N/A
	0.31 V	0	0	0	N/A
	0.85 V	0	0	0	N/A
	1.40 V	N/A	N/A	N/A	0
n_{AN} (-)	0.05 V	--	0	–0.087	0
	0.31 V	0	0	–0.087	0
	0.85 V	0.087	0.087	0	0.087
	1.40 V	0	0	–0.087	0
n_{Ochem} (-)	0.05 V	--	0	0	–0.92
	0.31 V	0	0	0	–0.92
	0.85 V	0	0	0	–0.92
	1.40 V	0.92	0.92	0.92	0

In the Introduction, we explain that the Sauerbrey equation refers to a flat surface and that any deviation from such an ideal state gives rise to a frequency change (see Δf_r in equation 3.2). Our experimental data indicate that the increase of the surface roughness by a given factor n (e.g. $n = 2$) increases the charge density associated with the electrochemical H adsorption and desorption as well as the surface oxide formation and reduction by the same factor n (here, $n = 2$). One would expect that the interfacial mass variation associated with these processes to scale up also by a factor of n but such a behavior is not observed. In fact, doubling the value of R does not double the value of interfacial mass change (it increases by a factor smaller than 2). However, the results presented in Figure 3.5 reveal a linear relationship between Δm and R for the four potential regions (the entire potential range EPR; the hydrogen adsorption range, HAR; the double-layer charging range, DLCR; and the surface oxide formation range, SOFR). These linear relationships allow the determination of the values of the y-intercepts (I) at $R = 1.00$ and the values of the respective slopes, S. It is important to add that each set of I and S values refers to a specific potential range (see Table 3.1). The linear trends observed in Figure 3.5 allow us to propose a modified version of the Sauerbrey equation that takes into account the surface roughness factor, which is as follows:

$$\Delta m_{R>1} = I + S(R-1) \tag{3.4}$$

where $I = \Delta m_{R=1}$ is the interfacial mass change for an atomically flat surface, thus for $R = 1.00$, and equals $\Delta m_{R=1} = - C_f \Delta f_{R=1}$; and $\Delta m_{R>1}$ is the interfacial mass change for an electrode the surface roughness of which is $R > 1.00$ and equals $\Delta m_{R>1} = - C_f \Delta f_{R>1}$. Thus, the modified Sauerbrey equation can also be written as follows:

$$\Delta m_{R>1} = - C_f \ \Delta f_{R=1} + S(R-1) \tag{3.5}$$

The observation that the values of *I* and *S* are different and that $I > S$ leads to very important remarks. The charge densities due to the electrochemical H adsorption and desorption as well as the surface oxide formation and reduction scale up with *R* but the interfacial mass variations do not. This implies that the surface roughness affects the structure of the interface, thus the number of H_2O molecules, anions, and H_3O^+ cations interacting with the Pt electrode surface. The "missing mass" can be interpreted as a lower degree of organization of the interface. Because H_2O molecules are involved in the hydration and transport of protons in the interfacial region, any modification of the double layer structure gives rise to different sequences of atomic level events and kinetics of electrochemical reactions involving protons, such as the hydrogen evolution and oxidation reactions (HER, HOR) as well as the oxygen evolution and reductions reactions (OER, ORR).

The possible dependence of the kinetics of these reactions on the surface roughness might have important consequences in the area of polymer electrolyte membrane fuel cells and water electrolysers, which employ Pt nanoparticles as electrocatalysts. The strong dependence of the interfacial mass variation on the surface roughness suggests that the interfacial behavior of Pt-based nanostructured catalysts (mainly nanoparticles) cannot be easily interpreted on the basis of experimental results obtained using single-crystal electrodes. These observations call for extensive research on the influence of surface roughness on the mechanisms and kinetics of electrochemical reactions, because it is reasonable to expect that the surface roughness will affect not only the HER, HOR, OER, and ORR, but also other processes such as electrodeposition and electro-dissolution. Because surface modifiers (e.g. surface smoothing agents) are often employed in industrial scale electrodeposition and electropolishing, it is expected that their interfacial behavior (surface coverage and orientation) might also depend on the morphology of

electrode materials. Consequently, application of EQCN in research on these processes might result in the observation of new phenomena that have received little attention until now.

3.4 Conclusions

We prepared Pt electrode of gradually increasing surface roughness and examined their behavior using cyclic-voltammetry and electrochemical quartz-crystal nanobalance. On the basis of these experiments, we report the values of interfacial mass changes associated with the electrochemical H adsorption and desorption as well as the surface oxide formation and reduction on Pt electrodes in relation to their surface roughness. These interfacial mass changes increase linearly with the surface roughness and their extrapolation to the roughness factor of 1.00 produces for the first time the interfacial mass responses for an *atomically flat polycrystalline Pt electrode*. The interfacial mass responses are converted to the interfacial molar mass changes expressed per 1 mol of Pt surface atom, which are then assigned to specific number of species interacting with a single Pt surface atom. The interfacial mass change for the entire potential range (EPR, here 0.05–1.40 V) is $\delta\Delta M_{EPR} = 45.1$ g mol_{Pt}^{-1}. The interfacial mass change for the hydrogen adsorption range (HAR) is $\delta\Delta M_{HAR} = 20.1$ g mol_{Pt}^{-1} and corresponds to 1 H_{UPD} adatom and 1.2 H_2O molecules. The interfacial mass change for the double-layer charging range (DLCR) is $\delta\Delta M_{DLCR} = 6.66$ g mol_{Pt}^{-1} and corresponds to 0.10 H_2O molecules and 0.087 anions. The interfacial mass change for the surface oxide formation range (SOFR) is $\delta\Delta M_{SOFR} = 18.4$ g mol_{Pt}^{-1} and corresponds to the addition 0.92 O adatoms and an unspecified number of H_2O and H_3O^+ species. The cyclic-voltammetry profiles for Pt electrodes of gradually increasing roughness reveal the same features and their normalization to a roughness factor of $R = 1.00$ yields overlapping profiles. This indicates that the polycrystalline nature of the electrodes remains the

same even when the surface roughness increases up to R = 13.0; thus, the ratio of the main crystallographic facets remains unaltered. Understanding of the nature and number of species interacting with each surface atom as the roughness of Pt electrodes gradually increases is of great importance to the polymer electrolyte membrane fuel cells and water electrolysers because it can affect the mechanisms and kinetics of the key electrochemical reactions involved in the conversion of chemicals into electrical energy and vice versa. The basic knowledge reported in this contribution will benefit computational efforts the objective of which is to model the platinum-polymer electrolyte membrane interface as a function of experimental parameters. Finally, the observation of a linear relationship between the interfacial mass variation and the surface roughness leads to a modified version of the Sauerbrey equation, which allows the determination of the interfacial mass response of Pt electrodes in different potential ranges in relation to its roughness.

3.5 References

(1) Sauerbrey, G. *Z. Phys.* **1959,** *155*, 206–222.

(2) Nomura, T.; Iijima, M. *Anal. Chim. Acta* **1981,** *131*, 97–102.

(3) Deakin, M. R.; Buttry, D. A. *Anal. Chem.* **1989,** *61*, 1147A–1154A.

(4) Hepel, M. In *Interfacial Electrochemistry: Theory, Experiment, and Applications;* Wieckowski, A., Ed.; Marcel Dekker: New York, 1999; pp 599–630.

(5) Gileadi, E. *Physical Electrochemistry: Fundamentals, Techniques and Applications;* WILEY-VCH: Weinheim, 2011; pp 253–264.

(6) Levi, M. D.; Salitra, G.; Levy, N.; Aurbach, D.; Maier, J. *Nat. Mater.* **2009,** *8*, 872–875.

(7) Tsai, W.; Taberna, P.; Simon, P. *J. Am. Chem. Soc.* **2014,** *136*, 8722–8728.

(8) Rice, C. A.; Betancourt, D.; Hepel, M. *Electrocatalysis* **2015,** *6,* 1–6.

(9) Trasatti, S. *J. Electroanal. Chem.* **1972,** *39,* 163–184.

(10) Jerkiewicz, G. *Prog. Surf. Sci.* **1998,** *57,* 137–186.

(11) Conway, B. E.; Jerkiewicz, G. *Electrochim. Acta* **2000,** *45,* 4075–4083.

(12) Jerkiewicz, G. *Electrocatalysis* **2010,** *1,* 179–199.

(13) Vetter, K. J.; Schultze, J. W. *J. Electroanal. Chem.* **1972,** *34,* 131–139.

(14) Vetter, K. J.; Schultze, J. W. *J. Electroanal. Chem.* **1972,** *34,* 141–158.

(15) Angerstein-Kozlowska, H.; Conway, B. E.; Sharp, W. B. A. *J. Electroanal. Chem.* **1973,** *43,* 9–36.

(16) Conway, B.E. *Prog. Surf. Sci.* **1995,** *49,* 331–452.

(17) Jerkiewicz, G.; Vatankhah, G.; Lessard, J.; Soriaga, M. P.; Park, Y. *Electrochim. Acta* **2004,** *49,* 1451–1459.

(18) Schumacher, R.; Borges, G.; Kanazawa, K. K. *Surf. Sci.* **1985,** *163,* L621–L626.

(19) Beck, R.; Pittermann, U.; Weil, K. G. *J. Electrochem. Soc.* **1992,** *139,* 453–461.

(20) Jerkiewicz, G.; Vatankahah, G.; Zolfaghari, A.; Lessard, J. *Electrochem. Commun.* **1999,** *1,* 419–424.

(21) Tremiliosi-Filho, G.; Jerkiewicz, G.; Conway, B. E. *Langmuir* **1992,** *8,* 658–667.

(22) Biegler, T. J.; Rand, D. A.; Woods, R. *J. Electroanal. Chem.* **1971,** *29,* 269–277.

(23) Shimazu, K.; Kita, H. *J. Electroanal. Chem.* **1992,** *341,* 361–367.

(24) Osawa, M.; Tsushima, M.; Mogami, H.; Samjeske, G.; Yamakata, A. *J. Phys. Chem. C* **2008,** *112,* 4248–4256.

(25) Jerkiewicz, G.; Vatankhah, G.; Tanaka, S.; Lessard, J. *Langmuir* **2011,** *27,* 4220–4226.

(26) Gamboa-Aldeco, M. E.; Herrero, E.; Zelenay, P. S.; Wieckowski, A. *J. Electroanal. Chem.* **1993,** *348,* 451–457.

(27) Kolics, A.; Wieckowski, A. *J. Phys. Chem. B* **2001,** *105,* 2588–2595.

(28) Birss, V. I.; Chang, M.; Segal, J. *J. Electroanal. Chem.* **1993,** *355,* 181–191.

(29) Frumkin, A. N.; Petrii, O. A. *Electrochim. Acta* **1975,** *20,* 347–359.

(30) Climent, V.; Feliu, J. M. *J. Solid State Electrochem.* **2011,** *15,* 1297–1315.

(31) Huang, J.; Malek, A.; Zhang, J.; Eikerling, M. H. *J. Phys. Chem. C* **2016,** *120,* 13587−13595.

(32) Reiss, H. in *Advances in Chemical Physics;* Prigogine, I., Ed.; Interscience: New York, 1965; Vol. 9, pp 1–84.

(33) *CRC Handbook of Chemistry and Physics*, 97th ed.; Boca Raton, FL, 2017; Chapter 4, p 143.

(34) Ataka, K.; Osawa, M. *Langmuir* **1998,** *14,* 951–959.

(35) Kunimatsu, K.; Samant, M. G.; Seki, H. *J. Electroanal. Chem.* **1989,** *258,* 163–177.

(36) Samant, M. G.; Kunimatsu, K.; Seki, H.; Philpott, M. R. *J. Electroanal. Chem.* **1990,** *280,* 391–401.

(37) Furuya, Y.; Mashio, T.; Ohma, A.; Dale, N.; Oshihara, K.; Jerkiewicz, G. *J. Chem. Phys.* **2014,** *141,* 164705.

Chapter 4

Influence of the Surface Roughness of Platinum Electrodes on the Calibration of the Electrochemical Quartz-Crystal Nanobalance

4.1 Introduction

The rising interest in sustainable energy storage and generation systems, such as water electrolysers and fuel cells, stimulates experimental research on the key electrochemical reactions occurring at their electrodes. The main objective of these research efforts is to understand the nature of electrochemical reactions and interfacial processes occurring in these systems that determine their efficiency and durability. The electrochemical quartz-crystal nanobalance (EQCN) is an important technique that measures *in-situ* mass changes associated with electrochemical processes occurring at the electrode surfaces.[1–3] It is also an attractive technique due to its high sensitivity and relatively low cost. Information acquired using the EQCN in conjunction with conventional electrochemical techniques, such as cyclic-voltammetry (CV), chronoamperometry (CA), and chronopotentiometry (CP), provides new insight into electrochemical processes and contributes to the understanding of their mechanisms at the atomic/molecular level. When evaluating the performance of electrochemical energy systems, one needs to examine the charge, energy, and mass balances. While the charge balance is typically studied using well-established electrochemical techniques and the energy (heat) balance using calorimetry and temperature-dependent studies, the mass balance assessment is frequently neglected due to lack of experimental approaches. However, the EQCN is a very suitable experimental approach and can measure interfacial mass changes even in the ng cm^{-2} range.[4]

A typical EQCN experimental setup employs a quartz-crystal resonator covered with a metallic layer (e.g. Au or Pt) that serves as a working electrode. Its resonant vibrational frequency (f_0) decreases upon mass addition and increases upon mass removal. The change in the resonant vibrational frequency (Δf) is converted into a mass changes (Δm) using the Sauerbrey equation:

$$\Delta m = -\frac{\sqrt{\mu_q \, \rho_q}}{2 \, f_0^2} \Delta f = -C_f \, \Delta f \tag{4.1}$$

where f_0 is the resonant frequency of the resonator prior to mass addition/removal, μ_q is the shear modulus of quartz (2.947×10^{11} g cm^{-1} s^{-2}), ρ_q is the density of quartz (2.648 g cm^{-3}), and C_f is the theoretical characteristic constant.[5] In the case of f_0 being 9.00 MHz, the theoretical characteristic constant equals 5.45 ng cm^{-2} Hz^{-1}. The technique was initially developed to study deposition of solids under vacuum conditions and was known as the quartz-crystal microbalance (QCM), it became an important electrochemical research tool.[1,6] The EQCN is applied in electrochemistry research with the objective of shedding light on the atomic/molecular level of interfacial processes, but its usefulness is strongly related to the accuracy of measurements and data analysis.

Ideally, one would like the frequency changes to be associated with the mass addition/removal, but there are other experimental factors that can cause a frequency change, such as temperature and pressure variation, density and viscosity changes in the electrode vicinity, stress/strain development in the deposit, and surface roughness modification.[1,2,7] Because typical CV, CA, and CP take only a few minutes, the temperature and pressure remain constant and their contribution to Δf is negligible. In the case of interfacial processes occurring at Pt electrodes, such as the electrochemical H adsorption/desorption or the surface oxide

formation/reduction, the density and viscosity of electrolyte do not change. In addition, these processes do not develop any stress/strain in the Pt deposit, thus their contribution to Δf is also negligible. However, the influence of surface roughness cannot be negligible because as it increases, the real surface area at which electrochemical processes occur also increases. The derivation of the Sauerbrey equation (equation 4.1) was based on the assumption that the resonator surface is completely flat. However, real electrode surfaces are never flat and their roughness has to be taken into account when interpreting EQCN results. There is a lot of interest in the interfacial electrochemical phenomena occurring at meso- and nano-structured or powder materials, because some electrochemical energy storage and generation technologies require large surface area materials.[8–10] However, the role of surface roughness is not taken into consideration because it has never been a subject of systematic research and there are no mathematical approaches. The influence of the surface roughness on the response of EQCN in the potential range of the electro-adsorption of H and surface oxide formation is the subject of a report of Kim *et al*.[11] They observed that an increase of the real surface by a factor *n* increased the charge associated with these interfacial electrochemical processes by exactly the factor of *n*, but the interfacial mass change by less than a factor of *n*. Based on those measurements, they proposed a modified version of the Sauerbrey equation that takes into account the surface roughness. The conversion of experimentally determined frequency changes to interfacial mass changes uses the Sauerbrey equation and the theoretical characteristic constant. However, it is unclear whether the theoretical value of the characteristic constant agrees with the one determined experimentally. In addition, it is unclear whether any deviation between these two values depends on the surface roughness of the EQCN resonator. Because the EQCN is an electroanalytical technique, each instrument should be calibrated using a suitable experimental approach so that the values of the theoretical and experimental characteristic constants (C_f and $C_{f,exp}$, respectively).[12] However, this

is not the case and, consequently, some quantitative results reported in the literature might be incorrect.

In this contribution, we report on the influence of the surface roughness of Pt-coated resonators on the value of the experimental characteristic constant. The surface roughness of Pt-coated resonators is steadily increased by Pt electrodeposition and the values of $C_{f,exp}$ are determined using Ag deposition. The surface roughness of the Pt electrodes is examined using the electro-adsorption of H as a probe and the atomic force microscopy. The values of $C_{f,exp}$ are compared to those determined using the Sauerbrey equation (C_f) and examine any correlations between these two.

4.2 Experimental

Electrochemical experiments were conducted using a Bio-Logic model SP-150 potentiostat/galvanostat and a Seiko-EG&G model QCA 922 quartz crystal analyzer. All electrochemical experiments were performed within a custom-built vibration-isolated Faraday cage, which was suspended on flexible rubber bands from an external frame to minimize mechanical interferences from the outside environment. Measurements were carried out in a custom-made Pyrex two-compartment electrochemical cell. The working and counter electrodes were placed in the main compartment and the reference electrode in the second one. The second compartment was connected to the main compartment through a Luggin capillary. A platinum-coated quartz-crystal resonator (Seiko-EG&G, QA-A9M-PT) having a resonant frequency of ca. 9.00 MHz served as the working electrode; it was placed in a Teflon holder that was attached horizontally to the bottom of the EQCN cell.[13] One of the Pt-coated sides on the resonator was in contact with the electrolyte; its geometric surface area was 0.196 cm^2. A platinum gauze (Alfa

Aesar, 99.9%) spot-welded to a Pt wire (Alfa Aesar, 99.95%) was used as a counter electrode and its surface area was more than ten times that of the working electrode. A reversible hydrogen electrode (RHE), which consisted of Pt wire (Alfa Aesar, 99.95%) covered with a thin layer of electrodeposited Pt black, was used as the reference electrode. A high purity 0.50 M aqueous H_2SO_4 electrolyte solution for CV and mass variation (MV) measurements was prepared using concentrated H_2SO_4 (Fluka Analytical, TraceSELECT ≥95%) and ultra-high purity (UHP) water (Millipore, 18.2 MΩ cm). A solution of 0.20 mM H_2PtCl_6 in 0.50 M aqueous H_2SO_4 was used to electrodeposit Pt to increase the electrode surface roughness. A solution of 1.5 mM Ag_2SO_4 in 0.50 M aqueous H_2SO_4 was used to electrodeposit Ag in order to calibrate the instrument. The 0.20 mM H_2PtCl_6 and 1.5 mM Ag_2SO_4 solutions were prepared using $H_2PtCl_6 \cdot 6H_2O$ (Alfa Aesar, 99.9%) and Ag_2SO_4 (Aldrich, 99.999%), respectively. Ultra-high purity Ar(g) (Praxair, 5.0 grade) was purged through the main compartment for 1 hour prior to the commencement of CV and MV measurements or prior to Pt electrodeposition to expel any reactive gasses from the solutions.

Preconditioning. Prior to the commencement of all experiments, the as-purchased Pt-coated resonator was preconditioned by potential cycling 1000 times in the range of E = 0.05–1.50 V using a potential scan rate of s = 50.0 mV s^{-1} in outgassed 0.50 M aqueous H_2SO_4 solution at T = 298 K. After the preconditioning, the electrolyte was exchanged for a new batch to ensure maximum cleanliness of the system, and then CV and MV measurements were conducted.

Increasing the surface roughness of electrodes via Pt electrodeposition. Platinum electrodeposition on the Pt-coated resonator was conducted to fine-tune the surface roughness of the working electrode. The Pt electrodeposition was accomplished using chronoamperometry at the potential of E = 0.20 V for t = 30.0 s in an outgassed 0.50 M aqueous H_2SO_4 solution containing 0.20 mM H_2PtCl_6 at T = 298 K. As the number of the Pt electrodeposition cycles increased, the value of R of the electrode was raised.

CV and MV measurements for roughened Pt electrodes. After the Pt electrodeposition, the electrochemical cell was thoroughly rinsed using UHP water and filled with a fresh batch of 0.50 M aqueous H_2SO_4 solution. Then, the electrodeposited Pt electrode was pretreated using potential cycling (ca. 300 times) in the E = 0.05–1.40 V range at a potential scan rate of s = 50.0 mV s^{-1} in outgassed 0.50 M aqueous H_2SO_4 solution at T = 298 K. This process is known as the electrochemical annealing; it releases any stress from the near-surface region of the electrodeposited Pt and produced a CV profile characteristic of a polycrystalline Pt electrode.[14] Afterward, the electrolyte was changed for a fresh batch of outgassed 0.50 M aqueous H_2SO_4 solution and CV and MV measurements were carried out simultaneously in the range of E = 0.05–1.40 V at a potential scan rate of s = 50.0 mV s^{-1} and T = 298K. Ten MV measurements were conducted and their average is reported in this contribution. This approach improved the signal-to-noise ratio of the MV transients. The electrochemically active surface area (A_{ecsa}) of the electrodeposited Pt electrode was calculated using the charge density (210 μC cm^{-2}) associated with the formation of one monolayer (ML) under-potential deposited H.[15] The values of the surface roughness factor (R) of the electrodeposited Pt electrodes were calculated by dividing A_{ecsa} by the geometric surface area (A_g = 0.196 cm^2 in this study) of the working electrode.

Analysis of the values of the experimental characteristic constant via Ag electrodeposition. The values of the experimental characteristic constant ($C_{f,exp}$) for the Pt electrodes having a gradually increasing surface roughness were investigated by means of a galvanostatic Ag electrodeposition. The Ag electrodeposition was conducted in 0.50 M aqueous H_2SO_4 solution containing 1.5 mM Ag_2SO_4 using chronopotentiometry (CP) by applying a defined current density of j = 50.0 μA cm^{-2} for pre-defined periods of time. Each electrodeposition time was adjusted in order to obtain the charge density required to form seven monolayers (ML) of Ag deposit. Thus, as the value of R gradually increased, the Ag electrodeposition time was also increased. Afterward, the electrodeposited Ag layer was stripped

by means of linear sweep voltammetry from the open circuit potential to 0.775 V at a potential scan rate of s = 1.0 mV s^{-1}. After the Ag stripping, the electrode and the cell were rinsed with 15 wt.% HNO_3 solution followed by thorough rinsing with UHP water. The Ag electrodeposition-stripping experiment was repeated three times to ensure good reproducibility of the results. Such determined three $C_{f,exp}$ values were averaged and the average value is reported in this paper. All the Ag electrodeposition experiments were conducted at room temperature (T = 298 K). The topography of the electrodeposited Ag layers was examined using an atomic force microscope (AFM), Veeco Instruments MultiMode V. The AFM measurements were performed in a contact mode using a silicon nitride tip (k = 0.12 N m^{-1}) at a tip speed of 1.0 μm s^{-1} under ambient conditions.

4.3 Results and discussion

The preparation of Pt electrodes of steadily increasing surface roughness and the characteristics of their surface morphology are discussed in *Chapter 3*.[11] Figure 4.1 presents CV profiles (A) and corresponding frequency variation (FV) transients (B) for Pt electrodes having a gradually increasing surface roughness recorded in 0.50 M aqueous H_2SO_4 at a potential scan rate of s = 50.0 mV s^{-1} and T = 298 K. The brown CV profile and FV transient were obtained using an as-received but preconditioned Pt electrode (see *Section 4.2 Experimental* for the details of preconditioning) having a roughness factor of R = 1.61. They are characteristic of a clean system and reveals the usual features associated with the electrochemical H adsorption/desorption as well as the surface oxide formation/reduction.[16,17]

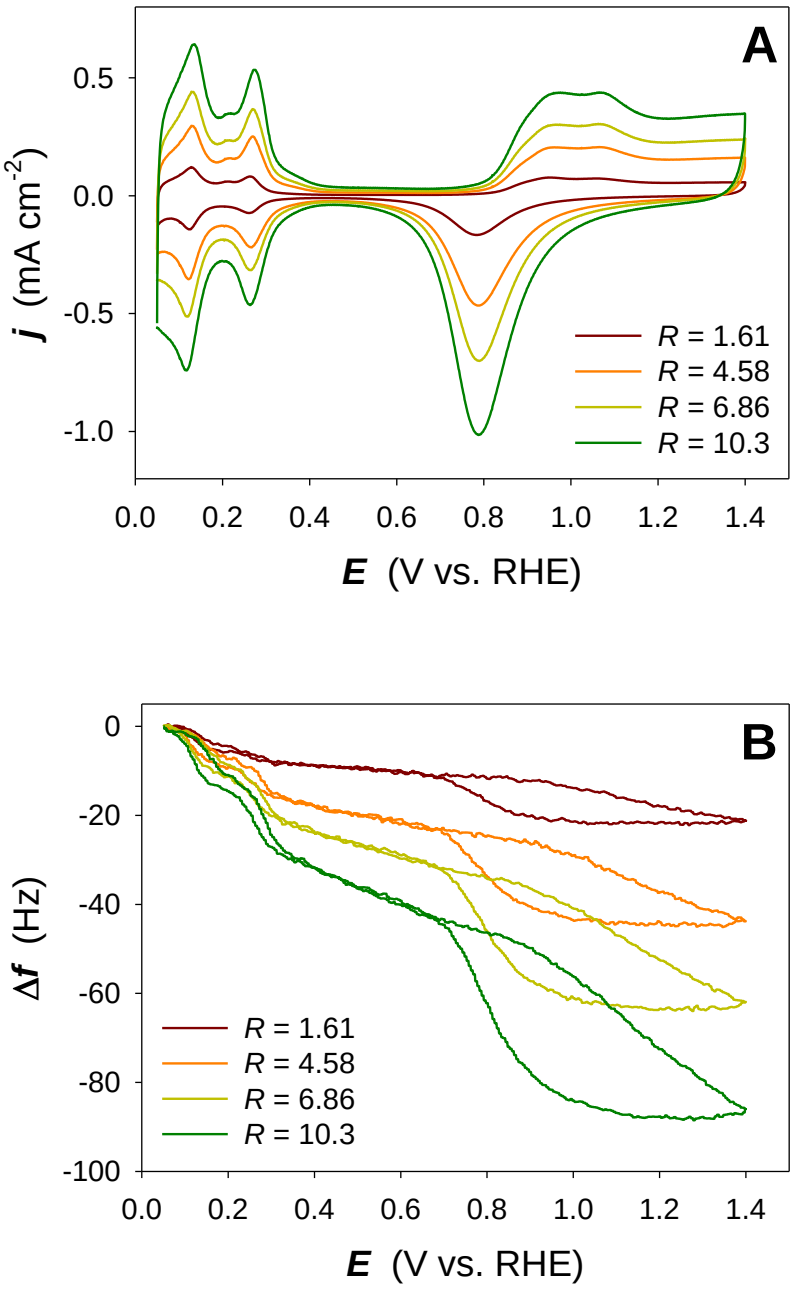

Figure 4.1. Cyclic-voltammetry profiles (**A**) and simultaneously recorded frequency variation transients (**B**) for Pt electrodes having the surface roughness factor of R = 1.61, 4.58, 6.86, and 10.3 acquired in 0.50 M aqueous H_2SO_4 at a potential scan rate of s = 50.0 mV s^{-1} and T = 298 K.

The subsequent CV profiles and FV transients refer to Pt electrodes of gradually increasing surface roughness. As the surface roughness of the Pt electrode increases by a factor of *n*, the corresponding current density values of each CV feature and the respective charge density values scale up by the same factor. However, the corresponding values of Δf increase by less than a factor of *n*. This behavior is the subject of a separate contribution and a detailed data analysis.[11] The values of *R* for each Pt electrode were obtained by comparing A_{ecsa} to A_g of the electrode, while the values of A_{ecsa} were determined by determining the charge density associated with the electrochemical H adsorption/desorption.[15] Therefore, the value of *R* is linearly related to the number of Pt surface atoms interacting with the electrolyte components facilitating the electro-adsorption of H.

In order to calibrate the EQCN system for Pt electrodes having a gradually increasing surface roughness, Ag was electrodeposited galvanostatically on each Pt electrode. The electrodeposition of Ag was extensively studied and is known to follow the Frank-van der Merwe mechanism.[18–21] According to this growth mechanism, the formation of a new atomic layer does not start until the formation of preceding layer is completed. The electrodeposit develops a smooth layer across the entire surface up to ca. ten MLs.[22] Figure 4.2A presents a charge density (*q*) versus time (*t*) profile for the Ag electrodeposition at a constant current density of $j = 50.0$ μA cm^{-2} on an as-received Pt electrode having a surface roughness of $R = 1.61$ in 0.50 M aqueous H_2SO_4 solution containing 1.5 mM Ag_2SO_4. As expected, the absolute value of *q* increases linearly with the electrodeposition time (it is negative because it is a cathodic process). Figure 4.2B presents a simultaneously recorded frequency variation (FV) transient associated with the Ag electrodeposition. It shows that the absolute value of Δf also increased linearly with the electrodeposition time; the value of Δf is negative because mass addition decreases the resonant frequency.

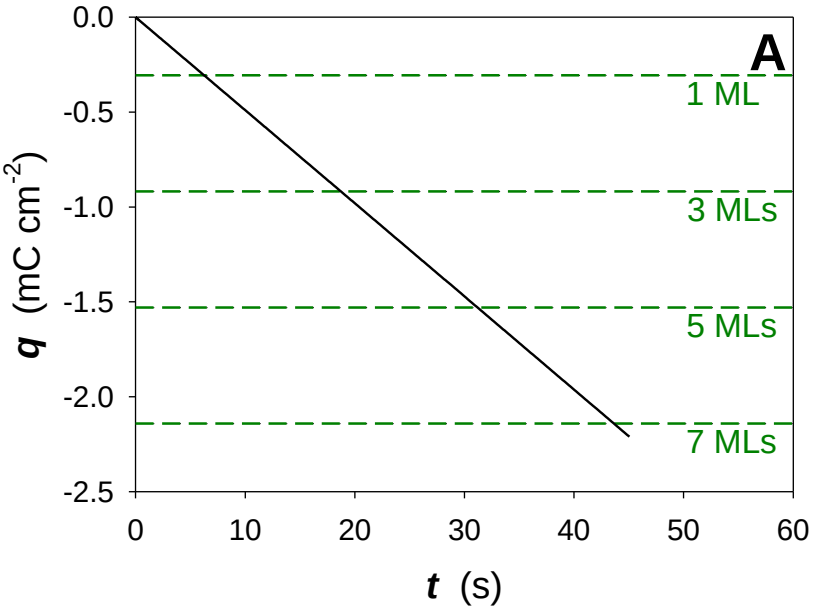
A
1 ML
3 MLs
5 MLs
7 MLs
0.0
-0.5
-1.0
-1.5
-2.0
-2.5
q (mC cm-2)
0
10
20
30
40
50
60
t (s)

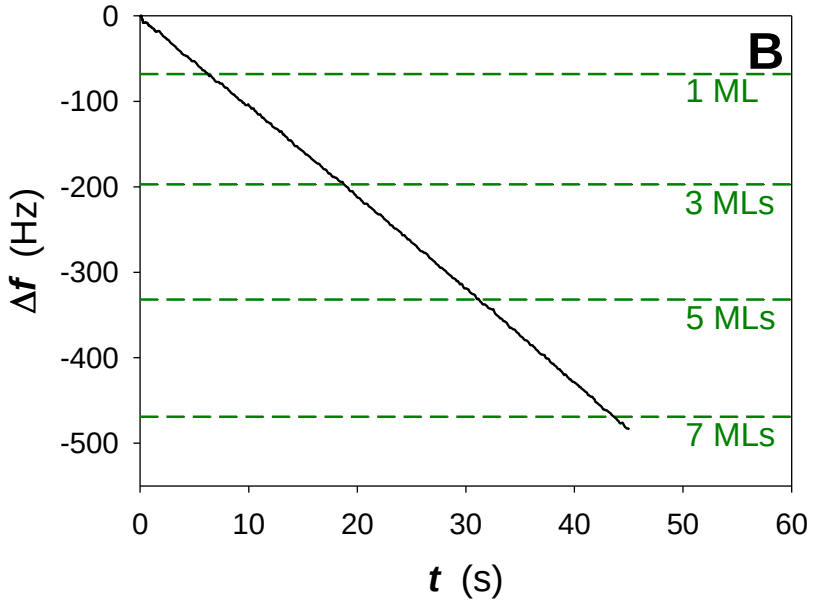
B
1 ML
3 MLs
5 MLs
7 MLs
0
-100
-200
-300
-400
-500
Δf (Hz)
0
10
20
30
40
50
60
t (s)

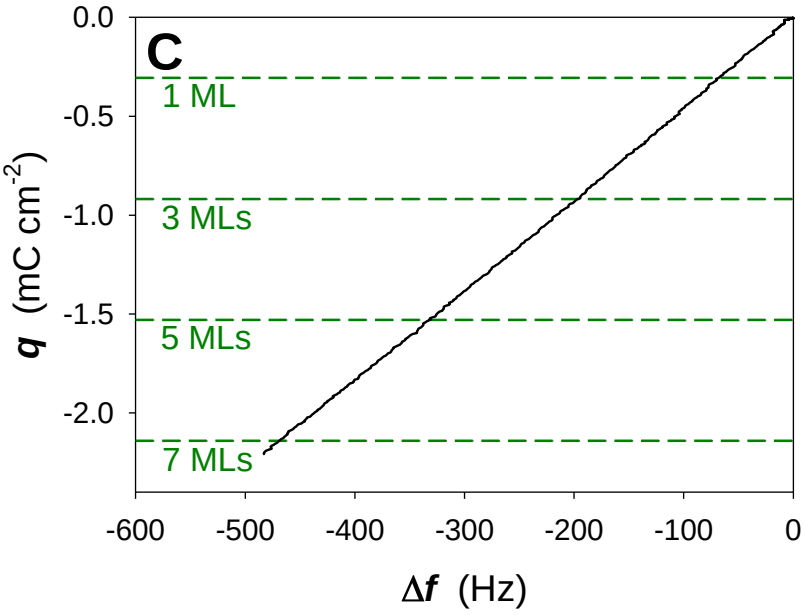

Figure 4.2. A charge density (q) versus time (t) profile (**A**) and a simultaneously recorded frequency variation transient (**B**) for Ag electrodeposition at a current density of j = 50.0 µA cm^{-2} on a Pt electrode having a surface roughness factor of R = 1.61 acquired in 0.50 M aqueous H_2SO_4 + 1.5 mM Ag_2SO_4 solution at T = 298 K; a charge density (q) versus frequency variation (Δf) plot (**C**) obtained by combining the plots shown in the graphs (**A**) and (**B**).

A combination of these two transients generates a linear plot of q versus Δf (Figure 4.2C). The green dashed lines in Figures 4.2A through 4.2C refer to the values of q corresponding to the Ag electrodeposit being 1, 3, 5, and 7 monolayers (MLs) in thickness. Application of the Faraday's law (equation 4.2) facilitates the conversion of the q values into values of Δm, bearing in mind that the number of electrons transferred per Ag atom is z = 1 and the atomic weight of Ag is W = 107.87 g mol^{-1}; F is the Faraday constant (F = 96485.3 C mol^{-1}).

$$q = \left(\frac{\Delta m}{W}\right) z\, F \qquad (4.2)$$

Rearrangement of this equation (isolation of Δm) and its substitution into equation 4.1 leads to the following formula, which allows determination of the value of the experimental characteristic constant:

$$C_{\mathrm{f,exp}} = -\left(\frac{W}{z\,F}\right)\left(\frac{q}{\Delta f}\right) \tag{4.3}$$

where $q/\Delta f$ is the slope of the plot shown in Figure 4.2C. Because the q versus Δf shows only one linear region, $C_{\mathrm{f,exp}}$ has only one value of $C_{\mathrm{f,exp}} = 5.18$ ng cm^{-2} Hz^{-1}. The tiny deviations from linearity over the initial 30 Hz region are due to the formation of Ag nuclei, which eventually merge and form a complete monolayer. Consequently, only the region corresponding to the formation of 2–7 MLs of Ag deposit is used in the determination of the value of $C_{\mathrm{f,exp}}$.[19,23–25] In *Appendix B*, we present analogous plots for Pt electrodes having different surface roughness values, namely 4.58, 6.86, and 10.3. These results are used to determine the value of $C_{\mathrm{f,exp}}$ for these four values of R.

In order to examine the surface morphology of the multi-layer Ag deposits, we employed atomic force microscopy (AFM) and conducted surface topography studies in the contact mode. Figures 4.3A and 4.3B depict AFM images and line profiles of the Pt electrodes having the surface roughness factor of 1.70 and 12.1, respectively. Figures 4.3C and 4.3D present AFM images and line profiles of the two Pt electrodes after electrodeposition of 5 MLs of Ag. Although we present AFM results for Ag deposits being 5 ML in thickness, there are representative of the overall trend. The AFM images presented here cover 5.00 μm in both the x and y directions as well as 400 nm and 800 nm in the z direction.

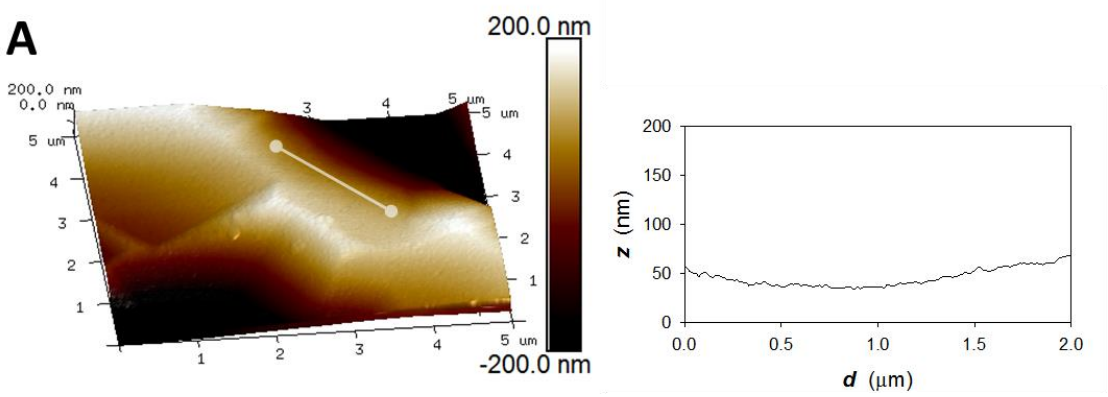
A
200.0 nm
200.0 nm
0.0 nm
-200.0 nm
z (nm)
d (µm)

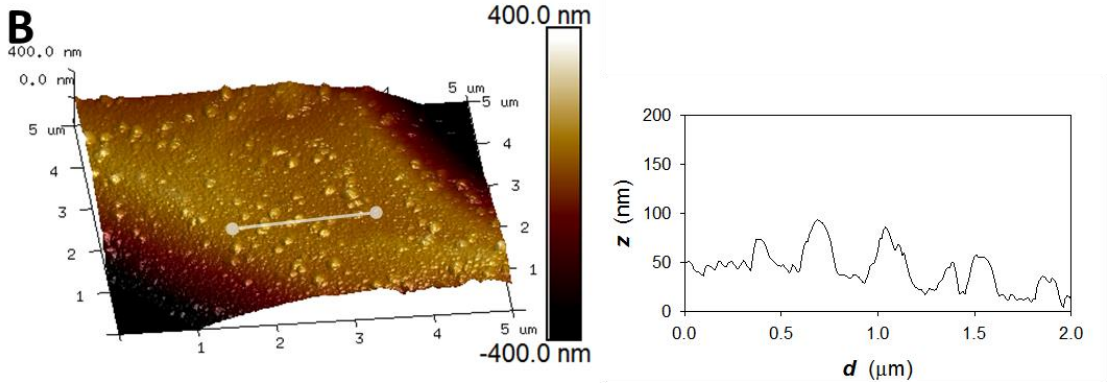
B
400.0 nm
400.0 nm
0.0 nm
-400.0 nm
z (nm)
d (µm)

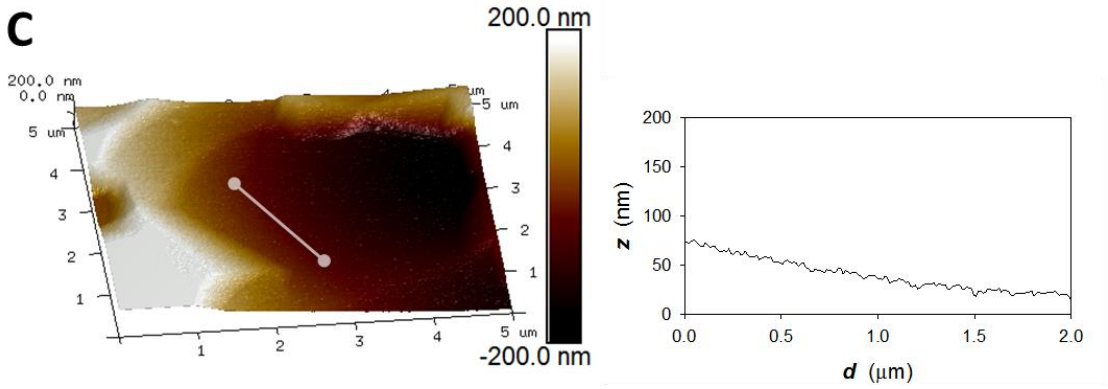
C
200.0 nm
200.0 nm
0.0 nm
-200.0 nm
z (nm)
d (µm)

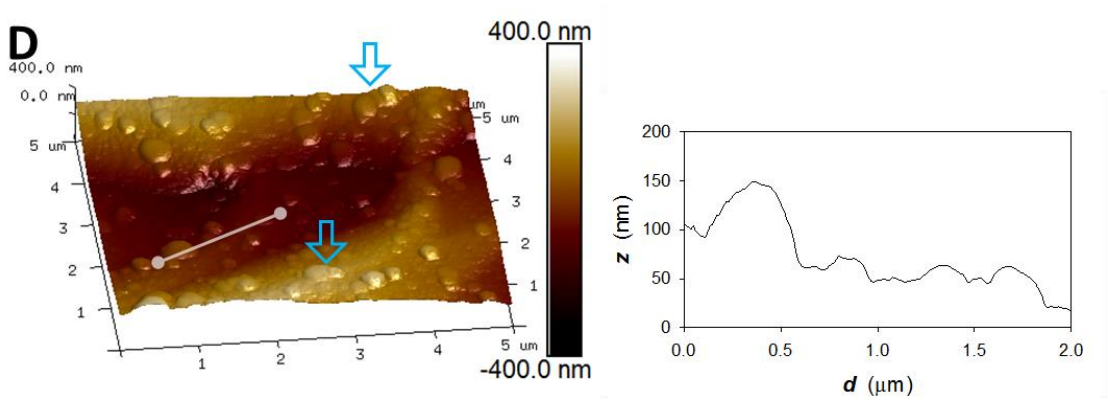

Figure 4.3. Atomic force microscopy images and line profiles for Pt electrodes prior to Ag electrodeposition having the surface roughness of R = 1.70 (**A**) and R = 12.1 (**B**). Atomic force microscopy images and line profiles of the same electrodes after electrodeposition of 5 MLs of Ag; the graphs (**C**) and (**D**) refer to R = 1.70 and R = 12.1, respectively. The blue arrows in the graphs (**D**) indicate large islands that develop through the merger of medium size islands.

In order to present the true (undistorted) morphology of the Pt surface prior to and after Ag deposition, the scale of the *x*, *y*, and *z* axes is the same. The AFM image and line profile of the Pt electrode with R = 1.70 prior to the electrodeposition of Ag (Figure 4.3A) reveal smooth faces and edges. After the electrodeposition of Ag, the surface preserves its main morphological features and shows similar characteristics (Figure 4.3C). Thus, the Ag deposit mimics the surface of the underlying Pt substrate, which is expected because the electrodeposition of Ag follows the Frank-van der Merwe growth mechanism. The AFM image and line profile of Pt electrode with R = 12.1 prior to the electrodeposition of Ag (Figure 4.3B) reveal a roughened surface with uniformly distributed small islands and randomly distributed medium size islands. The height and the width of the medium size islands are in the 40–80 nm and 100–300 nm ranges, respectively. After the electrodeposition of Ag (Figure 4.3D), the surface consists of mainly medium size and large islands; the small islands are practically indistinguishable. The average size of the medium size and large islands is significantly greater than the size of these features

prior to the electrodeposition of Ag. The large islands most likely develop through the merger of medium size islands (the blue arrows in Figure 4.3D). Following the electrodeposition of Ag, the height and the width of the medium size and large islands are in the 30–80 nm and 200–500 nm ranges, respectively. Although the AFM images and line profiles presented in Figures 4.3B and 4.3D reveal some structural changes (the large islands) brought about by the electrodeposition of Ag, the morphology and height of a majority of these surface features resemble that of the substrate prior to the formation of Ag deposit. We were not able to perform AFM measurements at identical locations on the electrode surface, but the AFM results are a good representation of the surface roughness of the Pt electrodes prior to and after their roughening through Pt electrodeposition, as well as prior to and after the electrodeposition of Ag.

In Figure 4.2 and *Appendix B*, we present an approach used to determine the value of $C_{f,exp}$ for Pt electrodes having different surface roughness, namely R = 1.61, 4.58, 6.86, and 10.3. We performed analogous experiments for other values of R covering the 1.61–13.0 range in order to identify any trend. The green squares in Figure 4.4 present the evolution of $C_{f,exp}$ values as s function of R; the black, horizontal dashed line represents the theoretical value of C_f, which is C_f = 5.45 ng Hz^{-1} cm^{-2}. The values of $C_{f,exp}$ are distributed over a relatively narrow range; it increases from 5.18 ng Hz^{-1} cm^{-2} for the lowest surface roughness of R = 1.61 to 5.98 ng Hz^{-1} cm^{-2} for the highest surface roughness of R = 13.0. An analysis of the trend using different mathematical equations revealed that they follow a logarithmic relationship.

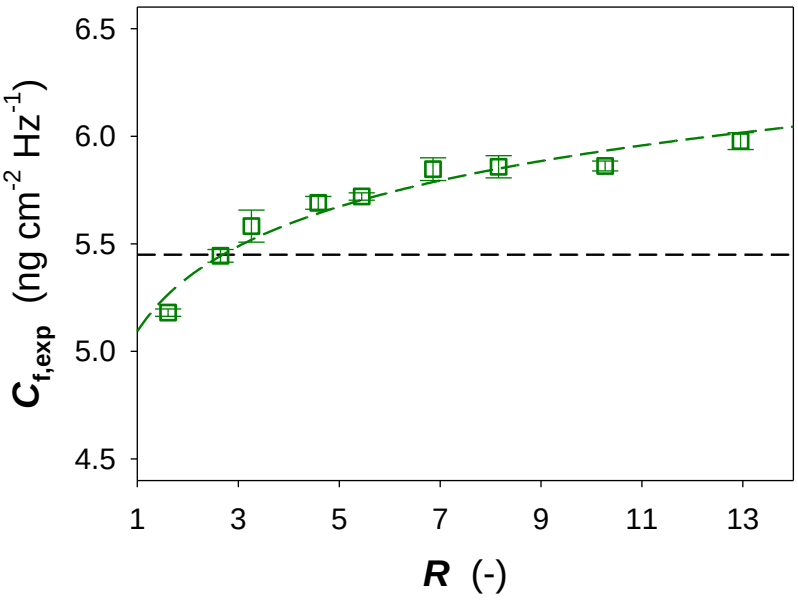

Figure 4.4. A plot showing the relationship between the values of the experimental characteristic constant ($C_{f,exp}$, green squares) and the surface roughness factor (R) for Pt-coated resonators. The black dashed line refers the value of the theoretical characteristic constant (C_f = 5.45 ng cm^{-2}).

The logarithmic equation presented below and developed through data fitting relates the values of $C_{f,exp}$ to C_f and R, and two fitting parameters, α and β:

$$C_{f,exp} = C_f \left(\alpha + \beta \ln R\right) \tag{4.4}$$

where $\alpha = 0.935 \pm 0.009$ and $\beta = 0.066 \pm 0.006$. The green dashed line represents the best fit using this mathematical expression (the square of the correlation coefficient equals 0.952). In the case of R = 1.00, thus the surface is polycrystalline in nature but atomically flat, the parameters α determines how the value of $C_{f,exp}$ relates to the value of C_f. The parameter β is a measure of the rise of $C_{f,exp}$ with increasing R. The experimental characteristic constant ($C_{f,exp}$) adopts the same

value as the theoretical one (C_f = 5.45 ng Hz^{-1} cm^{-2}) in the case of R = 2.69 (the cross-over point).

The theoretical and experimental values of the characteristic constant (C_f and $C_{f,exp}$) were employed to convert the FV transients (Figure 4.1B) into mass variation (MV) transients for Pt electrodes having the four values of R. The MV transients shown in Figure 4.5A were obtained using the theoretical characteristic constant (C_f = 5.45 ng Hz^{-1} cm^{-2}) and the MV transients presented in Figure 4.5B were obtained using the experimental characteristic constant ($C_{f,exp}$), with the value of $C_{f,exp}$ being different for each specific value of R, as in Figure 4.4. Although the MV transients shown in Figures 4.5A and 4.5B reveal the same characteristics, the values of Δm are different. Because $C_f = C_{f,exp}$ only in the case of R = 2.69 (the cross-over point), the difference in the values of Δm obtained using C_f and $C_{f,exp}$ is related to the magnitude of ΔR, where $\Delta R = R - 2.69$. We used the values of Δm presented in Figures 4.5A and 4.5B to determine the values of $\delta\Delta m$ covering the 0.05–1.40 V range, thus being defined by the following equation:

$$\delta\Delta m = \Delta m_{E=1.40\,\mathrm{V}} - \Delta m_{E=0.05\,\mathrm{V}} \tag{4.5}$$

The black triangles in Figure 4.6 present the values of $\delta\Delta m$ determined using the Δm data shown in Figure 4.5A, and the green squares in Figure 4.6 present the values of $\delta\Delta m$ determined using the Δm data shown in Figure 4.5B. In both instances, the values of $\delta\Delta m$ increase linearly with R, but the trends have slightly different slopes. The experimental data (the black triangles and green squares) were fitted using a linear regression and the fitting outcome is presented as black and green dashed lines; in both cases, the square of the correlation coefficient is 0.999.

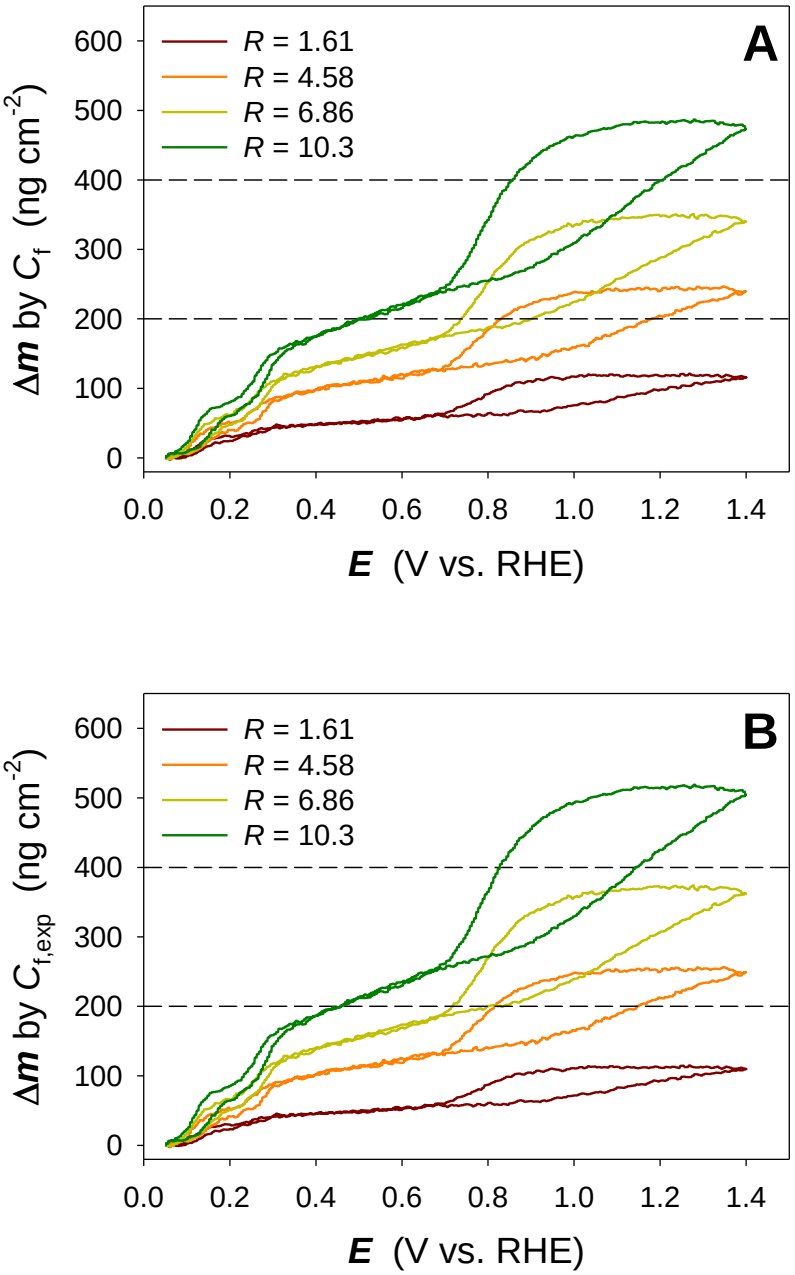

Figure 4.5. Mass variation transients converted from frequency variations transients shown Figure 1B using the C_f value (**A**) and the $C_{f,exp}$ values for specific values of R (**B**).

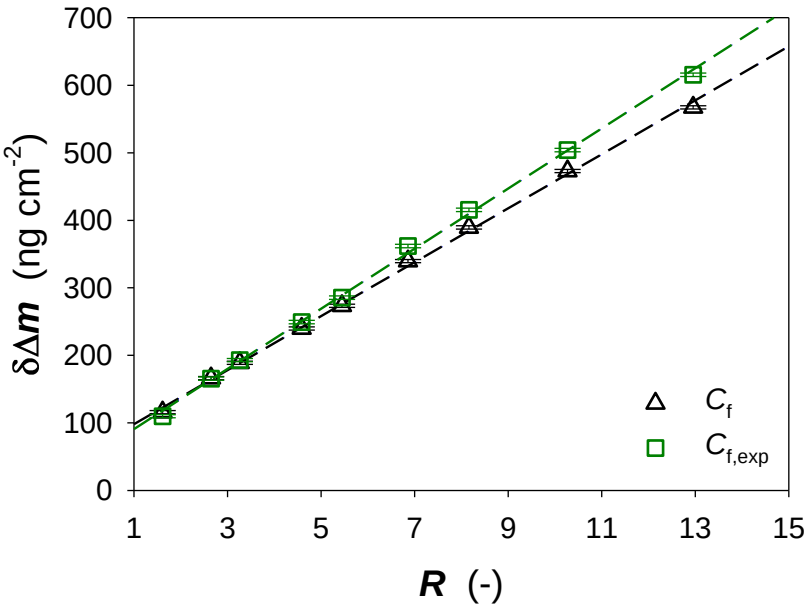

Figure 4.6. Values of the mass variation ($\delta\Delta m = \Delta m_{E=1.40\text{V}} - \Delta m_{E=0.05\text{V}}$) for a complete cyclic-voltammetry profile covering the 0.05–1.40 V range. The $\delta\Delta m$ values obtained using the value of C_f are shown as black triangles and those obtained using the values of $C_{f,exp}$ for specific values of R are shown as green square.

Their extrapolating to R = 1.00 yields the values of $\delta\Delta m$ for an atomically flat polycrystalline Pt electrode, and they are 98.2 ± 4.5 ng cm^{-2} (for C_f) and 90.7 ± 4.9 ng cm^{-2} (for $C_{f,exp}$), respectively; they differ by ca. 7.6%. In the case of the as-received Pt electrode having R = 1.61, the respective values of $\delta\Delta m$ are 116 ± 2 ng cm^{-2} (for C_f) and 110 ± 2 ng cm^{-2} (for $C_{f,exp}$); they differ by ca. 5.2%. EQCN measurements involve several sources of experimental uncertainty and the limit of detection (LOD) and the limit of quantification (LOQ) of the EQCN are 3 ng cm^{-2} and 9 ng cm^{-2}, respectively.[4] Because 5.2% of 116 ng cm^{-2} or 110 ng cm^{-2} corresponds to less than the LOQ of the EQCN, both the theoretical and experimental characteristic constants can be used to analyze the data obtained using the EQCN experimental setup employed in the course of our research.

The respective slopes of the $\delta\Delta m$ versus R plots (Figure 4.6) are 40.0 ± 0.5 gm cm^{-2} (for C_f) and

44.5 ± 0.6 ng cm^{-2} (for $C_{f,exp}$), thus they differ by ca. 11%. This difference indicates that in the case of Pt electrodes having significant surface roughness, the determination of $\delta\Delta m$ requires the knowledge of $C_{f,exp}$ because the application of C_f would results in a discrepancy that significantly exceed the technique's LOQ. Consequently, a similar analysis and an evaluation of $C_{f,exp}$ should be performed using a different EQCN setup than the one employed in the course of our research.

4.4 Conclusions

This study explores the influence of surface roughness of Pt electrodes on the frequency response of the electrochemical quartz-crystal nanobalance (EQCN). An entire set of Pt-coated resonators of gradually increasing surface roughness was prepared via Pt electrodeposition. Then, a thin layer of Ag (up to ca. 7 monolayers) was electrodeposited; the charge density (q) and frequency change (Δf) associated with this process were measured concurrently. Atomic force microscopy (AFM) was employed to examine the surface morphology of the Pt-coated resonators prior to and after Ag electrodeposition. The AFM results, images and line profiles, indicated that the electrodeposition of Ag followed the Frank-van der Merwe growth mechanism, thus that the Ag deposit mimicked the surface topography of the underlying Pt substrate. Plots of q versus Δf yielded the values of the experimental characteristic constant ($C_{f,exp}$) for each resonator having its unique value of the surface roughness factor (R). The values of $C_{f,exp}$ were found to differ from the value of the theoretical (calculated) C_f, which refers to an atomically flat surface. In addition, the values of $C_{f,exp}$ were found to increase logarithmically with rising values of R. The values of the theoretical and experimental characteristic constants were used to determine the interfacial mass changes ($\delta\Delta m = \Delta m_{E=1.40V} - \Delta m_{E=0.05V}$) associated with a complete cyclic-voltammetry profile covering the 0.05–1.40 V range. Because C_f and $C_{f,exp}$ have different values, the values of

$\delta\Delta m$ did not agree and their discrepancy increased with rising R. This discrepancy was small in the case of Pt electrodes being relatively smooth (as-received, polished Pt-coated resonators); it was smaller than the limit of quantification (LOQ) of the EQCN set-up, which was 9 ng cm^{-2}. Thus, in the case of as-received Pt-coated resonators and having relatively smooth surfaces, both C_f and $C_{f,exp}$ can be used to convert Δf results to Δm values. However, in the case of rough Pt-coated resonators as well as meso- and nano-structured materials, the conversion of Δf to Δm requires the knowledge of $C_{f,exp}$, which needs to be determined through calibrating the instrument. In the case of electrodes with an extended surface area, direct application of the theoretical characteristic constant would result in significant under-evaluation of mass changes associated with interfacial electrochemical processes. This is of particular importance to electrochemical technologies, such as polymer electrolyte membrane fuel cells and water electrolysers, where interfacial mass changes could shed light on the nature and number of electrolyte components interacting with electrode surfaces. The latter is very important because it affects the kinetics of electron transfer in the slowest reactions, i.e. the oxygen reduction and oxygen evolution reactions. The EQCN is a powerful technique that can be used to study other electrochemical processes, such as electro-oxidation and corrosion of metals and alloys, electrodeposition, and electro-polymerization. It can also be applied to monitor interfacial states of materials used in electrochemical supercapacitors. However, its application in quantitative data analysis requires knowledge of the morphology of electrode materials and the value of the characteristic constant. In summary, the EQCN is a very powerful and relatively inexpensive experimental technique that can be effectively used to investigate a broad range of electrochemical processes but its application requires determination of the limits of detection and quantification, as well as the characteristic constant.

4.5 References

(1) Hepel, M. In *Interfacial Electrochemistry: Theory, Experiment, and Applications;* Wieckowski, A., Ed.; Marcel Dekker: New York, 1999; pp 599–630.

(2) Gileadi, E. *Physical Electrochemistry: Fundamentals, Techniques and Applications;* Wiley-VCH: Weinheim, 2011; pp 253–264.

(3) Buttry, D. A. In *Electrochemical Interfaces: Modern Techniques for In-Situ Interface Characterization;* Abruna, H. D., Ed.; VCH: New York, 1991; pp 529–566.

(4) Kim, J.; Munro, A.; Beauchemin, D.; Jerkiewicz, G. *Anal. Chem.* **2016,** *88,* 10599–10604.

(5) Sauerbrey, G. *Z. Phys.* **1959,** *155,* 206–222.

(6) Bruckenstein, S.; Shay, M. *Electrochim. Acta* **1985,** *30,* 1295–1300.

(7) Kanazawa, K. K.; Gordon, J. G. *Anal. Chem.* **1985,** *57,* 1770–1771.

(8) Levi, M. D.; Salitra, G.; Levy, N.; Aurbach, D.; Maier, J. *Nat. Mater.* **2009,** *8,* 872–875.

(9) Tsai, W.; Taberna, P.; Simon, P. *J. Am. Chem. Soc.* **2014,** *136,* 8722–8728.

(10) Rice, C. A.; Betancourt, D.; Hepel, M. *Electrocatalysis* **2015,** *6,* 1–6.

(11) Kim, J.; Urchaga, P.; Baranton, S.; Coutanceau, C.; Jerkiewicz, G. *submitted*.

(12) Vatankhah, G.; Lessard, J.; Jerkiewicz, G.; Zolfaghari, A.; Conway, B. E. *Electrochim. Acta* **2003,** *48,* 1613–1622.

(13) Jerkiewicz, G.; Vatankhah, G.; Zolfaghari, A.; Lessard, J. *Electrochem. Commun.* **1999,** *1,* 419–424.

(14) Tremiliosi-Filho, G.; Jerkiewicz, G.; Conway, B. E. *Langmuir* **1992,** *8,* 658–667.

(15) Biegler, T.; Rand, D. A. J.; Woods, R. *J. Electroanal. Chem.* **1971**, *29*, 269–277.

(16) Jerkiewicz, G.; Vatankhah, G.; Lessard, J.; Soriaga, M. P.; Park, Y. *Electrochim. Acta* **2004,** *49,* 1451–1459.

(17) Jerkiewicz, G.; Vatankhah, G.; Tanaka, S.; Lessard, J. *Langmuir* **2011,** *27,* 4220–4226.

(18) Budevski, E. B. In *Comprehensive Treatise of Electrochemistry;* Conway, B. E.; Bockris, J. O'M.; Yeager, E.; Khan, S. U. M.; White, R. E., Eds.; Plenum Press: New York, 1983; Vol. 7, Chapter 7.

(19) Alonzo, D. C.; Scharifker, B. R. *J. Electroanal. Chem.* **1989,** *274,* 167–178.

(20) Garcia, S. G.; Salinas, D.; Mayer, C.; Vilche, J. R.; Pauling, H.-J.; Vinzelberg, S.; Staikov, G.; Lorenz, W. J. *Surf. Sci.* **1994,** *316,* 143–156.

(21) Vaskevich, A.; Rosenblum, M.; Gileadi, E. *J. Electroanal. Chem.* **1996,** *412,* 117–123.

(22) Esplandiu, M. J.; Schneeweiss, M. A.; Kolb, D. M. *Phys. Chem. Chem. Phys.* **1999,** *1,* 4847–4854.

(23) Budevski, E.; Staikov, G.; Lorenz, W. J. *Electrochemical Phase Formation and Growth;* VCH: New York, 1996; Chapter 4.

(24) Gabrielli, C.; Keddam, M.; Torresi, R. *J. Electrochem. Soc.* **1991,** *138,* 2657–2660.

(25) Oltra, R.; Efimov, I. O. *J. Electrochem. Soc.* **1994,** *141,* 1838–1842.

Chapter 5

Conclusions

During the course of this doctoral thesis work, the influence of the surface roughness of Pt electrodes on the frequency response, thus the mass response, of the electrochemical quartz-crystal nanobalance (EQCN) was studied. The EQCN is a powerful and relatively inexpensive technique for in-situ measurements of mass changes associated with interfacial electrochemical processes. Platinum electrochemistry and electrocatalysis play an important role in the development of electrocatalysts for hydrogen fuel cell and water electrolyser technologies. The Pt electrocatalysts applied in these technologies have very small sizes, meso- or nano-size, and their electrode surface is very roughness (the electrochemically active surface area is very large) because of the small size of the electrocatalysts. A considerable amount of research was conducted using the EQCN with the objective of gaining a better understanding of Pt electrocatalysis, but the influence of the surface roughness was not examined and, consequently, remained unknown. In this work, we first suggest a suitable methodology for the determination of the limits of detection and quantification (LOD and LOQ, respectively) of the EQCN measurements. The impact of the surface roughness on the mass response of the EQCN is analyzed. As outcomes of the analysis, we are able to determine the number of electrolyte compounds interacting with each Pt surface atom and report a modified version of the Sauerbrey equation. In addition, we calibrate the EQCN system for the more reliable data analysis for an electrode having a rough surface.

In *Chapter 2*, for the first time, we report a methodology for the determination of the values of LOD and LOQ of EQCN measurements for Pt electrodes in aqueous H_2SO_4 using

cyclic-voltammetry and concurrently measured frequency variation. The linear double-layer charging region in the frequency transient is selected as a baseline, and the standard deviation of the frequency data is obtained. Since the LOD and LOQ are defined as three times and ten times the standard deviation of the instrument signal from blanks, the values of LOD and LOQ are determined to be in the 2–3 ng cm^{-2} and 6–10 ng cm^{-2} ranges, respectively, depending on the electrolyte concentration. The variation of the LOD and LOQ values with the electrolyte concentration is attributed to the increased structural inhomogeneities of the electrolyte in the interfacial region. The values of LOD and LOQ are small enough to make this technique suitable for measuring interfacial mass changes associated with the electrochemical behavior of Pt electrodes.

In *Chapter 3*, for the first time, we report the response of the EQCN for atomically flat polycrystalline Pt electrodes. Platinum electrodes having a steadily increasing surface roughness are prepared through Pt electrodeposition, and their interfacial mass responses are examined simultaneously with cyclic-voltammetry measurements. Based on these experiments, the values of interfacial mass changes associated with the electrochemical H adsorption and desorption as well as the surface oxide formation and reduction on Pt electrodes are reported in relation to their surface roughness. They linearly increase with the surface roughness factor, and their extrapolation to the roughness factor of $R = 1.00$ produces the interfacial mass responses for atomically flat polycrystalline Pt electrodes. These interfacial mass change values are converted to the interfacial molar mass changes, revealing the number of H, O, water, and ionic species interacting with each Pt surface atom. In addition, the examination of the linear relationship between the interfacial mass changes and the surface roughness results in a proposal of a modified version of the Sauerbrey equation, which takes into account the surface roughness of the electrodes.

In *Chapter 4*, we report on the study of the influence of surface roughness of Pt electrodes on the value of experimental characteristic constant ($C_{f,exp}$) of the EQCN, as determined via Ag electrodeposition measurements. A thin layer of Ag is electrodeposited on the Pt electrodes of gradually increasing surface roughness, and the values of charge density and frequency change associated with the electrodeposition of Ag are measured. Atomic force microscopy images and line profiles of the Pt electrodes prior to and after Ag electrodeposition show that the morphology of the Ag deposits mimics the surface topography of the underlying Pt substrate. The slopes of the charge density versus frequency change plots yield the values of $C_{f,exp}$ for each Pt electrode (having its unique surface roughness), and the values differ from the theoretical characteristic constant (C_f). The values of $C_{f,exp}$ increase logarithmically with rising values of R. Both the values of C_f and $C_{f,exp}$ are used to determine the interfacial mass changes associated with the CV measurements. In the case of Pt electrodes having a relatively smooth surface, both values can be used to convert frequency changes to mass changes. However, in the case of rough Pt electrodes, the conversion of frequency changes to mass changes requires the knowledge of $C_{f,exp}$, which can be obtained through calibrating the instrument. This indicates that for electrodes with large surface roughness, direct application of the C_f value yields under-evaluated mass changes associated with interfacial electrochemical processes.

The new knowledge acquired using the EQCN is very important for the understanding of the nature of interfacial electrochemical processes occurring at Pt electrodes. Although in this work we employed Pt electrodes, the approach is universal and could be applied to other materials. For instance, it could be employed to study the interfacial behavior of other platinum-group or non-platinum-group metals that are of industrial importance and possess a meso- or nano-structure. These could be materials such as Ni, which finds application in electrochemical energy generation and storage systems. In addition, the EQCN could be a suitable technique to study the corrosion of metals or alloys. It is also a very suitable technique to study

electrodeposition of metallic or non-metallic materials. The EQCN can be easily combined with many electrochemical techniques with the objective of shedding new light on the nature of interfacial electrochemical processes. However, such research has to be conducted with a lot of diligence and the analysis of experimental data has to be thorough.

Chapter 6

Future Work

The outcome of my doctoral research project creates new knowledge as well as new research opportunities. In this final chapter, I would like to suggest three research projects that could be pursued as a follow-up on this thesis work. The research ideas described below could be expanded and become M.Sc. or Ph.D. thesis projects.

In the first part of my research, which is presented in *Chapter 2*, we used Pt-coated quartz-crystal resonators but other resonators (e.g. Au, Ag, Ni, Fe, etc.) are commercially available and could be employed in experimental research. Very few metallic materials reveal good adhesion to quartz and, consequently, an intermediate layer made of Cr or Ti is typically employed. The presence of the intermediate layer could contribute to the intrinsic noise level, thus to the LOD and LOQ of EQCN measurements. Because Au has good adhesion to quartz, the use of Au-coated resonators without and with an intermediate layer in the analysis of the EQCN noise level could shed light on the technique's LOD and LOQ.

In the second part of my research, which is presented in *Chapters 3* and *4*, we analyzed the influence of steadily increasing surface roughness of Pt electrodes on their frequency response. The surface roughness of the Pt electrodes was modified through Pt electrodeposition, which produced wave-like surface features and small/large islands. The height and size of these features were in the 40–80 nm and 100–300 nm ranges, respectively, and the electrode surface roughness factor was up to ca. $R = 13$. In this thesis work, we were able to control the value of the surface roughness factor; however, we were not able to control the shape and size of surface structures. It is desirable to examine the influence of the shape and size of surface features on the

EQCN frequency response. There are several methods that can produce specific surface structures, such as hemispheres, cones, tetrahedrons, pyramids, or cubes on the electrode surface. For example, photolithography, specific deposition (electrochemically or physically), or preferential etching (electrochemically or physically) techniques can be used to control the shapes and patterns of surface structures in the 10–100 nm range. In addition, atomic layer deposition technique could be employed because it can develop surface patterns that are below 10 nm in size, thus several atomic monolayers in size. Thus, through precise control of the size and shape of the surface structures, one could examine their influence on the frequency changes, thus the interfacial mass changes, associated with electrochemical processes. This research would shed light on the magnitude of LOD and LOQ for such patterned electrodes as well as the relationship between C_f and $C_{f,exp}$.

This project focused on the interfacial behavior of Pt electrodes as examined using the EQCN. There is a considerable amount of information available for Au-coated resonators but little is known about the interfacial mass response of other materials, such as Fe or Ni. A wide selection of electrode materials is commercially available and they can be used in experimental research to meet specific applications. For instance, Fe-coated electrodes could be used for a better understanding of its corrosion behavior. Nickel-coated electrodes could be used for a study of its electrocatalytic activity and durability in alkaline water electrolysis. Copper-coated electrodes could be effectively used in research on the reductive conversion of CO_2 into fuels.

Finally, once we manage to control the composition and surface morphology of EQCN resonators, we could analyze their frequency and mass responses during interfacial electrochemical processes with the objective of finding trends and mathematical data modeling. The mathematical modeling could incorporate parameters that take into account the geometry and size of surface features and the nature of the electrode material. Dedicated data modeling could lead to a new version of the Sauerbrey equation, which would be more versatile.

Appendix A

Appendix for Chapter 3

The current density (j) and the mass change (Δm) values of cyclic-voltammetry (CV) and mass variation (MV) transients shown in Figures 3.4A and 3.4B are divided by the corresponding values of the electrode roughness factor (R). Such normalized plots, namely j/R versus E and $\Delta m/R$ versus E, are presented in Figures A.1A and A.1B, respectively. Figure A.1A reveals that the CV profiles normalized for the roughness factor values overlap; the agreement is to ±1.9%, which is within the experimental uncertainty. Figure A.1B demonstrates that the MV transients normalized for the surface roughness factor do not overlap.

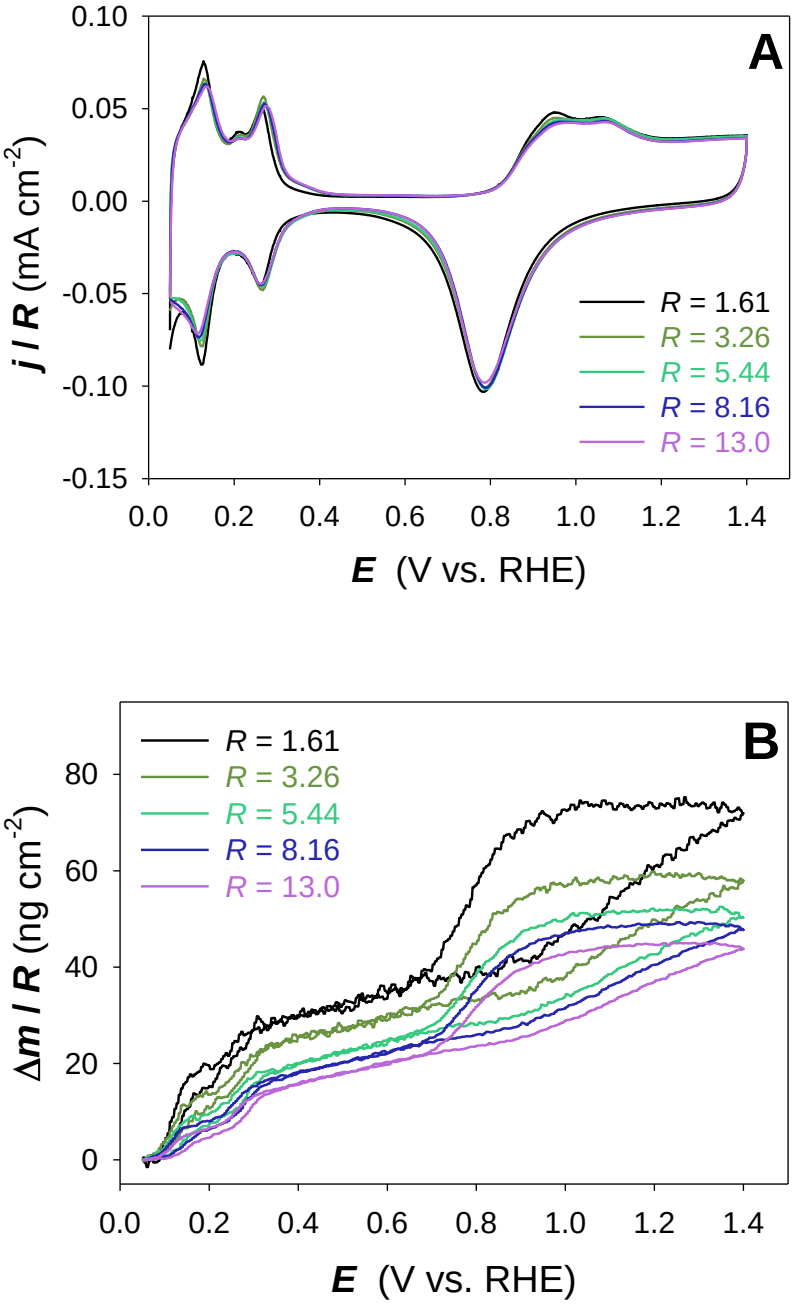

Figure A.1. Series of roughness factor-normalized CV profiles (**A**) and simultaneously recorded MV transients (**B**) for Pt electrodes of gradually increasing surface roughness ($1.61 \leq R \leq 13.0$) acquired in 0.50 M aqueous H_2SO_4 at a potential scan rate of s = 50.0 mV s^{-1} and T = 298 K.

Appendix B

Appendix for Chapter 4

Figures A.2A through A.2C show the charge density (q) versus frequency variation (Δf) plots for the Ag electrodeposition at a constant current density of j = 50.0 μA cm^{-2} on Pt electrodes having surface roughness factors of R = 4.58, 6.86, and 10.3, respectively, in 0.50 M aqueous H_2SO_4 solution containing 1.5 mM Ag_2SO_4. Their slopes are used to determine the value of $C_{f,exp}$ for each value of R. The green dashed lines refer to the values of q corresponding to the Ag electrodeposit being 1, 3, 5, and 7 monolayers (MLs) in thickness.

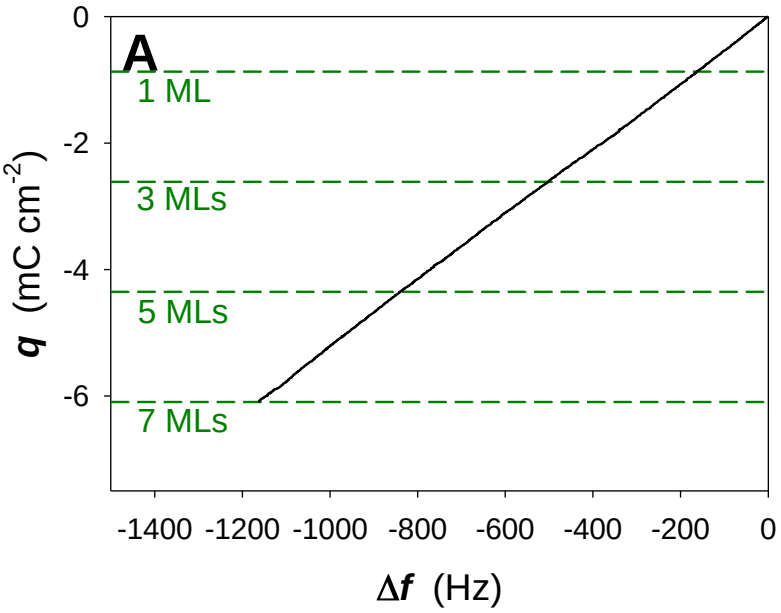

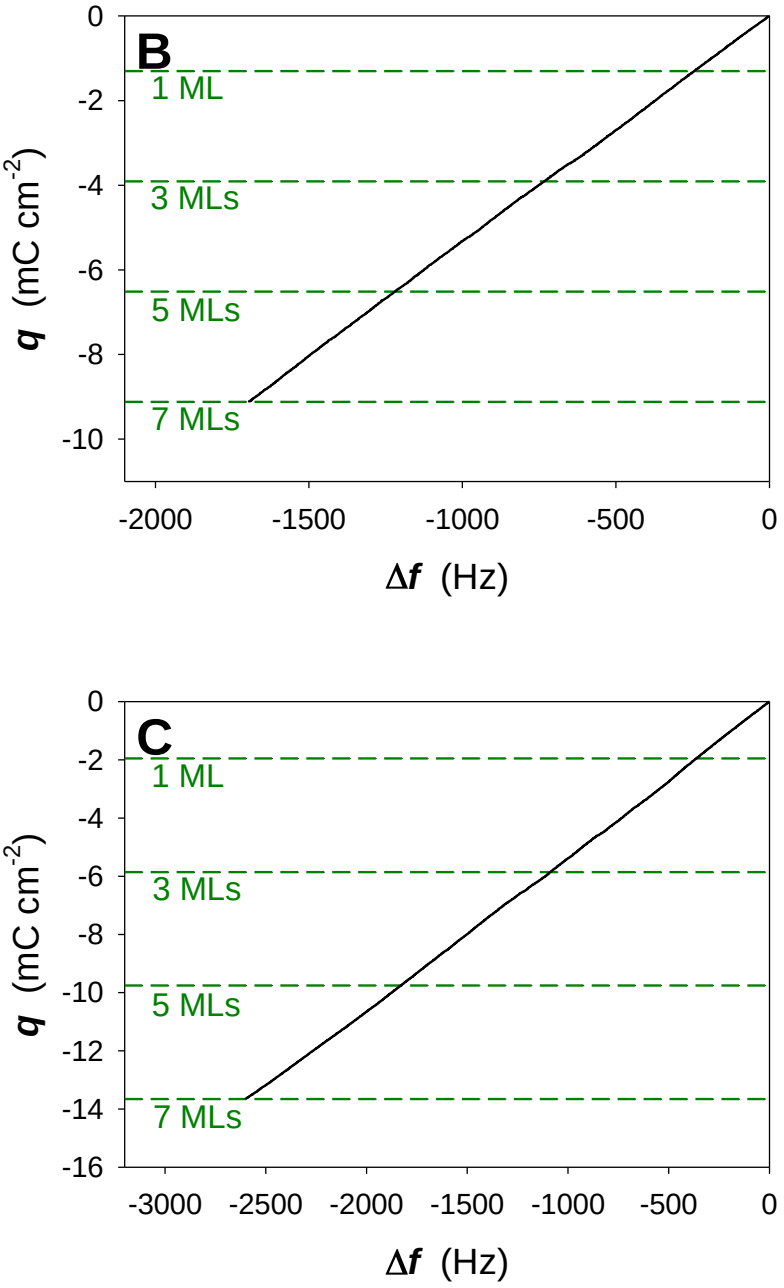

Figure A.2. Charge density (q) versus frequency variation (Δf) plots for the Ag electrodeposition on Pt electrodes having surface roughness factor of R = 4.58 (**A**), 6.86 (**B**), and 10.3 (**C**). The electrodeposition of Ag is accomplished at a current density of j = 50.0 μA cm^{-2} in 0.50 M aqueous H_2SO_4 + 1.5 mM Ag_2SO_4 solution at T = 298 K.